

10-22-2025 10:00 AM

Nonlinear Dynamics and Bifurcations in Tumor–Immune Models with Therapies

Ruchita Yaksh Amin

Supervisor: Yu, Pei, *The University of Western Ontario*

A thesis submitted in partial fulfillment of the requirements for the Doctor of Philosophy degree
in Applied Mathematics

© Ruchita Yaksh Amin 2025

Abstract

Cancer is one of the most serious health problems worldwide, responsible for millions of deaths each year. It develops when cells grow in an uncontrolled way and avoid detection by the immune system. Key immune players such as $CD4^+$ T cells and cytokines are essential for recognizing and controlling tumors, and many modern therapies aim to enhance or restore their function. Immunotherapy, in particular, has become one of the most promising approaches for reducing tumor growth and improving survival. In this thesis, mathematical models are used to study how tumors interact with immune cells and how treatments influence these interactions. We begin with a model that describes tumor, $CD4^+$ T cell, and cytokine dynamics in the absence of treatment. This helps identify the limits of natural immune control and shows how stability and oscillations in tumor size can occur, especially through Hopf bifurcations. The results suggest that when tumors have very low antigenicity, they can continue to grow unchecked, even if immune responses are strong. The analysis is then extended to include immunotherapy and combined treatments (polytherapy), where stability, equilibrium points, and bifurcation patterns are examined. Using normal form theory, we study the amplitude and stability of limit cycles, revealing how therapy can shift the system toward long-term tumor control or oscillatory behavior. We also explore virotherapy, a newer treatment that uses engineered viruses to infect and destroy cancer cells. A nonlinear model is developed for tumor–virus interactions, and bifurcation analysis shows how viral therapy can produce stable oscillations that represent ongoing cycles of tumor reduction. Numerical simulations are provided throughout to illustrate theoretical results. Overall, this work demonstrates how mathematical oncology can be used to understand tumor–immune–therapy interactions and to provide insights for improving cancer treatment strategies.

Keywords: Tumor model, Immunotherapy, Stability, Center manifold, Hopf bifurcation, Limit cycle, Normal Form, Virus-tumor interaction model, Virotherapy.

Summary for Lay Audience

These studies use mathematical models to analyze immune system and cancer tumor interactions. We considered three models to study tumor growth or shrinkage under different conditions: without treatment, immune therapy, and virus therapy. Using advanced mathematical tools, we explored when the system show steady tumor control, oscillations, or multiple possible states, and found important phenomena called bifurcations where small parameter changes cause sudden shifts towards the outcomes.

In the model without treatment, we found that very low tumor antigenicity leads to cancer progression no matter how strong the killing ability or cytokine levels are, showing that proper tumor recognizing is essential. Small parameter changes can push the system from control to escape, showing the limits of natural immunity.

Introducing immunotherapy, it changes the boundaries, sometimes stabilize or destabilize tumor control, depending on dose and timing. Near bifurcation points, small treatment changes can change tumor-immune cycles or create situations where both stable control and stable tumor growth coexist, making the outcome highly sensitive to initial conditions.

Oncolytic virotherapy adds viruses that infect and destroy tumor cells. The findings show that viral replication can either help long-term tumor control or allow cancer regrowth depending on infection rate, burst size, and clearance rate. Overall, the results highlight key factors that decide whether tumors are controlled or escaped, guiding for designing safer and more effective cancer therapies.

Co-Authorship Statement

I, Ruchita Amin, declare that the work presented in this thesis, “**Nonlinear Dynamics and Bifurcations in Tumor–Immune Models with Therapies,**” has been written by me under the supervision (co-authored) of Dr. Pei Yu.

Chapter 2: Ruchita Amin and Pei Yu, “*Bifurcation analysis on immunotherapy of a tumor model without treatment,*” *Discrete and Continuous Dynamical Systems - Series S*, 2025: 2025076 (Published).

Chapter 3: Ruchita Amin and Pei Yu, “*Dynamical Analysis of a Tumor Model with Immunotherapy Treatment,*” *Chaos, Solitons & Fractals*, 2025, (Submitted).

Chapter 4: Ruchita Amin and Pei Yu, “*Bifurcation Analysis and Complex Dynamics of a Virotherapy Model,*” *International Journal of Biomathematics*, 2025, (Submitted).

Acknowledgments

I would like to express my heartfelt gratitude to my supervisor, Professor Pei Yu, for his constant guidance and support throughout my Ph.D. studies. His calmness, encouragement, and generosity in sharing his knowledge of dynamical systems have been invaluable to me. I am especially thankful for the way he helped me to overcome challenges and inspired me with his passion for research. What I have learned from him will remain with me beyond this thesis and continue to guide me in my future career. It has been both an honor and a privilege to study under his supervision.

Additionally, I am deeply grateful to the Applied Mathematics and Mathematics Department at Western University for providing me with this wonderful opportunity. The experiences and skills I have gained here are truly vital. In particular, I thank Professor Wahl for her inspiring courses in mathematical biology, which played an important role in shaping this thesis, as well as other professors whose teaching and guidance have supported my growth. Moreover, I am grateful to the members of the Dynamical Systems Group for the weekly seminars that enriched my learning and fostered meaningful discussions, as well as to Professor Yu's and Professor Zou's groups for their encouragement and support.

Most of all, I owe my deepest gratitude to my family for their unconditional love and support. To my daughter, **Ruksha**, whose smiles and presence have been a constant source of joy and strength during this journey and to my husband, **Yaksh**, for his endless patience, assistance, and unwavering belief in me, even in the most difficult times. I am also grateful for the little life growing within me — our baby boy, **Ruksh**, whose presence has given me renewed courage and motivation during the final stages of this thesis.

This research was supported by the Natural Sciences and Engineering Research Council of Canada, No. R2686A02 (P. Yu).

Table of Contents

Abstract	ii
Summary for Lay Audience	iii
Co-Authorship Statement	iv
Acknowledgments	v
Table of Contents	vi
List of Tables	ix
List of Figures	x
1 Introduction	1
1.1 Overview of Immune Response	3
1.1.1 CD4 ⁺ T cells and Cytokines	4
1.1.2 Immune surveillance and tumour evasion	4
1.1.3 Immuno-oncology and Virotherapy	4
1.2 Mathematical Models in Immuno-Oncology	4
1.3 Dynamical Systems Approach	5
1.4 Mathematical Theories and Methodologies for Model Analysis	6
1.4.1 Analysis of equilibrium states and their stability	7
1.4.2 Bifurcation dynamics study	8
1.4.3 Hopf bifurcation	10
1.4.4 Methods for analyzing limit cycles and computing normal forms . .	11
Reduction and transformation to normal form	12
Focus Values and Limit Cycle Multiplicity	13

	Perturbation Methods and Symbolic Computation	13
	Geometric Interpretation and Dynamics	14
1.5	Thesis Outline	14
1.6	Contribution of the thesis	16
	References	16
2	Bifurcation Analysis on Immunotherapy of a Tumor Model Without Treatment	23
2.1	Introduction	23
2.2	Modeling and Reduction	24
2.3	Property of Solutions of System (2.5)	28
2.4	Equilibrium Solutions and Their Stability	29
2.4.1	Case $R_0 = 1$ (or $D = \frac{B}{C+1}$)	35
2.4.2	Case $R_0 > 1$ and codimension of Hopf bifurcation	38
2.5	Numerical Simulation	48
2.6	Conclusion	51
	References	52
3	Dynamical Analysis of a Tumor Model with Immunotherapy Treatment	54
3.1	Introduction	54
3.2	Mathematical Modeling	61
3.3	Solution Properties of Model (3.3)	63
3.4	Treatment with Cytokine ($G_1 = 0, G_2 > 0$).	65
3.4.1	Stability and bifurcation analysis	66
3.4.2	Limit cycle bifurcation and its stability	77
3.4.3	Stability at $G_2 = G_{2t}$ and center manifold reduction	81
3.5	Treatment with CD4 ⁺ T cells ($G_1 > 0, G_2 = 0$).	84
3.5.1	Stability and bifurcation of system (3.26)	86

3.5.2	Bifurcation of multiple limit cycles	92
3.6	Treatment with both CD4 ⁺ T cells and Cytokine ($G_1 > 0, G_2 > 0$).	97
	Remark	103
3.7	Conclusion	104
	References	105
4	Bifurcation Analysis and Complex Dynamics of a Virotherapy Model	111
4.1	Introduction	111
4.2	Modeling and Reduction	115
4.3	Positivity and Boundedness of Solutions	118
4.4	Equilibrium Solutions and Their Stability	120
4.5	Codimension of Hopf bifurcation	125
	4.5.1 Center manifold reduction	126
	4.5.2 Bifurcation of limit cycles and their stability	128
4.6	Simulation	134
4.7	Conclusion	136
	References	138
5	Conclusion and Future Work	142
5.1	Future Work	143
	Curriculum Vitae	145

List of Tables

2.1	Parameters used in system (2.2) [6].	26
2.2	Parameters used in system (2.5) [6].	28
3.1	Parameters used in system (3.2).	62
3.2	Parameters used in system (3.3) [15].	63
4.1	Model parameters for system (4.1) and their biological interpretation.	116

List of Figures

1.1	Percentage distribution of global cancer incidences and deaths.[16, 17] . . .	1
1.2	Percentage distribution of major cancer types by incidence and deaths in males and females.[18]	2
2.1	Bifurcation diagram for system (2.5) showing the equilibrium solutions E_0 , E_1 and E_2 , where solid and dotted lines/curves represent stable and unstable equilibrium solutions, respectively.	35
2.2	Phase portrait of system (2.5) at $R_0 = 1$, projected on the X - Y plane, showing the convergence of trajectories to the degenerate node $X = 1$, with the parameter values: $A = \frac{1}{10}$, $B = \frac{29}{3}$, $C = 1$, $D = \frac{B}{1+C} = \frac{29}{6}$, $E = \frac{3}{1000}$ and $F = 100$	39
2.3	Bifurcation diagram for Hopf bifurcations of system (2.5) yielding (a) one limit cycle bifurcating at $E = E_H - \mu$; and (b) two limit cycles bifurcating at $E = E_H + \mu$	49
2.4	Simulated limit cycles for system (2.5): (a) one stable limit cycle for $A = 0.1$, $B = 9.666667$, $C = 1$, $D = 3$, $E = 0.003$, $F = 100$; and (b) two limit cycles for $A = 0.9$, $B = 285.971087$, $C = 1$, $D = 13.617671$, $E = 0.092232$, $F = 20$, with the outer one stable and the inner one unstable, both them enclosing the stable equilibrium E_2	50
3.1	Different functions between helper T cells and cytotoxic T cells ($CD4^+$ and $CD8^+$).	56
3.2	Helper T cell activation and its role in immunity [26].	57

3.3	Bifurcation diagram of system (3.6) for (a) $A < 1$, (b) $A = 1$, and (c) $A \geq 1$, projected on the G_2 - X plane, showing the equilibria E_0 , E_1 and E_2 , marked by red, brown and blue colors, respectively. Solid and dotted lines/curves denote stable and unstable equilibria, respectively.	72
3.4	Simulated trajectories of system (3.6) for (a) $G_2 = \frac{9}{5}$, converging to the equilibrium E_2 ; and (b) $G_2 = \frac{183}{1075}$, converging to a stable limit cycle.	80
3.5	Simulated trajectories of system (3.26): (a) with parameters $A = \frac{9}{10}$, $B = 9$, $C = 1$, $D = 3$, $E = 1/10$, $F = 40$, $G_1 = \frac{165021347}{100000000}$, converging to equilibrium E_2 ; and (b) with parameters $A = \frac{2}{5}$, $B = 55$, $C = 1$, $D = \frac{1343113}{200000}$, $E = \frac{9}{10}$, $F = 6$, $G_1 = \frac{278715}{105167}$, converging to a stable limit cycle.	97
3.6	Simulated trajectories of system (3.38): (a) when $A = \frac{1}{10}$, $B = 57$, $C = 1$, $D = 4$, $E = \frac{3}{10}$, $F = 70$, $G_1 = \frac{165021347}{100000000}$, $G_2 = \frac{9}{5}$, converging to the equilibrium E_2 ; and (b) when $A = \frac{1}{10}$, $B = 50$, $C = 1$, $D = 6$, $E = 40$, $F = 10$, $G_1 = \frac{278715}{105167}$, $G_2 = \frac{183}{1075}$, converging to a stable limit cycle.	103
4.1	Function of oncolytic virotherapy (TA: Tumor Antigen, DC: Dendritic Cell) [9].	113
4.2	Bifurcation diagram for system (4.2) illustrating the equilibrium points E_0 , E_1 and E_2 . Stable equilibria are indicated by solid lines, while unstable equilibria are shown using dotted lines.	125
4.3	Simulations of model (4.2) for $A = 1$, $B = \frac{9}{10}$, $C = \frac{1}{10}$, $D_t = \frac{8}{9}$, with the initial condition: $X(0) = 0.4$, $Y(0) = 0$, $Z(0) = 0.1$ (a) $D = \frac{11}{10}$ and (b) $D = \frac{9}{10} \in (D_t, 1)$	135
4.4	Simulations of model (4.2) showing stable limit cycles: (a) $A = \frac{19}{20}$, $B = 9$, $C = 1$, $D = \frac{3107}{9900} < D_H = \frac{661}{1980}$, regular oscillation and (b) $A = \frac{3}{5}$, $B = 6$, $C = \frac{1}{5}$, $D = \frac{1}{5} < D_H = \frac{34459}{40350}$, slow faster motion.	135

Chapter 1

1 Introduction

Cancer, which arises from pathological disruptions in the normal process of cell division [1], has become a major global health concern and remains one of the leading causes of death worldwide [2]. In 2020 alone, more than 19.3 million new cases were diagnosed, resulting in nearly 10 million deaths [3, 4]. This alarming global burden underscores the urgent need for effective treatments that can target diverse cancer types [5–8].

The causes of cancer are multifaceted, ranging from genetic predispositions and lifestyle factors to stress and environmental influences. The dominant cause varies depending on cancer type and geographical location, making individualized treatment essential. While shifts in climate, industrialization, and modern dietary habits are suspected contributors to the rising incidence of cancer, further research is needed to establish definitive causal links [9–13].

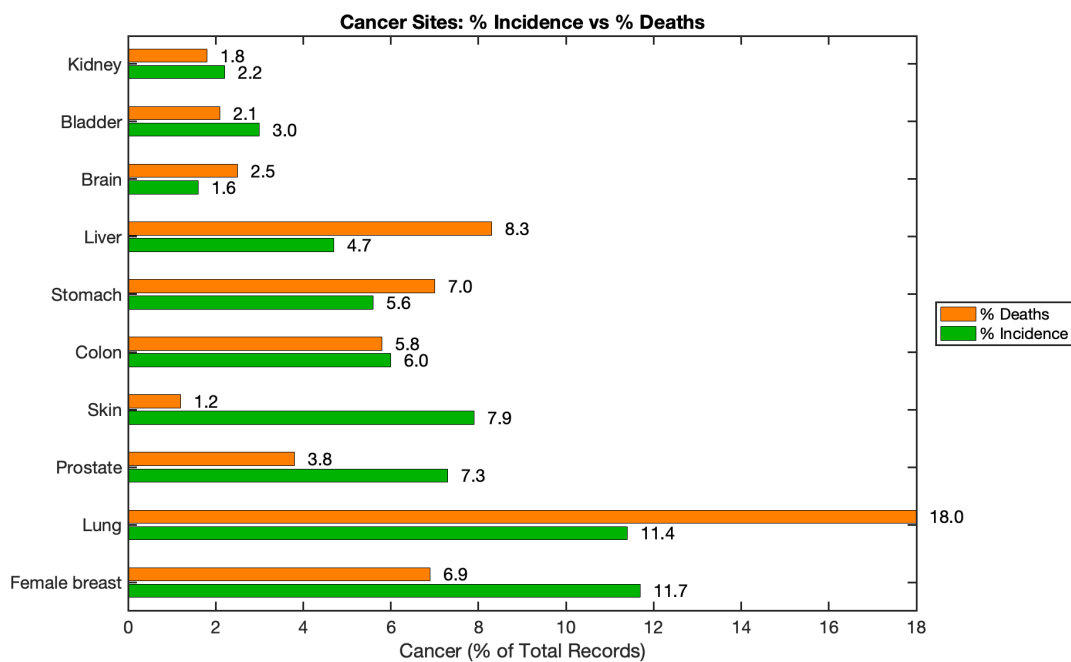


Figure 1.1: Percentage distribution of global cancer incidences and deaths.[16, 17]

Cancer affects every country. To monitor its global impact, the International Agency for Research on Cancer maintains the Global Cancer Observatory (GCO), which compiles and visualizes estimates of cancer incidence and mortality worldwide, providing us valuable data for cancer control strategies [14]. Its GLOBOCAN 2020 release covers 185 countries and offers interactive charts and tables you can explore by region and by sex [15]. As shown in Figure 1.1, the most common cancer types were female breast cancer (2.26 million; 11.7%), lung (2.21 million; 11.4%), skin (1.53 million; 7.9%), and prostate (1.41 million; 7.3%) and the leading causes of death due to cancer were lung (1.79 million; 18%), liver (0.83 million; 8.3%), stomach (0.77 million; 7.7%), and breast (0.68 million; 6.9%) [16, 17]. As shown in the bar graph in Figure 1.2, most cancer deaths in men were from lung (22%), prostate (10.5%), and liver (9%) cancers where as in women, mainly from breast (15.2%), lung (13.8%), and stomach (6.1%) cancers [18].

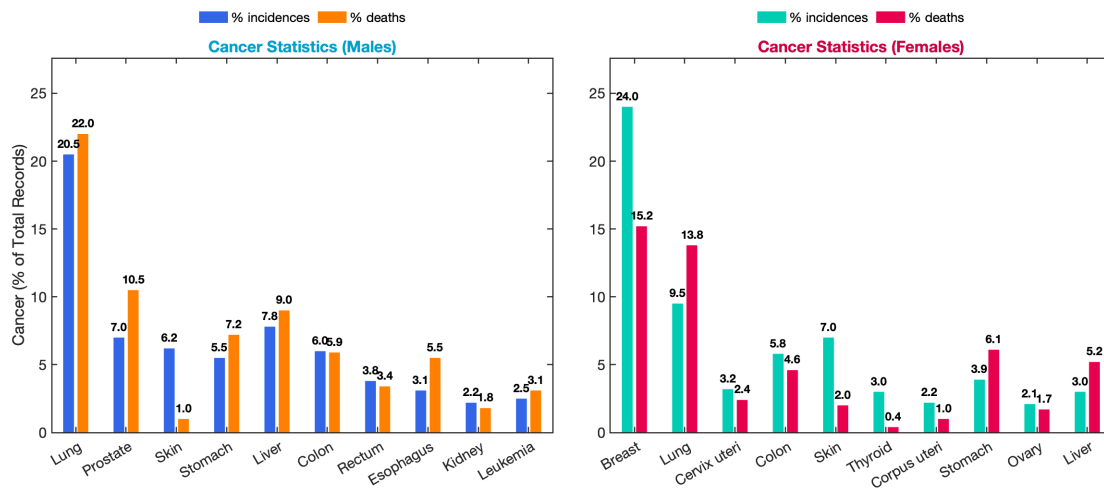


Figure 1.2: Percentage distribution of major cancer types by incidence and deaths in males and females.[18]

Fundamentally, cancer is characterized by uncontrolled cellular growth and the ability of malignant cells to escape immune surveillance. The human immune system, however, is equipped with powerful defenses; capable of recognizing and eliminating abnormal cells before they develop into full tumours. Key immune components—including CD4⁺ T cells,

cytokines, and cytotoxic lymphocytes—play crucial roles in tumour recognition and eradication [19, 20]. The emergence of immunotherapies, such as immune checkpoint inhibitors, adoptive T-cell transfer, and oncolytic virotherapy, has revolutionized modern oncology by harnessing and enhancing the body’s natural defenses [21–23].

Understanding these intricate interactions between tumours, immune responses, and therapeutic interventions has motivated the use of mathematical modeling. By formulating nonlinear differential equation systems, researchers can simulate tumour growth, immune activation, and treatment responses under diverse biological and therapeutic conditions. This interdisciplinary field, known as mathematical oncology, integrates biology, mathematics, and clinical data to investigate tumour–immune dynamics, predict patient outcomes, and optimize treatment strategies [24–26].

This thesis is devoted to exploring mathematical models that describe the interactions between tumours, $CD4^+$ T cells, and cytokines under varying therapeutic conditions. Specifically, it examines three interconnected models. The first analyzes the qualitative dynamics of tumour, $CD4^+$ T cell, and cytokine interactions in the absence of treatment. The second extends this framework to include immunotherapy and cytokine-based interventions. The third investigates bifurcation phenomena in tumour–immune systems, with a particular focus on the onset of oscillatory dynamics and multistability through Hopf bifurcation.

1.1 Overview of Immune Response

The immune system is broadly divided into two: natural and adaptive immunity [27]. While natural immunity provides the first line of defense through macrophages, dendritic cells, and natural killer (NK) cells, the adaptive immune response is slower but more specific and robust. T cells, including $CD4^+$ helper T cells and $CD8^+$ cytotoxic T lymphocytes (CTLs) play a key role in the body’s immune response [28, 29].

1.1.1 CD4⁺T cells and Cytokines

CD4⁺ T cells play a regulatory role in adapting immune responses by releasing cytokines such as interleukins (e.g., IL-2, IL-12) and interferon-gamma (IFN- γ) [30]. These cytokines enhance the cytotoxic activity of CD8⁺ T cells and NK cells help antigen to recognize infections. Depending on the microenvironmental cues, CD4⁺ T cells can differentiate into various subtypes (Th1, Th2, Th17, Treg), each with distinct functions [31].

1.1.2 Immune surveillance and tumour evasion

In normal conditions, immune cells can detect and eliminate transformed cells, a process termed "cancer immunosurveillance" [32]. However, tumours can evolve mechanisms to suppress immune responses, such as secreting immunosuppressive cytokines (e.g., TGF- β), downregulating antigen presentation, or inducing T cell exhaustion [33, 34].

1.1.3 Immuno-oncology and Virotherapy

Recent therapeutic advances have leveraged the immune system to fight cancer more effectively. Immune checkpoint inhibitors block inhibitory signals (e.g., PD-1/PD-L1, CTLA-4) which tumours use to suppress T cells, thereby restoring their effector function [35]. In parallel, oncolytic viruses—engineered to selectively infect and lyse tumour cells have emerged as promising tools in virotherapy. They not only cause direct tumour cell death but also stimulate systemic antitumour immunity by releasing tumour associated antigens [36, 37].

1.2 Mathematical Models in Immuno-Oncology

The classical logistic growth model has served as a starting point for modeling tumour progression, where tumour cells grow with natural rate and saturate due to limited resources

[38]. However, incorporating immune responses transform the system into a more biologically realistic, nonlinear model often analyzed using predator-prey or competition frameworks [39–41].

Recent models have considered interactions between tumours and multiple immune effectors, including $CD4^+$ T cells and cytokines. These models have been formulated as systems of ordinary differential equations (ODEs), and their qualitative behavior has been studied through equilibrium analysis, stability criteria, and bifurcation theory [42–45]. The inclusion of therapy such as cytokine infusion or virotherapy introduces new parameters that can significantly alter system dynamics and lead to multistability, periodic oscillations, or chaotic behavior [46, 47].

1.3 Dynamical Systems Approach

In this research, we employ advanced dynamical systems tools including center manifold theory, Lyapunov stability, Hopf bifurcation theory, and normal form analysis to study tumour–immune interaction models. We are particularly interested in identifying parameter regimes that lead to limit cycles, which correspond to periodic fluctuations in tumour size and immune activity. These oscillations can represent either successful immune surveillance or immune escape, depending on their stability and amplitude [48–50].

In later chapters, we investigate how therapeutic interventions shift these bifurcation thresholds and influence clinical outcomes. Our results contribute to a deeper understanding of the nonlinear dynamics underlying cancer progression and treatment response providing insight into the design of optimal therapeutic protocols.

1.4 Mathematical Theories and Methodologies for Model Analysis

Mathematical theories and methodologies provide a rigorous framework for understanding the complex, nonlinear dynamics observed in tumour-immune system interactions. These models often begin by formulating biologically meaningful assumptions grounded in immunology and oncology, then translating these into systems of ordinary differential equations (ODEs). These ODEs describe the rates of change of key populations, such as tumour cells, immune cells particularly $CD4^+$ T cells and cytokine concentrations over time.

A foundational step in analyzing such models is ensuring their biological consistency and mathematical well-posedness. This involves confirming that solutions remain positive and bounded, reflecting biologically realistic behavior such as non-negative population sizes and finite cytokine levels. After establishing this, researchers often proceed with identifying and classifying equilibrium points, which correspond to steady states in tumour progression or immune response.

The next step is to perform stability analysis of these equilibria using techniques such as linearization and the Routh–Hurwitz criteria. These tools help determine whether small perturbations will cause the system to return to equilibrium or diverge, indicating sensitivity of the immune response. However, due to the nonlinear nature of tumour – immune dynamics, equilibrium points may not always be accessible in closed form, requiring implicit or numerical techniques for stability assessment. Special attention is paid to coexistence states where tumour and immune populations persist together, as these often reveal rich dynamical behaviors including multi-stability and oscillations.

In certain parameter regimes, the system may undergo qualitative changes in its behavior such as transitioning from tumour suppression to escape through bifurcations. Hopf bifurcation, in particular, is of major interest in immuno-oncology, as it can lead to periodic solutions that reflect cyclical tumour growth and immune response. Identifying such bifur-

cations requires advanced tools such as center manifold theory and normal form analysis.

Beyond local analysis, global dynamics and the emergence of multiple stable attractors or limit cycles are investigated using numerical continuation and bifurcation software. These phenomena may correspond to alternative disease outcomes based on initial immune conditions or therapeutic timing. Hence, understanding the mathematical structure of the system has both theoretical and clinical significance, aiding in the design of optimized treatment strategies that exploit the immune system's nonlinear response to cancer.

1.4.1 Analysis of equilibrium states and their stability

A fundamental aspect of studying nonlinear dynamical systems involves analyzing their equilibrium states and determining the local behavior near these points. Equilibria correspond to steady states of the system where all time derivatives vanish, meaning that the system remains constant if initialized exactly at that point.

Consider a general autonomous system of ordinary differential equations in \mathbb{R}^n

$$\frac{dx}{dt} = F(x), \quad x \in \mathbb{R}^n, \quad (1.1)$$

where $F : \mathbb{R}^n \rightarrow \mathbb{R}^n$ is a smooth vector field. An equilibrium point x^* satisfies $F(x^*) = 0$.

To analyze the local dynamics near x^* , we linearize the system by computing the Jacobian matrix $A = DF(x^*)$. The behavior of the nonlinear system near x^* is governed by the properties of the linearized system:

$$\frac{dy}{dt} = Ay, \quad (1.2)$$

where $y = x - x^*$ is the perturbation from equilibrium.

The key to understanding the stability of x^* lies in the eigenvalues of the Jacobian matrix A . These eigenvalues are the roots of the characteristic polynomial:

$$f(\lambda) = \det(A - \lambda I) = \lambda^n + a_1\lambda^{n-1} + \cdots + a_{n-1}\lambda + a_n, \quad (1.3)$$

where $n = 3$ in our case. The nature of the eigenvalues are real or complex, positive or negative determines the type and stability of the equilibrium.

If all eigenvalues have negative real parts, the equilibrium is locally asymptotically stable (a sink). If any eigenvalue has a positive real part, the equilibrium is unstable (a source or saddle). If all eigenvalues are purely imaginary, the equilibrium is non-hyperbolic, and further analysis (e.g., center manifold theory) is needed to determine local dynamics.

In 3D systems, the characteristic polynomial takes the form:

$$\lambda^3 + a_1\lambda^2 + a_2\lambda + a_3 = 0. \quad (1.4)$$

One standard method to assess stability without computing roots explicitly is the Routh–Hurwitz criterion, which provides necessary and sufficient conditions for all roots of the polynomial to have negative real parts. For a third-degree polynomial, the equilibrium is stable if:

$$a_1 > 0, \quad a_3 > 0, \quad a_1a_2 > a_3.$$

These inequalities place constraints on the entries of the Jacobian matrix and, indirectly, on the system parameters. By analyzing how these coefficients change with parameters, one can identify bifurcation points where stability is lost or gained.

1.4.2 Bifurcation dynamics study

Bifurcation theory plays a central role in the qualitative analysis of nonlinear dynamical systems. It concerns itself with understanding how the structure of a system's solutions such as equilibrium points, periodic orbits, or more complex attractors—changes as system parameters are varied. Bifurcations mark critical thresholds where the behavior of the system can shift dramatically, making them essential tools in predicting transitions, instabilities, and emergent phenomena in mathematical models.

Broadly, bifurcations can be categorized into local and global types, depending on the

region of the phase space they affect. Local bifurcations are concerned with changes in the dynamics near equilibrium points or periodic orbits. These bifurcations typically occur when one or more eigenvalues of the Jacobian matrix cross critical values (such as zero or the imaginary axis) as a parameter changes. Among the most studied local bifurcations are:

- **Saddle-node bifurcation:** Two equilibrium points (one stable, one unstable) collide and annihilate.
- **Transcritical bifurcation:** Equilibria exchange stability as they intersect.
- **Pitchfork bifurcation:** Often observed in symmetric systems, where one equilibrium gives rise to two new branches.
- **Hopf bifurcation:** A pair of complex conjugate eigenvalues cross the imaginary axis, leading to the birth or death of a limit cycle.

In our analysis, special attention is given to the Hopf bifurcation, as it provides insight into the emergence of sustained oscillatory behavior. A supercritical Hopf bifurcation results in the formation of a stable limit cycle, while a subcritical Hopf can lead to the destabilization of the equilibrium and the potential for sudden transitions to large-amplitude oscillations.

These bifurcations, which depend on the variation of a single parameter, are classified as codimension-1 bifurcations. However, more intricate behaviors emerge when multiple parameters influence the system simultaneously. Codimension-2 bifurcations, such as the Bogdanov–Takens bifurcation, occur at points where two local bifurcation conditions are satisfied concurrently typically involving both a zero eigenvalue and a pair of purely imaginary eigenvalues. These bifurcation points act as organizing centers in parameter space and often give rise to richer dynamics, including the coexistence of steady states, periodic orbits, and homoclinic trajectories. Furthermore, higher-order generalizations of Hopf or Bogdanov–Takens bifurcations, depending on the vanishing of successive derivatives

or focus values, can lead to higher codimension scenarios that exhibit layered bifurcation structures and complex unfolding patterns.

In this study, we apply bifurcation analysis as a primary method to uncover how qualitative shifts in dynamical behavior emerge under parameter variation. Our focus lies particularly on Hopf bifurcations and their interaction with other bifurcation structures, exploring how oscillatory and multi-stable regimes arise and evolve—insights that are crucial for understanding both theoretical and applied nonlinear systems.

1.4.3 Hopf bifurcation

Hopf bifurcation is a fundamental phenomenon in nonlinear dynamical systems that describes the transition from a steady-state behavior to sustained oscillations as a parameter crosses a critical threshold. This type of bifurcation occurs when a pair of complex conjugate eigenvalues of the Jacobian matrix associated with an equilibrium point crosses the imaginary axis in the complex plane, leading to the loss (or gain) of stability of that equilibrium and the emergence (or disappearance) of a periodic solution known as a limit cycle.

Equation (1.5) extends system (1.1) by introducing a bifurcation parameter μ and considering a smooth dynamical system in \mathbb{R}^n

$$\frac{dx}{dt} = F(x, \mu), \quad (1.5)$$

where $x \in \mathbb{R}^n$, $\mu \in \mathbb{R}$ is a bifurcation parameter, and F is continuously differentiable. When μ is fixed, $F(x, \mu)$ reduces to $F(x)$ in (1.1). Let x_0 be an equilibrium point, i.e., $F(x_0, \mu) = 0$. Linearizing the system around x_0 , we obtain the Jacobian matrix $A(\mu) = D_x F(x_0, \mu)$. A Hopf bifurcation occurs at $\mu = \mu_c$ when:

- The Jacobian has a pair of purely imaginary eigenvalues $\lambda_{1,2} = \pm i\omega$, $\omega > 0$ at $\mu = \mu_c$.
- The real parts of the eigenvalues cross zero as μ varies through μ_c .

Under certain non-degeneracy and transversality conditions (satisfied generically), the Hopf bifurcation theorem guarantees the existence of a family of periodic solutions near $\mu = \mu_c$. We can discuss about types of Hopf bifurcation:

- **Supercritical Hopf bifurcation:** A stable limit cycle emerges from a stable equilibrium as it loses stability. The oscillations begin with small amplitude near the bifurcation point and grow continuously as the bifurcation parameter changes.
- **Subcritical Hopf bifurcation:** An unstable limit cycle collides with a stable equilibrium, meaning the amplitude of the unstable limit cycle shrinks to zero as it merges with the equilibrium, causing the equilibrium to become unstable. This causes the equilibrium to lose stability, often producing abrupt, large oscillations or bistability.
- **Lyapunov coefficient:** The nature of the bifurcation—supercritical or subcritical—is determined by computing the first Lyapunov coefficient, v_1 . This coefficient measures how nonlinear effects near the equilibrium influence the growth or decay of small perturbations and determines whether the emerging periodic orbit (limit cycle) is stable or unstable: if $v_1 < 0$, the bifurcation is supercritical and the limit cycle is stable; if $v_1 > 0$, the bifurcation is subcritical and the limit cycle is unstable.

1.4.4 Methods for analyzing limit cycles and computing normal forms

Understanding the behavior of dynamical systems near bifurcation points requires precise tools to capture the qualitative nature of the system's solutions. One of the most powerful approaches for analyzing oscillatory solutions particularly near a Hopf bifurcation is the reduction of the system to its normal form. This procedure simplifies the system while retaining the essential nonlinear features that govern the formation and stability of limit cycles.

Reduction and transformation to normal form

Near a Hopf bifurcation, the dynamics of a system can often be reduced to a two-dimensional invariant manifold where the behavior is governed primarily by the amplitude and phase of the oscillation. This is possible because, close to the bifurcation, the dynamics are dominated by a pair of complex eigenvalues that cross the imaginary axis, while other directions in the system decay or grow quickly. By focusing on this two-dimensional center manifold, one can describe the essential behavior using polar coordinates (r, θ) . In polar coordinates (r, θ) , the normal form for a classical (codimension-1) Hopf bifurcation can be expressed as [51]:

$$\begin{aligned}\frac{dr}{dt} &= r(v_0\mu + v_1r^2 + \cdots + v_kr^{2k} + \cdots), \\ \frac{d\theta}{dt} &= \omega_c + \tau_0\mu + \tau_1r^2 + \cdots + \tau_kr^{2k} + \cdots,\end{aligned}$$

where r is the oscillation amplitude, θ is the angular phase, and μ is the bifurcation (perturbation or unfolding) parameter. The normal form equations describe how r and θ evolve over time, with coefficients v_k (focus values) encoding the effects of nonlinearities. The coefficient v_k is the k th-order focus value, and its magnitude and sign determine the number and stability of limit cycles that may emerge from the bifurcation point.

The sign and magnitude of the first non-zero coefficient, v_1 , determine whether the limit cycle is stable (supercritical) or unstable (subcritical). If $v_1 \neq 0$, the bifurcation is a standard Hopf bifurcation (supercritical or subcritical). If $v_1 = 0$ but $v_2 \neq 0$, the system undergoes a generalized Hopf bifurcation (also called Bautin bifurcation), which can lead to multiple small-amplitude limit cycles. The order of the first non-zero v_k determines the codimension of the bifurcation and the maximum number of limit cycles that may arise locally.

Focus Values and Limit Cycle Multiplicity

The sign and order of the focus values v_k are critical in determining the number, amplitude, and stability of the bifurcating limit cycles. If the first k focus values vanish ($v_0 = v_1 = \dots = v_{k-1} = 0$) but $v_k \neq 0$, and if the Jacobian matrix formed by the partial derivatives of these coefficients with respect to the bifurcation parameters has full rank, i.e.,

$$\text{rank} \left(\frac{\partial(\mu_1, \mu_2, \dots, \mu_k)}{\partial(v_0, v_1, \dots, v_{k-1})} \Big|_{\mu=\mu_c} \right) = k \quad (1.6)$$

then the system admits exactly k small-amplitude limit cycles near the critical point. These bifurcations are referred to as generalized Hopf (or Bautin) bifurcations when higher-order focus values are involved. Such configurations are important because they represent codimension - k bifurcations, requiring k parameters to unfold all possible dynamical scenarios near the bifurcation point.

Perturbation Methods and Symbolic Computation

The computation of normal forms and focus values can be analytically intensive, particularly for higher-dimensional or nonlinear systems. One practical approach to handle such complexity is the method of multiple time scales, which systematically separates the fast and slow dynamics in the system and leads to averaged equations describing the evolution of the amplitude. Combined with small-parameter perturbation expansions, this technique is particularly useful for tracking amplitude equations and identifying the conditions for the appearance of limit cycles. Symbolic computational tools, such as Maple and Mathematica, are commonly used to automate the derivation of normal forms and focus values. These tools allow for the recursive calculation of transformation coefficients, normal form terms, and Lyapunov coefficients to arbitrary order, making it feasible to analyze systems where manual computation would be prohibitive.

Geometric Interpretation and Dynamics

From a geometric viewpoint, the dynamics of the amplitude equation $\frac{dr}{dt}$ determine whether oscillations grow, decay, or stabilize. The sign of the leading nonzero focus value determines the direction of bifurcation:

- If $v_1 < 0$, the bifurcation is supercritical, producing stable limit cycles.
- If $v_1 > 0$, it is subcritical, and the resulting cycles are unstable.

Higher-order focus values provide richer bifurcation structures. For instance, if the first focus value vanishes and the second is nonzero, multiple limit cycles may appear, and their stability alternates with each crossing of a critical curve in parameter space.

1.5 Thesis Outline

In this thesis, our research study focuses on understanding tumour–immune interactions and evaluating therapeutic strategies using mathematical modeling. It examines the dynamics of tumour cells, immune components like CD4⁺ T cells and cytokines, and therapeutic interventions, including immunotherapy and oncolytic virotherapy. Non-linear differential equations and bifurcation analyses are employed to capture complex behaviors, oscillations, and treatment effects. The overall goal is to provide theoretical insights that can provide effective cancer therapy strategies. This foundational understanding naturally leads to Chapter 2, where the untreated tumour–immune model is formulated and analyzed.

Chapter 2 presents a mathematical model of tumour cells, CD4⁺ T cells, and cytokines using differential equations with logistic growth and Michaelis–Menten kinetics. Hopf bifurcation analysis captures oscillatory behaviors, complemented by numerical simulations that illustrate system dynamics. The chapter discusses equilibrium solutions, stability, and bifurcation phenomena. It establishes a baseline understanding of tumour–immune interactions without treatment. Based on the untreated system, Chapter 3 extends this framework

to include immunotherapy interventions, allowing an exploration of treatment effects on tumour–immune dynamics.

Chapter 3 extends the previous model by incorporating immunotherapy, with a focus on cytokine-mediated tumour control and CD4⁺ T cells as key effectors. Helper T cells play a pivotal role in initiating immune responses by producing cytokines that activate cytotoxic T cells and white blood cells. Mathematical models, including the Kirschner–Panetta framework, provide insight into how tumour antigenicity and immuno-modulatory treatments influence tumour–immune dynamics. The model presented in this chapter shows that high-dose cytokine therapy can eliminate tumours, and that CD4⁺ T cells are more effective than low-dose cytokine therapy alone. Bifurcation analysis is performed under different therapeutic scenarios—including cytokine therapy, CD4⁺ T cell therapy, and combination treatments—to explore system dynamics. Following the analysis of both untreated and immunotherapy treated models, Chapter 4 investigates oncolytic virotherapy, which introduces an additional and highly significant layer of complexity through virus–tumour interactions.

Chapter 4 focuses on oncolytic virotherapy, a promising cancer treatment strategy that employs genetically engineered viruses to selectively infect and destroy tumour cells. A nonlinear dynamical model is developed to capture interactions among tumour cells, oncolytic viruses, and the immune response. The analysis includes equilibrium classification, stability evaluation, and bifurcation studies, revealing complex phenomena such as oscillatory behavior and tumour–virus coexistence. Mathematical techniques, such as center manifold theory, support the analysis, while simulations provide biological insight. Oncolytic viruses act through both direct tumour lysis and immune activation and both incorporated into the model to study tumour–virus–immune dynamics comprehensively.

Chapter 5 collectively represents our research studies which underscore the utility of mathematical models to predict tumour behavior, evaluate therapeutic strategies, and provide theoretical insights into cancer treatment. The findings emphasize that targeted inter-

ventions, whether through cytokines, immune cells, or oncolytic viruses, can significantly alter tumour dynamics, providing guidance for optimizing treatment protocols. By integrating fundamental biology with nonlinear dynamical modeling, this thesis contributes to a unified perspective on tumour–immune interactions and supports the design of more effective cancer therapies.

1.6 Contribution of the thesis

This thesis develops and analyzes mathematical models of tumour growth under various treatment scenarios, including immunotherapy and oncolytic virotherapy. It identifies key parameters and critical values at which the system’s behavior suddenly changes through bifurcation and stability analysis, revealing how small variations can drastically alter tumour dynamics.

Chapters 2 and 3 consider the tumour–immune model presented by Anderson, Jang & Yu [52] to analyze tumour dynamics without treatment and under immunotherapy, revealing oscillatory behaviors and the impact of CD4⁺ T cell and cytokine interventions. Chapter 4 incorporates a basic ordinary differential equation model expressed by Wodarz [53] and analyzes a nonlinear tumour–virus–immune model to capture the complex dynamics of oncolytic virotherapy, revealing critical insights into tumour control and oscillatory behavior.

By evaluating different therapeutic strategies, it offers theoretical guidance for optimizing cancer treatment timing and combination approaches. Methodologically, the thesis applies advanced nonlinear dynamics tools, such as focus value and limit cycle analysis, to biologically realistic tumour models. Overall, this research advances both the theoretical understanding and practical implications of tumour control mechanisms.

References

- [1] Matthews, H.K., Bertoli, C., de Bruin, R.A.M. Cell cycle control in cancer, *Nature Reviews Molecular Cell Biology*, **23**(1) (2022) 74–88. doi:10.1038/s41580-021-00404-3
- [2] Hanahan, D. Hallmarks of Cancer: New Dimensions, *Cancer Discovery*, **12**(1) (2022) 31–46. doi:10.1158/2159-8290.CD-21-1059
- [3] Ferlay, J., Colombet, M., Soerjomataram, I., Parkin, D.M., Piñeros, M., Znaor, A., Bray, F. Cancer statistics for the year 2020: An overview, *International Journal of Cancer*, **149**(4) (2021) 778–789. doi:10.1002/ijc.33588
- [4] Chhikara, B.S., Parang, K. Global Cancer Statistics 2022: the trends projection analysis, *Journal of Medical Virology*, **94**(10) (2022) 4656–4667. doi:10.1002/jmv.28091
- [5] Desai, A., Scheckel, C., Jensen, C.J., Orme, J., Williams, C., Shah, N., Leventakos, K., Adjei, A.A. Trends in prices of drugs used to treat metastatic non-small cell lung cancer in the US from 2015 to 2020, *JAMA Network Open*, **5**(1) (2022) e2144923–e2144923. doi:10.1001/jamanetworkopen.2021.44923
- [6] Wen, J., Wang, S., Guo, R., Liu, D. CSF1R inhibitors are emerging immunotherapeutic drugs for cancer treatment, *European Journal of Medicinal Chemistry*, **245** (2023) 114884. doi:10.1016/j.ejmech.2022.114884
- [7] Xu, M., Peng, R., Min, Q., et al. Bisindole natural products: A vital source for the development of new anticancer drugs, *European Journal of Medicinal Chemistry*, **2022**, 114748. doi:10.1016/j.ejmech.2022.114748
- [8] Zigrossi, A., Hong, L.K., Ekyalongo, R.C., Cruz-Alvarez, C., Gornick, E., Diamond, A.M., Kastrati, I. SELENOF is a new tumour suppressor in breast cancer, *Oncogene*, **41**(9) (2022) 1263–1268. Publisher: Nature Publishing Group UK London.

- [9] Saller, J.J., Boyle, T.A. Molecular pathology of lung cancer, *Cold Spring Harbor Perspectives in Medicine*, **12**(3) (2022) a037812. Cold Spring Harbor Laboratory Press.
- [10] Cheung, E.C., Vousden, K.H. The role of ROS in tumour development and progression, *Nat. Rev. Cancer*, **22**(5) (2022) 280–297. doi:10.1038/s41568-022-00460-x
- [11] Kumari, S., Sharma, V., Tiwari, R., Maurya, J.P., Subudhi, B.B., Senapati, D. Therapeutic potential of p53 reactivation in prostate cancer: Strategies and opportunities, *European Journal of Pharmacology*, **919** (2022) 174807. doi:10.1016/j.ejphar.2022.174807
- [12] Feola, S., Chiaro, J., Martins, B., et al. A novel immunopeptidomic-based pipeline for the generation of personalized oncolytic cancer vaccines, *eLife*, **11** (2022) e71156. doi:10.7554/eLife.71156
- [13] Eala, M.A.B., Robredo, J.P.G., Dee, E.C., Lin, V., Lagmay, A.M.F.A. Climate crisis and cancer: perspectives from the hardest hit, *Lancet Oncology*, **23**(3) (2022) e92.
- [14] Ferlay, J., Ervik, M., Lam, F., Laversanne, M., Colombet, M., Mery, L., Piñeros, M., Znaor, A., Soerjomataram, I., Bray, F. Global Cancer Observatory: Cancer Today, *International Agency for Research on Cancer*, Lyon, France (2024). Available at: <https://gco.iarc.who.int/today>, accessed [DD Month YYYY].
- [15] International Agency for Research on Cancer Global Cancer Observatory, *GCO*, (2020). Available at: <https://gco.iarc.fr>
- [16] Sung, H., Ferlay, J., Siegel, R.L., Laversanne, M., Soerjomataram, I., Jemal, A., Bray, F. Global cancer statistics 2020: GLOBOCAN estimates of incidence and mortality worldwide for 36 cancers in 185 countries, *CA: A Cancer Journal for Clinicians*, **71**(3) (2021) 209–249. doi:10.3322/caac.21660

- [17] Ferlay, J., Colombet, M., Soerjomataram, I., Parkin, D.M., Piñeros, M., Znaor, A., Bray, F. Cancer statistics for the year 2020: An overview, *International Journal of Cancer*, **149**(4) (2021) 778–789. doi:10.1002/ijc.33588
- [18] Sabarwal, A., Kumar, K., Singh, R.P. Hazardous effects of chemical pesticides on human health–Cancer and other associated disorders, *Environmental Toxicology and Pharmacology*, **63** (2018) 103–114.
- [19] Dunn, G.P., Old, L.J., Schreiber, R.D. The immunobiology of cancer immunoediting and immunotherapy, *Immunity*, **21**(2) (2004) 137–148. doi:10.1016/j.immuni.2004.07.017
- [20] Abbas, A.K., Lichtman, A.H., Pillai, S. Cellular and Molecular Immunology, *Elsevier Health Sciences*, **9th ed** (2017).
- [21] Mellman, I., Coukos, G., Dranoff, G. Cancer immunotherapy comes of age, *Nature*, **480**(7378) (2011) 480–489. doi:10.1038/nature10673
- [22] Ribas, A., Wolchok, J.D. Cancer immunotherapy using checkpoint blockade, *Science*, **359**(6382) (2018) 1350–1355. doi:10.1126/science.aar4060
- [23] Chiocca, E.A., Rabkin, S.D. Oncolytic viruses and their application to cancer immunotherapy, *Cancer Immunol Res*, **2**(4) (2014) 295–300. doi:10.1158/2326-6066.CIR-14-0037
- [24] de Pillis, L.G., Radunskaya, A.E. A mathematical model of immune response to tumour invasion, *Math Comput Model*, **37**(11) (2003) 1221–1244. doi:10.1016/S0895-7177(03)00121-2
- [25] d’Onofrio, A. tumour-immune system interaction: modeling and bifurcation analysis, *Math Comput Model*, **37**(11) (2003) 1155–1162. doi:10.1016/S0895-7177(03)00117-0

- [26] Kuznetsov, V.A., Knott, G.D. Modeling tumour regrowth and immunotherapy, *Math Biosci*, **163**(2) (2000) 115–133. doi:10.1016/S0025-5564(99)00062-5
- [27] Murphy, K., Weaver, C. Janeway’s Immunobiology, *Garland Science*, **9th ed** (2016).
- [28] Coico, R., Sunshine, G. Immunology: A Short Course, *Wiley-Blackwell*, **7th ed** (2015).
- [29] Abbas, A.K., Lichtman, A.H., Pillai, S. Basic Immunology: Functions and Disorders of the Immune System, *Elsevier*, **6th ed** (2020).
- [30] Zhu, J., Paul, W.E. CD4 T cells: fates, functions, and faults, *Blood*, **112**(5) (2008) 1557–1569. doi:10.1182/blood-2008-05-078154
- [31] Zhu, J., Yamane, H., Paul, W.E. Differentiation of effector CD4 T cell populations, *Annu Rev Immunol*, **28** (2010) 445–489. doi:10.1146/annurev-immunol-030409-101212
- [32] Schreiber, R.D., Old, L.J., Smyth, M.J. Cancer immunoediting: integrating immunity’s roles in cancer suppression and promotion, *Science*, **331**(6024) (2011) 1565–1570. doi:10.1126/science.1203486
- [33] Gajewski, T.F., Schreiber, H., Fu, Y.X. Innate and adaptive immune cells in the tumour microenvironment, *Nat Immunol*, **14**(10) (2013) 1014–1022. doi:10.1038/ni.2703
- [34] Spranger, S., Bao, R., Gajewski, T.F. Melanoma-intrinsic β -catenin signaling prevents anti-tumour immunity, *Nature*, **523**(7559) (2015) 231–235. doi:10.1038/nature14404
- [35] Sharma, P., Allison, J.P. The future of immune checkpoint therapy, *Science*, **348**(6230) (2015) 56–61. doi:10.1126/science.aaa8172
- [36] Russell, S.J., Peng, K.W., Bell, J.C. Oncolytic virotherapy, *Nat Biotechnol*, **30**(7) (2012) 658–670. doi:10.1038/nbt.2287

- [37] Engeland, C.E., Ungerechts, G. Oncolytic viruses: a new class of immunotherapy drugs, *Nature Rev Drug Discov*, **19**(10) (2020) 697–710. doi:10.1038/s41573-020-0073-9
- [38] Murray, J.D. *Mathematical Biology I: An Introduction*, Springer, **3rd ed** (2002).
- [39] Kirschner, D., Panetta, J.C. Modeling immunotherapy of the tumour–immune interaction, *J Math Biol*, **37**(3) (1998) 235–252. doi:10.1007/s002850050134
- [40] Arciero, J.C., Jackson, T.L., Kirschner, D.E. A mathematical model of tumour-immune evasion and siRNA treatment, *Discrete Contin Dyn Syst Ser B*, **4**(1) (2004) 39–58. doi:10.3934/dcdsb.2004.4.39
- [41] Wodarz, D., Komarova, N.L. *Dynamics of Cancer: Mathematical Foundations of Oncology*, World Scientific, (2014).
- [42] Eladdadi, A., Isaacson, D. A mathematical model for the effects of HER2 signaling pathway on cell cycle progression in breast cancer cells, *Bull Math Biol*, **70**(6) (2008) 1707–1729. doi:10.1007/s11538-008-9323-5
- [43] Kareva, I., Berezovskaya, F., Castillo-Chavez, C., Karev, G. Hierarchical population dynamics of cancer: implications for treatment and control, *J Theor Biol*, **263**(3) (2010) 370–378. doi:10.1016/j.jtbi.2009.11.019
- [44] Eftimie, R., Bramson, J.L., Earn, D.J. Interactions between the immune system and cancer: a brief review of non-spatial mathematical models, *Bull Math Biol*, **73**(1) (2011) 2–32. doi:10.1007/s11538-010-9526-3
- [45] Choi, Y., et al. Mathematical modeling of CD4+ T cell responses in cancer immunotherapy, *J Theor Biol*, **422** (2017) 232–244. doi:10.1016/j.jtbi.2017.05.010
- [46] Ghosh, S., Banerjee, S., Sarkar, R.R. A mathematical study of cytokine therapy for immuno-oncology, *Math Biosci*, **317** (2019) 108266. doi:10.1016/j.mbs.2019.108266

- [47] Banerjee, S., Bose, A., Pal, S. Bifurcation analysis of a tumour-immune interaction model with time delay, *Chaos Solitons Fractals*, **126** (2019) 111–123. doi:10.1016/j.chaos.2019.05.027
- [48] Kuznetsov, Y.A. Elements of Applied Bifurcation Theory, *Springer*, **3rd ed** (2004).
- [49] Perko, L. Differential Equations and Dynamical Systems, *Springer*, **3rd ed** (2001).
- [50] Chow, S.N., Li, C., Wang, D. Normal forms and bifurcation of planar vector fields, *Cambridge University Press*, (1994).
- [51] P. Yu, Computation of normal forms via a perturbation technique, *J. Sound Vib.*, **211** (1998), 19-38. doi: 10.1006/jsvi.1997.1347.
- [52] L. Anderson, S. Jang, J. L. Yu, Qualitative behaviour of system of tumour-CD4⁺-cytokine interactions with treatments, *Math. Meth. Appl. Sci.*, **38** (2015), 4330-4344. doi: 10.1002/mma.3370.
- [53] D. Wodarz, Computational modeling approaches to studying the dynamics of oncolytic viruses, *Mathematical Biosciences & Engineering*, **10**(3), 939–957, 2013.

Chapter 2

2 Bifurcation Analysis on Immunotherapy of a Tumor

Model Without Treatment

2.1 Introduction

According to the World Health Organization, cancer continues to be the second foremost cause of death globally, but how it develops and spreads is still not well understood. The most prevalent malignancies include prostate, breast, lung, colon, and rectum cancers. Approximately three percent of the deaths related to cancer are use of cigarettes, having a high body mass index, limited amounts of vegetables and fruits, drinking alcohol, and not physical activity. Numerous tumors can be treated if they are diagnosed early and treated appropriately [1]. Even after successful cancer treatment, recurrence might still happen later. We must focus on both more effective treatment options and prevention measures.

A few treatments have been existing for a long time and are frequently utilized. They provide quick results by eliminating cancer cells, but there are significant downsides. In most situations, there is no selectivity for tumor cells, therefore they destroy healthy cells nearby. Further, the negative impacts are severe and might continue for a long time [2]. Different techniques are needed for treating different types of cancers. However, this is not the only situation, since the diversity of a particular disease makes it impossible to follow a similar form of therapy even for individuals experiencing the same kind of cancer [3].

Immunotherapy is a rapidly increasing and expanding branch of cancer treatment. It focuses on improving patients' immune system against cancer. Current immunotherapies include cytokines, inhibitors of checkpoints, targeted antigens, immunizations, adoptive cell transfer, and oncolytic bacteria, etc. To increase the effectiveness of the therapy, they can be employed either alone or in conjunction with radiotherapies, chemotherapies, surgery, or

targeted treatments. Immunotherapy involves using cytokines in combination with adoptive cellular immunotherapy (ACI) [3, 4]. A protein hormone known as cytokines plays an equally crucial role in native and adaptive immunity. Activated T cells primarily form cytokines during cell-mediated immune responses [5].

To distinguish the complex relations amongst the various aspects of the tumor microhabitat, mathematical modeling is a predominant tool. In this thesis, we introduce a mathematical model describing the behaviors of the tumor cells, the CD4⁺ T cells, and the cytokine interactions, in the form of ordinary differential equations (ODEs) [6], and focus on the study of the case with no treatment. We use a logistic growth function for the tumor cells, and Michaelis-Menten kinetics with various half-saturation values for all functional forms. Hopf bifurcation analysis is given to show the oscillating behaviors in the model. Numerical simulations are represented to illustrate the theoretical predictions.

remainder of the thesis is organized as follows. In the next section, we will study the basic solution features of the proposed system. Then, we investigate the stability and bifurcations from equilibrium solutions in Sect. 2.4, with the center manifold reduction discussed. Analysis on the codimension of Hopf bifurcation is given in Sect. 2.4.2 to show the existence of maximal number of bifurcating limit cycles. Numerical simulations are presented in Sect. 2.5, and finally conclusions are drawn in Sect. 2.6.

2.2 Modeling and Reduction

In this section, we introduce a mathematical model describing the dynamical behaviours of the tumor cells, the CD4⁺ T cells, and the cytokine interactions, and focus on the study for the case with no treatment. Let the mass concentration of the tumor cells, CD4⁺ T cells and cytokine be denoted by x, y and z , respectively. Then, the proposed model is described by the following ordinary differential equations (ODEs) [6]:

$$\begin{aligned}
\frac{dx}{dt} &= xf(x) - d(x, z), \\
\frac{dy}{dt} &= g_y(x, y) - a_y(y) + I_1(t), \\
\frac{dz}{dt} &= g_z(x, y, z) - a_z(z) + I_2(t),
\end{aligned} \tag{2.1}$$

where the function $f(x)$ represents the tumor cells per capita growth rate, $d(x, z)$ denotes the tumor cells loss caused by cytokines, $g_y(x, y)$ is the CD4⁺ T cells proliferation through contacts with the tumor cells. Here, the function $g_z(x, y, z)$ represents cytokine secretion by CD4⁺ T cells activated by tumor cells. It does not depend on z , since cytokines do not self-proliferate; the cytokine loss are denoted by the functions $a_y(y)$ and $a_z(z)$, respectively, while immunotherapy treatments are represented by $I_1(t)$ and $I_2(t)$, which may be time-dependent.

In this research work, a logistic growth function is utilized for the tumor cells, and Michaelis-Menten kinetics with various half-saturation values is used for all functional forms. As a result, it is anticipated that the tumor's development is reduced as well as the tumor cells' ability to produce the CD4⁺ T cells and an anticancer cytokine. With these assumptions, the model (2.1) can be rewritten as

$$\begin{aligned}
\frac{dx}{dt} &= rx\left(1 - \frac{x}{K}\right) - \frac{\delta xz}{m + x}, \\
\frac{dy}{dt} &= \frac{\beta xy}{k + x} - ay + I_1, \\
\frac{dz}{dt} &= \frac{\alpha xy}{b + x} - \mu z + I_2,
\end{aligned} \tag{2.2}$$

where all the parameters r , K , m , a , b , k , μ , β , δ and α are positive constants, and $I_1(t) \geq 0$ and $I_2(t) \geq 0$ denote the regular remedies of the CD4⁺ T cells and the cytokine in keeping with a unit time, respectively. The parameters and their organic interpretations are summarized in Table 2.1.

Table 2.1: Parameters used in system (2.2) [6].

Parameter	Biological meaning	Unit
m	half saturation constant of the tumor-killing rate	cm^3
β	Maximum CD4^+ T cells production rate	day^{-1}
k	half saturation constant of the CD4^+ T cells production rate	cm^3
a	death rate of the CD4^+ T cells	day^{-1}
b	half saturation constant of the cytokine production rate	cm^3
μ	cytokine loss rate	day^{-1}
r	growth rate of the tumor	day^{-1}
K	carrying capacity of the tumor	cm^3
δ	maximum tumor killing rate by cytokine	day^{-1}
α	maximum production rate of cytokine	day^{-1}
I_1	treatment by CD4^+ T cells	$\text{cm}^3 \text{day}^{-1}$
I_2	treatment by Cytokine	$\text{cm}^3 \text{day}^{-1}$

All variables are expressed per unit cell volume (cm^3); hence tumour cells, immune cells, and cytokines are represented as mass concentrations (e.g. IU/cm^3). Cytokine data reported experimentally in IU/mL are converted into equivalent volumetric units before nondimensionalization to maintain dimensional consistency across the model. In order to simplify the analysis in the following sections, we introduce the scaling:

$$x = KX, \quad y = \frac{Kr^2}{\alpha\delta} Y, \quad z = \frac{Kr}{\delta} Z, \quad t = \frac{1}{r} \tau$$

into system (2.2) to obtain the dimensionless model:

$$\begin{aligned} \frac{dX}{d\tau} &= X\left(1 - X - \frac{Z}{A + X}\right), \\ \frac{dY}{d\tau} &= Y\left(\frac{BX}{C + X} - D\right) + I_1, \\ \frac{dZ}{d\tau} &= \frac{XY}{E + X} - FZ + I_2, \end{aligned} \tag{2.3}$$

where the six new positive parameters are defined as

$$\begin{aligned}
A &= \frac{m}{K}, & B &= \frac{\beta}{r}, & C &= \frac{k}{K}, & D &= \frac{a}{r}, \\
E &= \frac{b}{K}, & F &= \frac{\mu}{r}, & I_1 &= \frac{G_1 r^3 K^2}{\alpha \delta^2}, & I_2 &= G_2 r.
\end{aligned}
\tag{2.4}$$

In this research work, we shall explore the dynamical behaviors of the model (2.3) in the full 6-dimensional parameters space, particularly for the case without treatment, i.e., $I_1 = I_2 = 0$. Thus, system (2.3) is reduced to

$$\begin{aligned}
\frac{dX}{d\tau} &= X\left(1 - X - \frac{Z}{A + X}\right), \\
\frac{dY}{d\tau} &= Y\left(\frac{BX}{C + X} - D\right), \\
\frac{dZ}{d\tau} &= \frac{XY}{E + X} - FZ,
\end{aligned}
\tag{2.5}$$

with the non-negative initial conditions:

$$X(0) = X_0 \geq 0, \quad Y(0) = Y_0 \geq 0, \quad Z(0) = Z_0 \geq 0. \tag{2.6}$$

We shall give an analysis on the generic dynamics of the system (2.5) in terms of the 6-dimensional (A, B, C, D, E, F) parameters space. We pay particular attention on the analysis of Hopf and generalized Hopf bifurcation. We apply Hopf bifurcation theory to prove the existence of multiple limit cycles, giving rise to different types of bistable states. The new parameters and their biological meaning are given in Table 2.2.

The dimensionless model (2.5) will be studied in the next several sections. We shall consider the property of solutions, the equilibria and their stability, and pay particular attention to the dynamics of the tumor cells, the CD4⁺ T cells, and the cytokine interactions.

Table 2.2: Parameters used in system (2.5) [6].

Parameter	Biological meaning	value
A	half saturation constant of the tumor-killing rate	0.1
B	Maximum CD4 ⁺ T cells production rate	6
C	half saturation constant of the CD4 ⁺ T cells production rate	1
D	death rate of the CD4 ⁺ T cells	3
E	half saturation constant of the cytokine production rate	0.1
F	cytokine loss rate	5000

2.3 Property of Solutions of System (2.5)

First, we consider the property of solutions of the system (2.5) and have the following result.

Theorem 2.3.1 *The solution of system (2.5) is positive if the given initial condition is positive, and it is bounded.*

Proof We begin by considering the well-posedness of the solutions of system (2.5). The existence and uniqueness of the solution of (2.5), subject to initial conditions (2.6), follow from the elementary theory of ODEs. We consider the solution of this initial value problem, $(X(\tau), Y(\tau), Z(\tau)) \in \mathbb{R}_+^3$. Since the variables represent densities and concentrations of physical quantities, the system must remain non-negative for all $\tau > 0$. We first consider the tumor equation. Using the variation principal, we obtain from the first equation in (2.5) that

$$X(\tau) = X(0) e^{\int_0^\tau [1 - X(s) - \frac{Z(s)}{A + X(s)}] ds},$$

which clearly indicates that $X(\tau) \geq 0$, for $\tau > 0$ if $X(0) \geq 0$. Similarly, it follows from the second equation in (2.5) that

$$Y(\tau) = Y(0) e^{\int_0^\tau [\frac{BX(s)}{C + X(s)} - D] ds},$$

implying that $Y(\tau) \geq 0$ for $\tau > 0$ if $Y(0) \geq 0$. Finally, the third equation in (2.5) gives

$$Z(\tau) = e^{-F\tau} \left[Z(0) + \int_0^\tau \left(\frac{X(s)Y(s)}{E + X(s)} \right) e^{Fs} ds \right].$$

This shows that $Z(\tau) > 0$ for $\tau > 0$ if $Z(0) \geq 0$, by noticing that $X(\tau) > 0$ and $Y(\tau) > 0$ for $\tau > 0$.

Next, we prove that the solution of system (2.5) is bounded. First of all, it is easy to see from the first equation in (2.5) that the following inequality holds:

$$\frac{dX}{d\tau} = X \left(1 - X - \frac{Z}{A + X} \right) \leq X(1 - X).$$

It is obvious that the solution of the DE: $\frac{dX}{d\tau} = X(1 - X)$ is bounded, and actually it converges to the equilibrium $X = 1$. Then, by the comparison principle we know that X is bounded. Next, consider the variable Z . Suppose it is unbounded, i.e., $Z(\tau) \rightarrow +\infty$ as $\tau \rightarrow \infty$. Then, it follows from the first equation in (2.5) that $X(\tau) \rightarrow 0$ as $\tau \rightarrow \infty$, and thus the second equation in (2.5) yields $Y(\tau) \rightarrow 0$ as $\tau \rightarrow \infty$. Hence, the limit equation of the third equation in (2.5) becomes $\frac{dZ}{d\tau} = -FZ$, implying that $Z(\tau) \rightarrow 0$ as $\tau \rightarrow \infty$, leading to a contradiction. Therefore, Z is bounded. Finally, suppose Y is unbounded, i.e., $Y(\tau) \rightarrow +\infty$ as $\tau \rightarrow \infty$. Then, again it follows from the third equation in (2.5) that $\frac{X(\tau)Y(\tau)}{E + X(\tau)} - FZ(\tau) \rightarrow +\infty$ as $\tau \rightarrow \infty$ since X and Z are bounded, yielding that $\frac{dZ(\tau)}{d\tau} \rightarrow +\infty$ as $\tau \rightarrow \infty$, giving $Z(\tau) \rightarrow +\infty$ as $\tau \rightarrow \infty$, a contradiction. Thus, Y is also bounded.

2.4 Equilibrium Solutions and Their Stability

Simply letting $\frac{dX}{d\tau} = \frac{dY}{d\tau} = \frac{dZ}{d\tau} = 0$ yields three equilibrium solutions:

Two boundary equilibria: $E_0 = (0, 0, 0)$, $E_1 = (1, 0, 0)$;

One positive (interior) equilibrium:

$$E_2 = (X_2, Y_2, Z_2) = \left(\frac{CD}{B-D}, \frac{F(E+X_2)Z_2}{X_2}, (1-X_2)(A+X_2) \right).$$

Define

$$B_t = (C+1)D. \quad (2.7)$$

Then, we have the following theorem for the existence and stability of the equilibria.

Theorem 2.4.1 *For the system (2.5), the two boundary equilibria E_0 and E_1 exist for all parameter values, while the positive equilibrium E_2 exists for $B > B_t$. E_0 is always a saddle-focus; E_1 is locally asymptotically stable (LAS) for $B < B_t$ and unstable for $B > B_t$; while E_2 is LAS for $B_t < B < B_H$ and unstable for $B > B_H$. A transcritical bifurcation happens between E_1 and E_2 at $B = B_t$, and a Hopf bifurcation occurs from E_2 at the critical point $B = B_H$, where B_H is defined in the proof.*

Proof Since the two boundary equilibrium solutions are not related to any parameters, they exist for all parameter values. The positive equilibrium E_2 requires $Z_2 > 0$, that is, $X_2 = \frac{CD}{B-D} < 1$, yielding $B > B_t$.

The stability of the three equilibrium solutions can be easily determined from the Jacobian matrix of (2.5), evaluated at the equilibria. The Jacobian matrix of (2.5) is given by

$$J(X, Y, Z) = \begin{bmatrix} 1 - 2X - \frac{AZ}{(A+X)^2} & 0 & -\frac{X}{A+X} \\ \frac{BCY}{(C+X)^2} & \frac{BX}{C+X} - D & 0 \\ \frac{EY}{(E+X)^2} & \frac{X}{E+X} & -F \end{bmatrix}. \quad (2.8)$$

Evaluating J at the boundary equilibria E_0 and E_1 , we have

$$J(E_0) = \begin{bmatrix} 1 & 0 & 0 \\ 0 & -D & 0 \\ 0 & 0 & -F \end{bmatrix} \quad \text{and} \quad J(E_1) = \begin{bmatrix} -1 & 0 & -\frac{1}{A+1} \\ 0 & \frac{B}{C+1} - D & 0 \\ 0 & \frac{1}{E+1} & -F \end{bmatrix}.$$

It is easy to see from $J(E_0)$ that the population-free equilibrium E_0 is a saddle-focus with a stable manifold lying on the non-negative Y - Z plane. This indicates that the tumor may not be eliminated without any treatment even if it is very small. The equilibrium E_1 is LAS for $B < B_t$, and unstable for $B > B_t$. A transcritical bifurcation occurs between E_1 and E_2 at the critical point $B = B_t$ (which will be shown next), but E_2 only exists for $B > B_t$.

Next, consider the stability of E_2 . Note that the tumor size in E_2 is always smaller than the normalized carrying capacity 1 (the non-normalized carrying capacity is K). Evaluating the Jacobian matrix of system (2.5) at the positive equilibrium E_2 , we obtain

$$J(E_2) = \begin{bmatrix} \frac{D[(A-2C-1)D-B(A-1)]C}{[(A-C)D-AB](B-D)} & 0 & \frac{CD}{(A-C)D-AB} \\ \frac{[(A-C)D-AB][(C+1)D-B][(C-E)D+EB]F}{C^2BD} & 0 & 0 \\ \frac{E[(A-C)D-AB][(C+1)D-B]F}{D[(C-E)D+BE]C} & \frac{CD}{(C-E)D+BE} & -F \end{bmatrix}. \quad (2.9)$$

A direct computation yields the characteristic polynomial for E_2 :

$$P_{E_2}(\lambda) = \lambda^3 + a_1\lambda^2 + a_2\lambda + a_3, \quad (2.10)$$

where

$$\begin{aligned}
a_1 &= F + 1 - \frac{(B - B_t)[(A + 2)CD + (B - B_t)A]}{[CD + B - B_t][(A + 1)CD + (B - B_t)A]} \\
a_2 &= F - \frac{(B - B_t)CDF[(A + E + 2)CD + (B - B_t)(A + E)]}{(CD + B - B_t)[(A + 1)CD + (B - B_t)A][(E + 1)CD + (B - B_t)E]}, \quad (2.11) \\
a_3 &= \frac{DF(B - B_t)}{(1 + C)D + B - B_t}
\end{aligned}$$

It is easy to see that $a_3 > 0$ due to the existence condition $B > B_t$ for E_2 . At the critical point $B = B_t$, $a_1 = F + 1 > 0$, $a_2 = F > 0$ and $a_3 = 0$, at which $E_2 = E_1$, implying that a transcritical bifurcation occurs between E_1 and E_2 .

To simplify the analysis on the stability of E_2 , we let

$$B = B_t + h, \quad (h \geq 0). \quad (2.12)$$

Then, the transcritical bifurcation point $B = B_t$ becomes $h = 0$. We want to consider the bifurcation from E_2 as h is increasing. Thus, substituting (2.12) into (2.11) yields

$$a_1(h) = F + 1 - h Q_1(h), \quad a_2(h) = F - h Q_2(h), \quad a_3(h) = h Q_3(h),$$

in which Q_1 , Q_2 and Q_3 are given by

$$\begin{aligned}
Q_1(h) &= \frac{[(A + 2)CD + hA]}{(CD + h)[(A + 1)CD + hA]}, \\
Q_2(h) &= \frac{CDF[(A + E + 2)CD + h(A + E)]}{(CD + h)[(A + 1)CD + hA][(E + 1)CD + hE]}, \\
Q_3(h) &= \frac{DF}{(1 + C)D + h},
\end{aligned}$$

which clearly indicates that $Q_k(h) > 0$, $k = 1, 2, 3$ for $h > 0$. By the Routh-Hurwitz criteria, it is known that E_2 is LAS for $a_1(h) > 0$, $a_3(h) > 0$ and $\Delta_2(h) = a_1(h)a_2(h) - a_3(h) > 0$. At the critical point $h = 0$, $a_1 > 0$, $a_2 > 0$, $a_3 = 0$, and so $\Delta_2 > 0$. When h is increasing

from $h = 0$, both a_1 and a_2 are decreasing from positive values, while a_3 is increasing from 0. Hence, $\Delta_2 = a_1 a_2 - a_3$ crosses zero before either a_1 or a_2 does, implying that the only bifurcation can happen from E_2 is Hopf bifurcation. Clearly, Bogdanov-Takes (B-T) bifurcation is not possible since it requires that $a_2 = a_3 = 0$. Further, to investigate if it is possible to have Hopf bifurcation from E_2 , we derive the detailed expression for Δ_2 as follows:

$$\Delta_2(h) = F(F + 1) - \frac{hFQ_4(h)}{(CD+h)^2[(A+1)CD+hA]^2[(C+1)D+h][(E+1)CD+hE]},$$

where where

$$\begin{aligned} Q_4(h) = & A^2E(D + 1)h^5 \\ & + AD[AC(5E+1)(D+1) + 2CE(D+1) + (A+C)E + (A+E)CF]h^4 \\ & + CD^2(10A^2CDE + 4A^2CD + 10A^2CE + 4A^2CF + 8ACDE \\ & + 4ACEF + 5A^2C + 4A^2E + A^2F + 2ACD + 13ACE + AEF \\ & + 3ACF + CDE + CEF + A^2 + 2AC + 3AE + CE)h^3 \\ & + C^2D^3(10A^2CDE + 6A^2CD + 10A^2CE + 6A^2CF + 12ACDE \\ & + 6ACEF + 9A^2C + 6A^2E + 3A^2F + 6ACD + 21ACE + 9ACF \\ & + 3AEF + 3CDE + 3CEF + 4A^2 + 10AC + 10AE + 3AF + CD \\ & + 5CE + 2CF + EF + 2A + E)h^2 \\ & + C^3D^4(5A^2CDE + 4A^2CD + 5A^2CE + 4A^2CF + 8ACDE + 4ACEF \\ & + 7A^2C + 4A^2E + 3A^2F + 6ACD + 15ACE + 9ACF + 3AEF + 3CDE \\ & + 3CEF + 5A^2 + 14AC + 11AE + 6AF + 2CD + 7CE + 4CF + 2EF \\ & + 8A + 4C + 4E + 2F)h \\ & + C^4D^5(A+1)(ACDE+ACD+ACE+ACF+CEF+CDE+2AC \\ & +AE+ AF + CD+ 3CE+ 2CF + EF + 2A+ 4C+ 3E+ 2F + 4). \end{aligned}$$

It can be seen that $Q_4(0) = F(F + 1) > 0$ and $\Delta_2 \rightarrow -\infty$ as $h \rightarrow \infty$ (since the coefficient of h^5 is positive), implying that $\Delta_2(h)$ has at least one positive root, and it may have multiple positive roots. The smallest root of $\Delta_2(h)$, denoted by h_H , defines a critical Hopf bifurcation point. In terms of the bifurcation parameter B , the Hopf critical point is given by $B_H = B_t + h_H$. Thus, the equilibrium E_2 is LAS for $B_t < B < B_H$ (or $0 < h < h_H$) and unstable for $B > B_H$. Hopf bifurcation occurs from E_2 at the critical point $B = B_H$.

This completes the proof for Theorem 2.4.1.

Define the basic reproduction number as

$$R_0 = \frac{B}{(C + 1)D}, \quad (2.13)$$

where R_0 represents the ratio between the immune cell growth rate and the combined effects of immune suppression and natural decay. It quantifies the ability of $CD4^+$ T cells to expand in response to tumour stimulation when the tumour is small.

The dynamics and bifurcations of system (2.5) can be simply described as follows: the equilibrium E_0 is always a saddle-focus; the equilibrium E_1 is LAS for $R_0 < 1$ and unstable for $R_0 > 1$; while the equilibrium E_2 exists for $R_0 > 1$ and is LAS for $1 < R_0 < \frac{B_H}{(C+1)D}$, and unstable for $R_0 > \frac{B}{(C+1)D}$. A transcritical bifurcation happens between E_1 and E_2 at the critical point $R_0 = 1$, and Hopf bifurcation occurs from E_2 at the critical point $R_0 = \frac{B_H}{(C+1)D}$. Note that E_0 is a population-free equilibrium, E_1 is a disease-free equilibrium, and E_2 is an endemic equilibrium.

Biologically, R_0 measures how effectively the immune response can “reproduce” or sustain itself relative to its loss rate. $R_0 > 1$ indicates that $CD4^+$ T cells can grow sufficiently to expand the immune response and control the tumour, while $R_0 < 1$ signals insufficient growth, leading to tumour persistence. Here, the “reproducing” quantity is the $CD4^+$ T-cell population, and R_0 sets the threshold for immune effectiveness.

The bifurcation diagram projected on the B - X plane for system (2.5) is shown in Fig-

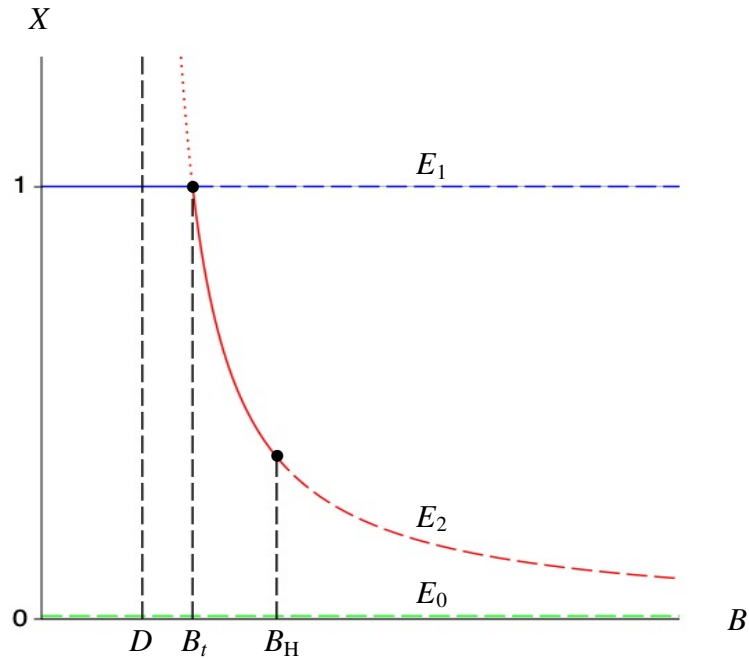


Figure 2.1: Bifurcation diagram for system (2.5) showing the equilibrium solutions E_0 , E_1 and E_2 , where solid and dotted lines/curves represent stable and unstable equilibrium solutions, respectively.

ure 2.1, in which three equilibria E_0 , E_1 and E_2 with stability are depicted. The transcritical bifurcation point B_t and the Hopf bifurcation point $B = B_H$ are specified.

To further explore the dynamics and bifurcation of system (2.5), we discuss two cases in the following: (1) $R_0 = 1$ for which we use center manifold theory to investigate the stability of equilibria; and (2) $R_0 > 1$ for which we consider Hopf bifurcation and pay particular attention to the codimension of the Hopf bifurcation.

2.4.1 Case $R_0 = 1$ (or $D = \frac{B}{C+1}$)

When $R_0 = 1$ or $D = \frac{B}{C+1}$, system (2.5) is in a critical situation, i.e., the equilibria E_1 and E_2 coincide at the critical point $B = B_t$ and complex dynamics of the system happens on the center manifold, while the equilibrium E_0 is still a saddle-focus.

For this critical case, in order to keep the parameter B in the analysis, we treat D as a bifurcation parameter and change the equation $B = (C + 1)D$ to $D = \frac{B}{C+1}$. Then, define

$D_t = \frac{B}{C+1}$ at which $R_0 = 1$. At the critical point, the equilibrium solutions become

$$E_0 = (0, 0, 0), \quad E_1 = E_2 = (1, 0, 0). \quad (2.14)$$

We have following theorem.

Theorem 2.4.2 *For the system (2.5) at the critical point $R_0 = 1$, the equilibria E_1 and E_2 coincide to become a degenerate stable node. There is no backward bifurcation for this critical case.*

Proof Since at $R_0 = 1$, the system (2.5) has a simple zero eigenvalue at $E_1 (= E_2)$, implying that it is a degenerate node. To study the stability of E_1 , We need to find the differential equation describing the dynamics on the center manifold, and then discuss the stability of E_1 . To achieve this, we first perform a reduction analysis on the center manifold by introducing an affine transformation, given by

$$\begin{pmatrix} X \\ Y \\ Z \end{pmatrix} = \begin{pmatrix} 1 \\ 0 \\ 0 \end{pmatrix} + \begin{bmatrix} \frac{-1}{(E+1)(A+1)} & 1 & \frac{1}{A+1} \\ F & 0 & 0 \\ \frac{1}{E+1} & 0 & F-1 \end{bmatrix} \begin{pmatrix} u \\ v \\ w \end{pmatrix}, \quad (2.15)$$

into (2.5) with $D = \frac{B}{1+C}$ to obtain the system,

$$\begin{aligned} \frac{du}{d\tau} &= -\frac{CBu\{u - (E+1)[(A+1)v + w]\}}{(C+1)^2(A+1)(E+1)}, \\ \frac{dv}{d\tau} &= -v - v^2 - \frac{(AF+1)w^2}{(A+1)^3} - \frac{(AF+A+2)vw}{(A+1)^2} - \frac{u(P_1u - P_2v - P_3w)}{(A+1)^3(E+1)^3(C+1)^3(F-1)}, \\ \frac{dw}{d\tau} &= -Fw + \frac{u[CB(E+1) - (C+1)^2EF]\{u - (E+1)[(A+1)v + w]\}}{(E+1)^3(A+1)(C+1)^2(F-1)}, \end{aligned} \quad (2.16)$$

where

$$P_1 = F(CB(A + 1)(E + 1) + (C + 1)^2(1 - AE)) - (E + 1)(C + 1)^2,$$

$$P_2 = (E + 1)(A + 1)\{F[CB(A + 1)(E + 1) + (C + 1)^2(A + E + 2)] \\ - (A + 2)(C + 1)^2(E + 1)\},$$

$$P_3 = (E + 1)\{(E + 1)(C + 1)^2(AF^2 - 2) \\ + [CB(A + 1)(E + 1) - (C + 1)^2(A(1 + 2E) - E - 2)]F\}.$$

Note that the linear part of system (2.16) is in Jordan canonical form, having eigenvalues 0, -1 and $-F$.

Then applying center manifold theory and letting

$$v = au^2, \quad w = bu^2,$$

and balancing the coefficients in the equations:

$$\frac{dv}{d\tau} = 2au\dot{u}, \quad \text{and} \quad \frac{dw}{d\tau} = 2bu\dot{u},$$

together with (2.16) yields

$$a = -\frac{(AEF + E - F + 1)(C^2 + 1) + \{[(2 - B)A - B]E - B(A + 1) - 2\}F(E + 1)C}{(A + 1)^2(E + 1)^3(C + 1)^2(-1 + F)},$$

$$b = \frac{-C^2EF + CBE - 2CEF + CB - EF}{(E + 1)^2(A + 1)(C + 1)^2(-1 + F)}.$$

Hence, the center manifold up to the second order is defined as

$$W^c = \{(u, v, w) | v = au^2 + O(u^3), w = bu^2 + O(u^3)\},$$

and the differential equation describing the dynamics on the center manifold is given by

$$\frac{du}{d\tau} = -\frac{CB}{(E + 1)(C + 1)^2(A + 1)}\{u^2 - [a(A + 1) + b](E + 1)u^3 + O(u^4)\}, \quad (2.17)$$

which clearly indicates that the equilibrium E_1 is a stable degenerate node since the coefficient of u^2 is negative.

When $D = \frac{B}{1+C}$, the system still has four parameters A , B , C and D . We give a brief summary on the dynamics and bifurcation of the system (2.5) at $R_0 = 1$. It can be seen from (2.17) that $u = 0$ defines a degenerate stable node on the center manifold. Now, the system (2.5) has only two equilibria E_0 and E_1 , and $Y_1 = 0$ still holds for the critical case. Back to the original equilibrium solution using (2.15), we have

$$X_1 = 1 - \frac{u}{(1+E)(1+A)}, \quad (2.18)$$

which shows that $X_1 = 1$ when $u = 0$. The above stability for u implies that E_1 is a degenerate stable node, and so that no backward bifurcation can occur. Simulation of system (2.5) for the critical case $R_0 = 1$ is shown in Figure 2.2, indicating that all trajectories with different initial conditions converge to the degenerate node E_1 .

2.4.2 Case $R_0 > 1$ and codimension of Hopf bifurcation

In this subsection, we consider the case $R_0 > 1$, and particularly investigate the codimension of the Hopf bifurcation discussed in the previous sections.

First, we describe the underlying concept of the technique used to study the codimension of Hopf bifurcation. The basic idea is to identify the dominant values that can be used to quantify the number of limit cycles bifurcating from a Hopf critical point and their stability for a given nonlinear dynamical system associated with a Hopf bifurcation. These dominant values are often known as focus values, and they may be derived by computing the normal forms for a general n -dimensional nonlinear systems. To be more specific, consider the following general n -dimensional autonomous differential system,

$$\frac{dZ}{d\tau} = AZ + f(Z), \quad Z \in R^n, \quad f : R^n \rightarrow R^n, \quad (2.19)$$

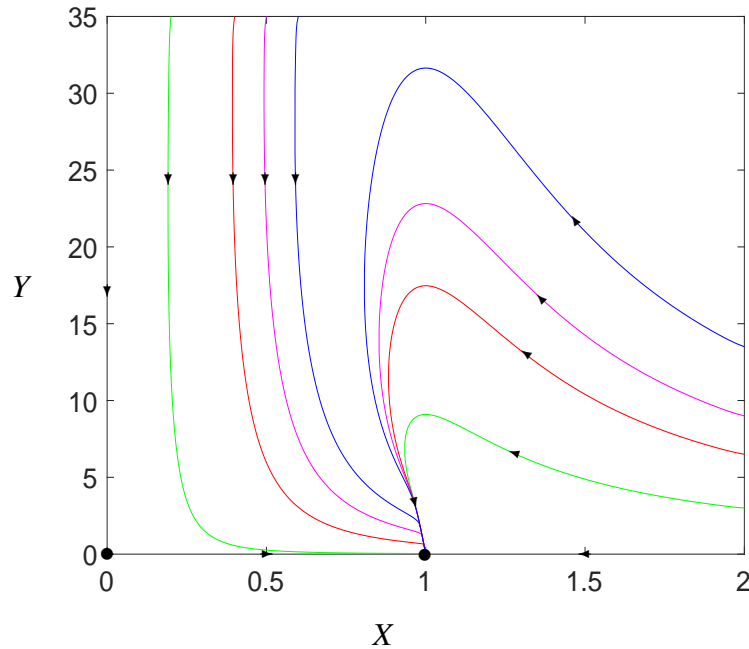


Figure 2.2: Phase portrait of system (2.5) at $R_0 = 1$, projected on the X - Y plane, showing the convergence of trajectories to the degenerate node $X = 1$, with the parameter values: $A = \frac{1}{10}$, $B = \frac{29}{3}$, $C = 1$, $D = \frac{B}{1+C} = \frac{29}{6}$, $E = \frac{3}{1000}$ and $F = 100$.

where the linear and nonlinear components of the system are denoted by AZ and $f(Z)$, respectively. For our purpose, without loss of generality, assume that $f(0) = Df(0) = 0$, which indicates that the system's fixed point is $Z = 0$. In general, the matrix A may have eigenvalues with real parts that are negative, positive, or zero, and as a result, the system may contain stable, unstable, or center manifolds. To compute the normal form, the first step is typically to apply a linear transformation T to the given system, converting its linear portion to the Jordan canonical form, which is the system's normal form for the linear part. Thus, applying the linear transformation $Z = TX$ to the system results in the system,

$$\frac{dX}{d\tau} = JX + f(X), \quad X \in \mathbb{R}^n, \quad f: \mathbb{R}^n \rightarrow \mathbb{R}^n, \quad (2.20)$$

where $J = \text{diag}(J_1, J_2, J_3)$, in which J_1 , J_2 and J_3 are in Jordan canonical forms, having zero, negative and positive real parts, respectively. It should be noted that in real applications, the unstable manifold is usually assumed null since the system is unstable when it

contains unstable manifold.

Now, based on the system (2.20), we suppose that J_1 is two dimensional and contains a pair of purely imaginary eigenvalues $\pm i\omega_c$ at a critical point, and J_3 is null. Then, we compute the normal form associated with Hopf and generalized Hopf bifurcations by employing center manifold theory, normal form theory and computer algebra systems to obtain the following normal form in polar coordinates [7]:

$$\begin{aligned}\frac{dr}{d\tau} &= r(v_0\mu + v_1r^2 + v_2r^4 + \cdots + v_kr^{2k} + \cdots), \\ \frac{d\theta}{d\tau} &= \omega_c + t_0 + t_1r^2 + t_2r^4 + \cdots + t_kr^{2k} + \cdots,\end{aligned}\tag{2.21}$$

where the motion's amplitude and phase are denoted by r and θ , respectively. The k th-order focus value is v_k ($k = 0, 1, 2, \dots$). We can derive v_0 and t_0 using a linear analysis. The second equation in (2.21) can be used to calculate the frequency of the bifurcating periodic motion, whereas the first equation in (2.21) can be applied to examine bifurcation and the stability of limit cycles. When all the focus values are given in terms of the original system parameters, if we can use k parameters such that $v_0 = v_1 = \cdots = v_{k-1} = 0$ but $v_k \neq 0$ at the critical point specified by $\mu_c = (\mu_{1c}, \dots, \mu_{kc})$, and the following condition holds:

$$\text{rank}\left[\frac{\partial(v_0, v_1, \dots, v_{k-1})}{\partial(\mu_1, \mu_2, \dots, \mu_k)}(\mu_c)\right] = k,\tag{2.22}$$

then the system can bifurcate k limit cycles around the origin (the equilibrium) from the Hopf critical point, by using appropriate perturbations on μ . More details on the topic of bifurcation of limit cycles can be found in [7–9].

We have the result for the codimension of Hopf bifurcation in the following theorem.

Theorem 2.4.3 *For the system (2.5), when $C = 1$, $B = \frac{D(3-A)}{1-A}$ ($A < 1$), the codimension of the Hopf bifurcation from the equilibrium E_2 is 4, implying that at least 4 small-amplitude limit cycles exist around the equilibrium E_2 .*

Proof Since the computation of the focus values is extremely complicated for general case, we make a simplification by setting $C = 1$, $B = \frac{D(3-A)}{1-A}$ (with $A < 1$) in system (2.5), yielding the new system,

$$\begin{aligned}\frac{dX}{d\tau} &= X\left(1 - X - \frac{Z}{A + X}\right), \\ \frac{dY}{d\tau} &= \frac{DY(2X - 1 + A)}{(1 - A)(1 + X)}, \\ \frac{dZ}{d\tau} &= \frac{XY}{E + X} - FZ,\end{aligned}\tag{2.23}$$

which has three equilibria:

$$E_0 = (0, 0, 0),$$

$$E_1 = (1, 0, 0),$$

$$E_2 = \left(\frac{1 - A}{2}, \frac{F(A + 1)^2(1 - A + 2E)}{4(1 - A)}, \frac{(A + 1)^2}{4}\right).$$

Since we are interested in the Hopf bifurcation which occurs from E_2 , we similarly use the Jacobian matrix of the system to determine the stability of E_2 , which produces

$$J(E_2) = \begin{bmatrix} 0 & 0 & \frac{A - 1}{A + 1} \\ \frac{DF(A + 1)^2(A - 2E - 1)}{(A - 3)(A - 1)^2} & 0 & 0 \\ \frac{E(A + 1)^2F}{(A - 1)(A - 2E - 1)} & \frac{A - 1}{A - 2E - 1} & -F \end{bmatrix},$$

yielding the characteristic polynomial,

$$P_{E_2}(\lambda) = \lambda^3 + a_1\lambda^2 + a_2\lambda + a_3,$$

where

$$a_1 = F, \quad a_2 = \frac{F(A + 1)E}{1 - A + 2E}, \quad a_3 = \frac{FD(A + 1)}{3 - A},$$

showing that all a_i 's are positive. To find a Hopf bifurcation critical point, we choose E as the bifurcation parameter and let

$$\Delta_2 = F(A + 1) \frac{E[F(3 - A) - 2D] - D(1 - A)}{((3 - A)(1 - A + 2E))} = 0,$$

from which we find the Hopf critical point defined as

$$E_H = \frac{D(1 - A)}{F(3 - A) - 2D}.$$

Since $A < 1$ and $E \gg D$, we know that $E_H > 0$. Thus, the equilibrium E_2 is LAS for $E > E_H$, and unstable for $0 < E < E_H$. Hopf bifurcation occurs from E_2 at the critical point $E = E_H$.

To compute the focus values for system (2.23) at $E = E_H$, we introduce the following affine transformation,

$$\begin{pmatrix} X \\ Y \\ Z \end{pmatrix} = \begin{pmatrix} \frac{1 - A}{2} \\ \frac{F(A + 1)^2(A - 1 - 2E)}{4(A - 1)} \\ \frac{(A + 1)^2}{4} \end{pmatrix} + \begin{bmatrix} 0 & \frac{(1 - A)\sqrt{D_2(3 + 2A - A^2)}}{(1 + A)^2 D_2} & \frac{1 - A}{F(A + 1)} \\ \frac{F^2(3 - A)}{F(3 - A) - 2D_2} & 0 & \frac{-D_2(1 + A)}{F(3 - A) - 2D_2} \\ 1 & 0 & 1 \end{bmatrix} \begin{pmatrix} u \\ v \\ w \end{pmatrix},$$

where $D_2 = \sqrt{D}$, into (2.23) to obtain the system whose linear part is in Jordan canonical

form:

$$\begin{aligned}
\frac{du}{d\tau} &= \omega_c v + \frac{(2F^3 - 2DF)A^2 + (-8F^3 - 4D^2 + 4DF)A + 6F^3 - 4D^2 + 6DF}{(A+1)(A-3)F((D-F^2)A + 3F + D)} u^2 \\
&\quad + \frac{2(-AF^2 + AD + 2DF + F^2 + D)D}{F^2(-AF^2 + AD + 3F^2 + D)(-3 + A)} w^2 + \dots, \\
\frac{dv}{d\tau} &= -\omega_c u + V_{11}v^2 + V_{12}w^2 + \dots, \\
\frac{dw}{d\tau} &= -Fw + \frac{4(D-F)F}{F(-AF^2 + AD + 3F^2 + D)(A+1)} v^2 \\
&\quad - \frac{4(D-F)D}{F(-AF^2 + AD + 3F^2 + D)(A-3)} w^2 + \dots,
\end{aligned} \tag{2.24}$$

in which

$$\omega_c = \sqrt{\frac{D(A+1)}{3-A}},$$

while other lengthy expressions denoted by \dots are omitted for simplicity. $V_{11} = \frac{V_{11n}}{V_{11d}},$

$V_{12} = \frac{V_{12n}}{V_{12d}}$ with

$$\begin{aligned}
V_{11n} &= (D - F^2)A^4 + 4(2F^2 - D)A^3 + 2[11F^2 - (2D^2 + 2F + 1)D]A^2 \\
&\quad + 4[6F^2 - 2D^2 + (2F + 1)D]A - 4D^2 + (4F - 3)D - 9F^2, \\
V_{11d} &= \omega_c(A+1)^2((-F^2 + D)A + 3F^2 + D), \\
V_{12n} &= -D\{(D - F^2)A^4 - 4[F^3 - 2F^2 - (F - 1)D]A^3 \\
&\quad + 2[12F^3 - 11F^2 - 2D^2 - (2F - 1)D]A^2 \\
&\quad - 4[9F^3 - 6F^2 + 2D^2 + (F - 1)D]A - 4D^2 + (4F - 3)D - 9F^2\}, \\
V_{12d} &= \omega_c(A+1)(A-3)F^2[(D - F^2)A + 3F^2 + D].
\end{aligned}$$

Now, we apply the Maple program in [7] for computing the normal forms associated with Hopf and generalized Hopf bifurcations to get the amplitude equation in the normal form

up to 9th-order as follows:

$$\frac{dr}{d\tau} = r[v_0\mu + v_1r^2 + v_2r^4 + v_3r^6 + v_4r^8 + O(r^{10})], \quad (2.25)$$

where $\mu = E - E_H$, is a perturbation parameter, and v_0, v_1, v_2, v_3 , and v_4 are the zero-order, 1st-order, 2nd-order, 3rd-order, and 4th-order focus values.

The transversal condition is obtained by using a linear analysis as

$$v_0 = -\frac{(1+A)[(A-3)F+2D]^2}{2(1-A)(3-A)[(3-A)F^2+(1+A)D]} < 0, \quad (2.26)$$

indicating that E is decreasing to cross the Hopf critical point $E = E_H$, which agrees with the above result: E_2 is LAS for $E > E_H$ and unstable for $E < E_H$.

The equation (2.25) can be utilized to do bifurcation analysis, and the sign of v_1 indicates whether the Hopf bifurcation is supercritical or subcritical, while the signs of higher-order focus values can determine the stability of multiply bifurcating limit cycles. The general necessary and sufficient condition for the existence of multiple limit cycles is given in (2.22). For our system (2.24), using the Maple program [7], we obtain the focus values v_1, v_2, v_3 and v_4 as follows:

$$v_1 = \frac{(1-A)(3-A)v_{1a}}{16D(A+1)^4[(A-3)F+2D][(3-A)F^2+(A+1)D][(3-A)F^2+4(A+1)D]},$$

$$v_2 = \frac{(A-1)v_{2a}}{144v_{2d}},$$

$$v_3 = \dots,$$

$$v_4 = \dots,$$

where

$$\begin{aligned}
v_{1a} = & (3A^2 - 6A - 1)(A - 1)^2(A - 3)^3F^5 + 4D(3A - 5)(A - 3)(A + 1)^2F^4 \\
& - D(A + 1)(A - 3)[4(A + 1)(A - 7)D + (A - 1)^2(A - 3)(15A^2 - 26A - 1)]F^3 \\
& - 4D^2(A + 1)^2[2D(A + 1)(A - 3) - A^4 + 8A^3 - 20A^2 + 4A - 31]F^2 \\
& - 4D^2(A + 1)^2[8(A + 4)(A + 1)D + (3A - 1)(3 - A)(A - 1)^3]F \\
& + 8D^3(A + 1)^3[5D(A + 1) - (A - 3)(A - 1)^2],
\end{aligned}$$

$$v_{2a} = \dots ,$$

$$\begin{aligned}
v_{2d} = & D^3F^2(A + 1)^{10}[(A - 3)F + 2D][D(9A + 9) + F^2(3 - A)] \\
& \times [D(A + 1) + F^2(3 - A)]^3[4D(A + 1) + F^2(3 - A)]^3
\end{aligned}$$

The lengthy expressions for v_{2a} , v_3 and v_4 are omitted here for brevity.

Since v_k 's contain 3 parameters, A , D and F , it might be possible to have solutions such that $v_1 = v_2 = v_3 = 0$, but $v_4 \neq 0$, yielding at most 4 limit cycles. Based on the focus values v_1 , v_2 and v_3 , we first use the Maple-built command *eliminate* to get a solution $D(A, F)$ and two resultants: $R_1(A, F) = R_0(A, F)R_{1a}(A, F)$ and $R_2(A, F) = R_0(A, F)R_{2a}(A, F)$, where

$$\begin{aligned}
R_0(A, F) = & F(1 - A)(3 - A)[1 + 3A(2 - A)][1 + A + (3 - A)F] \\
& \times [4(1 + A) + (3 - A)F]\{(3 - A)[8F^2 - (1 - A)^2] + (A + 17)F\} \\
& \times \{(3 - A)[F^2 + 4(1 - A)^2] + 4(1 + 5A)F\} > 0, \quad (\text{for } A < 1 < F).
\end{aligned}$$

$R_{1a}(A, F)$ and $R_{2a}(A, F)$ are two lengthy polynomials in A and F . Then, we use the Maple-built command *resultant* to obtain a lengthy resultant polynomial in A :

$$R_{12}(A) = -C_0(1 - A)^5 62(3 - A)^4 80(1 + 6A - 3A^2)^1 0R_{12a} R_{12b} R_{12c} R_{12d} R_{12e},$$

where C_0 is a big integer, and

$$\begin{aligned}
R_{12a} &= (A^6 - 21A^5 + 100A^4 - 174A^3 + 117A^2 - 77A + 22) \\
&\quad \times (A^8 - 34A^7 + 262A^6 - 850A^5 + 1344A^4 - 758A^3 + 810A^2 - 22A + 15) \\
&\quad \times (692356A^8 - 8273296A^7 + 38723436A^6 - 86480443A^5 + 93238801A^4 \\
&\quad \quad - 34912614A^3 - 19718394A^2 + 10915137A + 3619593), \\
R_{12b} &= 21472041204A^{16} - 478685886756A^{15} + 4655191749410A^{14} \\
&\quad - 34305698817233A^{13} + 215384167112585A^{12} - 969873671993323A^{11} \\
&\quad + 2873132220801823A^{10} - 5219368638878410A^9 + 4808258364989540A^8 \\
&\quad - 631844839107146A^7 - 1746598670362432A^6 + 369616640399739A^5 \\
&\quad + 316560031040433A^4 - 78293927207799A^3 - 8702697485457A^2 \\
&\quad + 2044756430064A + 188337117438,
\end{aligned}$$

$$\begin{aligned}
R_{12c} = & 167799312A^{16} - 3958473216A^{15} + 42320529064A^{14} \\
& -271935782032A^{13} + 1172853133196A^{12} - 3585911951970A^{11} \\
& +7985864531153A^{10} - 13061138801753A^9 + 15498297078232A^8 \\
& -12684785748056A^7 + 5940193043694A^6 + 296535775826A^5 \\
& -2874589615504A^4 + 2350575838674A^3 - 1033536360511A^2 \\
& +259226146431A - 30413518092,
\end{aligned}$$

$$\begin{aligned}
R_{12d} = & 90882A^{22} - 2679318A^{21} + 35478081A^{20} - 277959600A^{19} \\
& +1424448720A^{18} - 4950964386A^{17} + 11507199649A^{16} \\
& -15822195200A^{15} + 3505374380A^{14} + 38022655684A^{13} \\
& -98266484414A^{12} + 143736947488A^{11} - 150810106072A^{10} \\
& +126898351068A^9 - 91109565046A^8 + 54088899456A^7 \\
& -23425253534A^6 + 6141349874A^5 - 727614883A^4 \\
& +53692176A^3 - 25228552A^2 + 5826598A + 882677,
\end{aligned}$$

$$R_{12e} = \dots ,$$

$$R_{12f} = \dots ,$$

where R_{12e} and R_{12f} are respectively 386-degree and 1908-degree polynomials in A . It is easy to verified that R_{12c} and R_{12d} have no real solutions for $A \in (0, 1)$, while R_{12a} , R_{12b} and R_{12e} have only 9 real solutions for $A \in (0, 1)$. Then, we use these 9 solutions to obtain 4 positive solutions for F . Among theses 4 sets of solutions (A_k, F_k) , $k = 1, 2, 3, 4$, we use the above obtained formula $D(A, F)$ to verify that only one solution satisfies $D > 0$. This

unique solution is given by

$$\begin{aligned} A &= 0.9434673546 \cdots, & B &= 154.3184037325 \cdots, & C &= 1, \\ D &= 4.2421050801 \cdots, & E &= 0.4459655614 \cdots, & F &= 5.6930540630 \cdots, \end{aligned} \quad (2.27)$$

where $E = E_H$. Note that 1000-digit point accuracy has been used in the above computations in order to guarantee the correctness of conclusion. With this solution, we have

$$\omega_c = 0.2053782428 \cdots, \quad v_0 = v_1 = v_2 = v_3 = 0, \quad v_4 = 0.1785278748 \cdots \times 10^{-7} \neq 0,$$

which shows that the system (2.5) can have at most 4 small-amplitude limit cycles arising from Hopf bifurcation. Finally, we check the formula in (2.22) to obtain

$$\text{rank} \left[\frac{\partial(v_1, v_2, v_3)}{\partial(A, D, F)} \right]_{(2.27)} = -0.2636627563 \cdots \times 10^{-14} < 0,$$

which indeed shows that 4 small-amplitude limit cycles can bifurcate from E_2 near the critical point defined in (2.27). Note that v_0 is excluded in the above formula since $E = E_H$ has separately solved the equation $v_0 = 0$.

The proof of Theorem 2.4.3 is complete.

2.5 Numerical Simulation

In this section, we use numerical simulation to demonstrate the theoretical results obtained in the previous sections. However, it should be pointed out that realising the bifurcation of 4 small-amplitude limit cycles using numerical simulation is extremely difficult. It is theoretically possible for the system to exhibit four small-amplitude limit cycles, as established via higher-order Lyapunov coefficients. However, numerically capturing all four is extremely challenging because the cycles are very close in phase space and have tiny amplitudes near critical parameter values. Small numerical errors or sensitivity to initial

conditions can merge or distort trajectories, and high-order nonlinear terms require very precise computation and fine parameter tuning. Thus, while theory guarantees up to four limit cycles, numerical simulations typically reveal only one or two. In fact, to the best of our knowledge, so far in the literature, the limit cycle simulation is only success for 3 limit cycles, for example see [10]. We shall present two simulations, one for one limit cycle, and the other for two limit cycles. The bifurcation diagrams for these limit cycle bifurcations are shown in Figure 2.3.

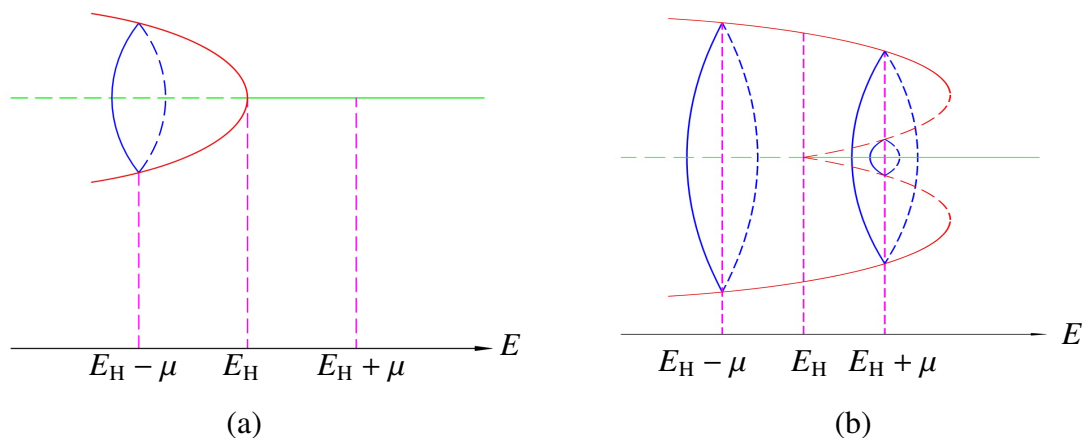


Figure 2.3: Bifurcation diagram for Hopf bifurcations of system (2.5) yielding (a) one limit cycle bifurcating at $E = E_H - \mu$; and (b) two limit cycles bifurcating at $E = E_H + \mu$.

We take the following parameter values for simulation of one stable limit cycle, as shown in Figure 2.4(a):

$$A = 0.1, \quad B = 9.666667, \quad C = 1, \quad D = 3, \quad E = 0.003, \quad F = 100.$$

To show the existence of two limit cycles, we choose $A = 0.9$ and $F = 20$, and then solve $v_1 = 0$ to get $\sqrt{D} = 3.69021284$. Further, taking perturbation on \sqrt{D} as $\sqrt{D} = 3.69021284 + 0.0001$, leading to $D = 13.6176708$ and $E_H = 0.09223153$, which yields one small-amplitude limit cycle. To get one more small limit cycle, we take $\mu = 0.2 \times 10^{-10}$ to

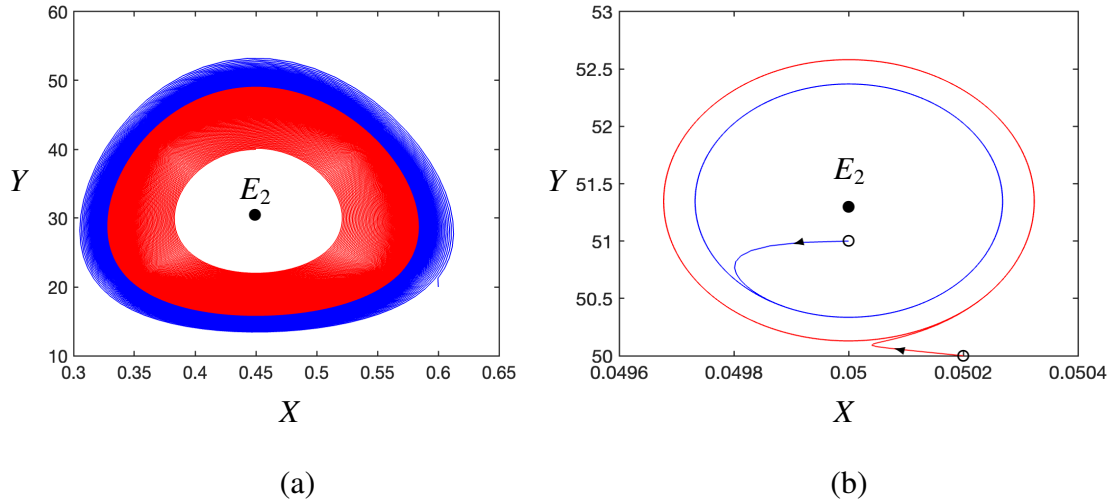


Figure 2.4: Simulated limit cycles for system (2.5): (a) one stable limit cycle for $A = 0.1$, $B = 9.6666667$, $C = 1$, $D = 3$, $E = 0.003$, $F = 100$; and (b) two limit cycles for $A = 0.9$, $B = 285.971087$, $C = 1$, $D = 13.617671$, $E = 0.092232$, $F = 20$, with the outer one stable and the inner one unstable, both them enclosing the stable equilibrium E_2 .

get

$$v_0\mu = -0.22778579 \times 10^{-10}, \quad v_1 = 0.18776581 \times 10^{-7}, \quad v_2 = -0.32816726 \times 10^{-5},$$

which yields the following normal form equation for the amplitudes of bifurcating limit cycles:

$$\frac{dr}{d\tau} = r[v_0\mu + v_1r^2 + v_2r^4 + O(r^6)].$$

Solving the above equation, we obtain the approximate solutions for the amplitudes of the two limit cycles: $r_1 \approx 0.041783$ and $r_2 \approx 0.063054$.

The simulated limit cycles are shown in Figure 2.4. Figure 2.4(a) depicts one stable limit cycle. Two trajectories (in red and blue colors) start from two initial points, one is outside the limit cycle and one is inside the limit cycle. Both them converge to the limit cycle (the intersection of the red and blue trajectories) which encloses the unstable equilibrium E_2 . Bifurcation of two limit cycles is given in Figure 2.4(b), where only the bigger limit cycle is shown since the existence of the small limit cycle is due to that both the

bigger limit cycle and the equilibrium E_2 are stable (E_2 is stable because $v_0\mu < 0$). Again, two initial points (marked by the two circles in Figure 2.4(b)) are chosen from outside and inside the bigger stable limit cycle. However, due to extremely slow convergence, unlike Figure 2.4(a), it does not show the two trajectories converging to the exact bigger stable limit cycle, but it clearly indicates the direction of convergence.

2.6 Conclusion

In this research study, a mathematical model consisting of tumor cells, CD4⁺ T cells, and cytokine relations has been studied for examining how the CD4⁺ T cells might influence tumor reduction and latency. Although the CD4⁺ T cells do not directly destroy the tumor cells, they can produce and deploy cytokines to modulate tumor growth. We apply stability and bifurcation theory to investigate the stability of equilibria and the oscillating behaviours arising from Hopf bifurcation. Center manifold theory and normal form theory are employed to study bifurcation of limit cycles. The bifurcation results obtained in this research work indeed indicate that the model can have complex dynamical behaviors, which may be more proper to describe the real situation.

Our study shows that the tumor cells are persist when no treatment is applied, irrespective to the size of the tumor. In the current study, the CD4⁺ T cells are treated as a single type and the simplest tumor-suppressing cytokine. No direct relations are assumed between the tumor and CD4⁺ T cells. It is shown that without treatment, a patient with very low tumor antigenicity would experience tumor expanding to its maximum size, regardless whether the tumor destruction rate and the cytokine production rate are high [11]. On the other hand, if either of these two rates is high and the maximum CD4⁺ T production rate is not excessively low, tumor recurrence can happen, and its size can be managed to a smaller extent. However, complete elimination of the tumor is not possible without intervention. In order to completely eliminate tumor cells while the CD4⁺ T cells are administered, we

aim to assess if immunotherapy itself is adequate in the next research.

References

- [1] A. M. Knowles, J. P. Selby, Introduction to the Cellular and Molecular Biology of Cancer, (4th ed.), Oxford University Press Inc. New York, 2005.
- [2] B. Mansoori, A. Mohammadi, S. Davudian, S. Shirjang, B. Baradaran, The Different Mechanisms of Cancer Drug Resistance: A Brief Review, *Adv. Pharm. Bull.*, **7** (2017), 339-348. doi: 10.15171/apb.2017.041.
- [3] P. Parsonidis, I. Papatotiriou, Adoptive Cellular Transfer Immunotherapies for Cancer, *Cancer Treat. Res. Commun.*, **32** (2022), 1-7. doi: 10.1016/j.ctarc.2022.100575.
- [4] R Eftimie, J. L. Bramson and DJD Earn, Interactions Between the Immune System and Cancer: A Brief Review of Non-spatial Mathematical Models, *Bull. Math. Biol.*, **73** (2011), 2-32. doi: 10.1007/s11538-010-9526-3.
- [5] E. G. Mahlbacher, C. K. Reihmer, B. H. Frieboes, Mathematical modeling of tumor-immune cell interactions, *J. Theor. Biol.*, **469** (2019), 47-60. doi: 10.1016/j.jtbi.2019.03.002.
- [6] L. Anderson, S. Jang, J. L. Yu, Qualitative behaviour of system of tumor-CD4⁺-cytokine interactions with treatments, *Math. Meth. Appl. Sci.*, **38** (2015), 4330-4344. doi: 10.1002/mma.3370.
- [7] P. Yu, Computation of normal forms via a perturbation technique, *J. Sound Vib.*, **211** (1998), 19-38. doi: 10.1006/jsvi.1997.1347.
- [8] J. Jiang, P. Yu, Multistable phenomena involving equilibria and periodic motions in predator-prey systems, *Int. J. Bifurcation and Chaos*, **27** (2017), 28. doi: 10.1142/S0218127417500432.

- [9] M. Han, P. Yu, Normal Forms, Melnikov Functions, and Bifurcations of limit cycles, *Springer-Verlag, New York*, 2012, doi: 10.1007/978-1-4471-2918-9.
- [10] W. Zhang, L. M. Wahl, P. Yu, Modelling and analysis of recurrent autoimmune disease, *SIAM J. Appl. Math.*, **74** (2014), 1998-2025. doi: 10.1137/140955823.
- [11] H. C. Wei, J. L. Yu, C. Y. Hsu, Periodically pulsed immunotherapy in a mathematical model of Tumor, CD4⁺ T cells, and antitumor cytokine interactions, *Comput. Math. Methods Med.*, **2017**(4) (2017) (12 pages). doi: 10.1155/2017/2906282.

Chapter 3

3 Dynamical Analysis of a Tumor Model with Immunotherapy Treatment

3.1 Introduction

Cancer is a disease in which certain cells in the body grow and divide abnormally and uncontrollably. If left untreated, these abnormal cells can spread to other parts of the body through the blood or lymph system. Tumor cells do not follow the normal rules that control how cells grow and stay balanced. This can interfere with the signals that control cell growth, causing them to stop working properly in all types of human tumors [1]. The treatment plan for cancer is largely determined by its stage. Cancer staging often relies on the TNM system, which assesses the tumor's size (T), whether it has reached nearby lymph nodes (N), and if it has spread (metastasized) to distant parts of the body (M). Cancer is usually divided into five stages. In stages 0 and 1, the tumor is small and hasn't spread (in place). In stages 2 and 3, the tumor is bigger and may have spread to nearby tissues or lymph nodes. Stage 4 means that the cancer has spread to other parts of the body [2, 3]. Based on the stage, doctors recommend appropriate treatments, which may include surgery, chemotherapy, radiation therapy, immunotherapy, virotherapy, or other options. In some situations, a combination of treatments is used for example, one to shrink the tumor and another to remove it.

Cancer is treated using various standard therapies, including surgery, chemotherapy, radiation therapy [4], virotherapy [5], hormonal therapy [6], and immunotherapy [7]. Surgery is often the primary approach, but additional treatments are commonly needed to reduce recurrence risk. In cases where tumors are large or in sensitive areas like the face or eyelids, extensive tissue removal may be required, leading to complications. Radiation is frequently

used post-surgery for inoperable or large tumors, though it may not always improve survival [8]. Chemotherapy remains widely used but can damage healthy cells, causing side effects and potential recurrence [9]. These limitations have led to growing interest in immunotherapy, which enhances the immune system's ability to fight cancer [10, 11].

The Tumor Immuno-Surveillance Hypothesis, originally proposed in 1957, suggests that the immune system continuously monitors the body for emerging tumor cells and eliminates them before they can develop into detectable cancers. Some tumors express unique antigens that can be recognized by immune cells. Supporting this idea, modern mathematical models of tumor-immune interactions build on this concept to explore how the immune system controls tumor growth and how tumors may escape [12]. Immunotherapy mainly activates CD8⁺ T cells, NK cells, and macrophages [13], with studies confirming their potency in killing cancer cells [14, 15]. However, the evolving complexity of tumor-immune interactions within the tumor microenvironment presents challenges in designing effective immunotherapies.

Immunotherapy helps the body's immune system find and attack cancer cells in two main ways: passive and active. Passive immunotherapy gives the body parts of the immune system directly, like special antibodies and changed T cells called CAR-T cells. Active immunotherapy helps the immune system get stronger to fight cancer by using cancer vaccines, proteins called cytokines, and cell therapies [16]. We can now better understand the human immune system's complexity using deep learning, probability models, and a mix of different methods, along with powerful computers to run detailed biological simulations [17].

The immune system acts like the body's defense team, protecting it from infections and diseases. The immune system starts with special cells made in the bone marrow through a process called hematopoiesis. These cells have two main types: myeloid and lymphoid. Myeloid cells include neutrophils, monocytes, macrophages, and dendritic cells, which help fight infections and clean the body [18, 19]. Lymphoid cells include B cells, T cells,

and natural killer (NK) cells, which are part of the body's targeted defense system. Each type of cell has a unique role, working together to protect the body in a well-organized way [20].

T cells are one of the two primary types of lymphocytes (a type of white blood cell) that play a key role in the immune system. They can be categorized into two main types of effector cells: helper T cells and cytotoxic T cells. Helper T cells are one of the two main types of T cells in the human immune system. Both helper and cytotoxic T cells come from stem cells in the bone marrow and grow to maturity in the thymus. The main difference between them is the type of receptors found on their surfaces. As T cells grow in the thymus, they develop special receptors on their surface called T Cell Receptors (TCRs) along with co-receptors named CD4 (T helper) and CD8 (T-killer). All T cells have TCRs, but only helper T cells have CD4, and only cytotoxic T cells have CD8. That's why helper T cells are also called $CD4^+$ T cells [21].

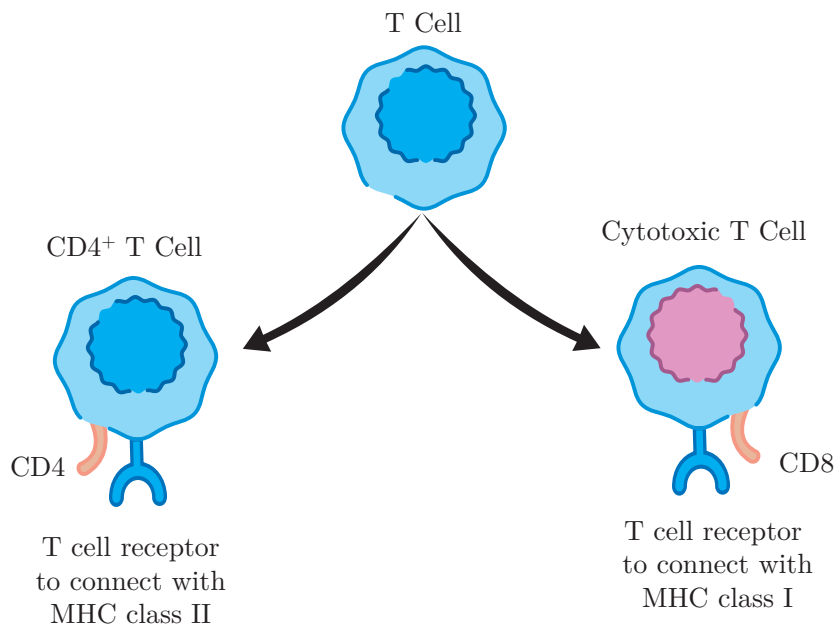


Figure 3.1: Different functions between helper T cells and cytotoxic T cells ($CD4^+$ and $CD8^+$).

A newly grown T cell is called a naïve T cell until it meets an antigen and becomes

active. The T cell has a special receptor (TCR) that recognizes only one kind of antigen, but it cannot bind to antigens directly. Instead, it recognizes antigens only when they are attached to certain molecules called Major Histocompatibility Complex (MHC) Class I and Class II [22] (see Figure 3.1). MHC class I molecules show pieces of proteins from inside the cell, including those from viruses [23]. MHC class II molecules display protein pieces from outside germs. These are taken in, broken down, and shown on the cell surface to $CD4^+$ T cells, helping trigger the immune response and support antibody production [24, 25].

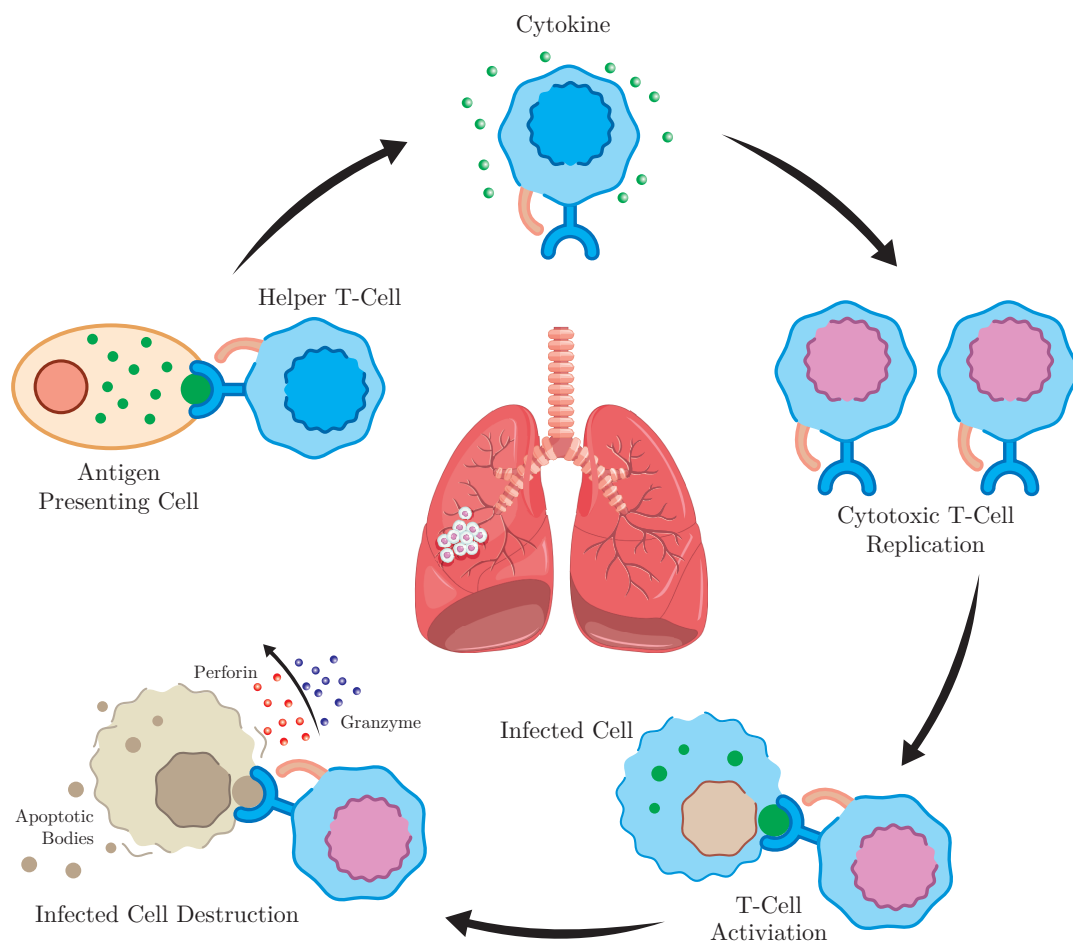


Figure 3.2: Helper T cell activation and its role in immunity [26].

Helper T cells are very important in the adaptive immune system and are needed for most immune responses. They do not produce toxins or antibodies, nor do they attack germs directly. Instead, they help by releasing signals called cytokines, which activate

other immune cells and guide the body's defense against infections. The cytokines made by helper T cells also help activate cytotoxic T cells and phagocytes like macrophages. Phagocytes eat and remove infected cells, while cytotoxic T cells release substances to kill harmful cells. By activating these cells, helper T cells play an important role in guiding the immune system to fight infections [27], see the illustration given in Figure 3.2.

Cancer vaccines stimulate the body's immune system by boosting the activity of cytotoxic T lymphocytes against tumor-specific antigens. Meanwhile, immune signaling is controlled by cytokines such as interleukin-2 (IL-2) and interferon- α (IFN- α). These are the only cytokines which are approved by the U.S. Food and Drug Administration (FDA) for cancer therapy, as they have shown reasonable medical efficacy [28]. IL-2 stimulates natural killer (NK) and T cells to target tumors, while IFN- α triggers a comparable immune response, although it does not provide the same prolonged survival advantages as IL-2 [16, 29–31].

Mathematical models, especially systems of ordinary differential equations (ODEs), are widely used to study tumor-immune dynamics [32–35]. Studies show that immunotherapy alone often cannot eliminate tumors but can delay recurrence [35, 36]. Due to cancer's complexity and variability, immunotherapy is sensitive to initial conditions and typically used alongside other treatments. Modeling helps clarify interactions within the tumor microenvironment and predict treatment outcomes [37–40]. As cancer biology evolves, mathematical tools play a growing role in analyzing tumor growth and immune responses, highlighting the importance of both adaptive and innate immunity in cancer control [41].

In the following, we provide an overview of one of the mathematical models related to tumor-immune dynamics. Around 2000, Kirschner and Panetta [42] developed a simple

3-dimensional ODE model, described by

$$\begin{aligned}\frac{dE}{dt} &= cT - \mu_2 E + \frac{p_1 E I_L}{g_1 + I_L} + s_1, \\ \frac{dT}{dt} &= r_2 T(1 - bT) - \frac{aET}{g_2 + T}, \\ \frac{dI_L}{dt} &= \frac{p_2 ET}{g_3 + T} - \mu_3 I_L + s_2,\end{aligned}\tag{3.1}$$

to investigate the tumor-immune interactions, which incorporates three key state variables: effector immune cells (E), which include CD8+ T cells, macrophages, or NK cells; tumor cells (T); and the cytokine IL-2 (IL), which plays a role in activating immune cells. The system of equations used in the model captures the dynamics between these variables, illustrating how they influence each other in the context of immune response to tumors. Note that the parameters s_1 and s_2 can be either zero or positive, while all other parameters are positive. The tumor follows logistic growth in the absence of an immune response, while its elimination by effector cells is governed by Michaelis-Menten kinetics. Effector cell and IL-2 production also follow similar kinetics, combining external treatments s_1 and s_2 . Using tumor antigenicity as a bifurcation parameter, the study presented in [42] investigated the dynamics of tumor-immune interactions by analyzing a one-parameter bifurcation diagram under the assumption $s_1 = s_2 = 0$, highlighting the role of antigenicity. The model was then extended to explore various treatment strategies, specifically involving effector cell therapy ($s_1 > 0$, $s_2 = 0$), and cytokine therapy ($s_1 = 0$ and $s_2 > 0$), or both ($s_1 > 0$ and $s_2 > 0$). Kirschner and Panetta [42] conclude that the immune response to tumors is significantly influenced by the level of tumor antigenicity and the presence of immunomodulatory treatments. Tumors with low recognition tend to escape immune attack, while highly recognizable ones may shrink but not disappear. Some tumors show cycles of growth and dormancy. Among treatments, adoptive cellular immunotherapy (ACI) works well, while IL-2 alone has limited success and can cause side effects at high doses. However, combining ACI with IL-2 is the most effective approach, demonstrating that enhancing the immune

system can be crucial in cancer treatment.

As discussed below, our model is based on different assumptions than earlier studies. In the model by [42], tumor clearance is primarily driven by cytotoxic effector cells. In contrast, our model (3.2) attributes tumor control mainly to cytokines, with $CD4^+$ T cells acting as effectors instead of $CD8^+$ T cells. Although $CD4^+$ T cells do not directly kill tumor cells, they secrete cytokines that suppress tumor growth. Model (3.2) explores interactions among tumor cells, $CD4^+$ T cells, and cytokines, focusing on the role of $CD4^+$ T cells in promoting tumor regression or dormancy. Consistent with [43], our results show that tumor cells persist without treatment, though $CD4^+$ T cells help slow their growth. Simulations indicate that high-dose cytokine therapy can eradicate tumors, whereas low doses may not. Furthermore, $CD4^+$ T cells are more effective than low-dose cytokine treatment alone, though both are effective when cytokines are administered at high levels.

This paper presents a mathematical model that explains how the immune system works, especially on its role in treatment strategies in cancer treatment. The remainder of the paper is organized as follows. Section 3.2, develops the mathematical framework of the system. Section 3.3 focuses on the model's solutions and key properties. In Section 3.4, under cytokine treatment, we conduct a detailed analysis of equilibrium solutions, stability, and bifurcation behaviors (Section 3.4.1) and limit cycle bifurcations and their stability (Section 3.4.2). Section 3.5 investigates treatment with $CD4^+$ T cells and bifurcation of multiple limit cycles (Section 3.5.2). Section 3.6 considers combination therapy involving both $CD4^+$ T cells and cytokines. Finally, Section 3.7 summarizes the main findings, discusses their potential implications, and presents the conclusion.

3.2 Mathematical Modeling

Consider the following model developed by Anderson [15], described by the system of ODEs:

$$\begin{aligned}\frac{dx}{dt} &= rx\left(1 - \frac{x}{K}\right) - \frac{\delta xz}{m+x}, \\ \frac{dy}{dt} &= \frac{\beta xy}{k+x} - ay + I_1, \\ \frac{dz}{dt} &= \frac{\alpha xy}{b+x} - \mu z + I_2,\end{aligned}\tag{3.2}$$

where x, y and z represent the densities of the tumor cells, CD4⁺ T cells, and antitumor cytokines, respectively. The tumor cells exhibit a logistic growth, and the interactions among the variables are modelled using Michaelis-Menten kinetics, each governed by distinct half-saturation constants. This formulation captures regulated tumor growth, along with constrained CD4⁺ T cell and cytokine production as influenced by tumor presence.

All parameters $r, K, m, a, b, k, \mu, \beta, \delta$ and α are assumed to be positive constants. The term $rx(1 - \frac{x}{K})$ models per capita growth rate of tumor cells and $\frac{\delta xz}{m+x}$ represents their reduction due to cytokine activity. The recruitment of CD4⁺ T cells through interaction with tumor cells is represented by $\frac{\beta xy}{k+x}$, and their natural decay is modeled by ay . Cytokine production driven by CD4⁺ T cells is given by $\frac{\alpha xy}{b+x}$, and their degradation is represented by μz . Immunotherapy is incorporated through the time-dependent input functions $I_1 \geq 0$ and $I_2 \geq 0$, where $I_1(t)$ models CD4⁺ T cell therapy and $I_2(t)$ represents cytokine-based treatment. A comprehensive list of the model parameters, including their biological interpretations and units, is given in Table 3.1 of [15]. All population densities are measured per unit volume, and time is measured in days.

We non-dimensionalize the model by introducing the following substitutions:

$$x = KX, \quad y = \frac{Kr^2}{\alpha\delta} Y, \quad z = \frac{Kr}{\delta} Z, \quad t = \frac{1}{r} \tau,$$

Table 3.1: Parameters used in system (3.2).

Parameter	Biological meaning	Unit
m	half-saturation constant of the tumor-killing rate	cm^3
β	Maximum CD4^+ T cells production rate	day^{-1}
k	half-saturation constant of the CD4^+ T cells production rate	cm^3
a	death rate of the CD4^+ T cells	day^{-1}
b	half-saturation constant of the cytokine production rate	cm^3
μ	cytokine loss rate	day^{-1}
r	growth rate of the tumor	day^{-1}
K	carrying capacity of the tumor	cm^3
δ	maximum tumor killing rate by cytokine	day^{-1}
α	maximum production rate of cytokine	day^{-1}
I_1	treatment by CD4^+ T cells	$\text{cm}^3\text{day}^{-1}$
I_2	treatment by Cytokine	$\text{cm}^3\text{day}^{-1}$

which yield the following dimensionless model:

$$\begin{aligned} \frac{dX}{d\tau} &= X\left(1 - X - \frac{Z}{A + X}\right), \\ \frac{dY}{d\tau} &= Y\left(\frac{BX}{C + X} - D\right) + G_1, \\ \frac{dZ}{d\tau} &= \frac{XY}{E + X} - FZ + G_2, \end{aligned} \tag{3.3}$$

with positive initial conditions:

$$X(0) = X_0 \geq 0, \quad Y(0) = Y_0 \geq 0, \quad Z(0) = Z_0 \geq 0. \tag{3.4}$$

The new parameters in system (3.3) are defined as

$$\begin{aligned} A &= \frac{m}{K}, \quad B = \frac{\beta}{r}, \quad C = \frac{k}{K}, \quad D = \frac{a}{r}, \\ E &= \frac{b}{K}, \quad F = \frac{\mu}{r}, \quad G_1 = \frac{I_1\alpha\delta^2}{r^3K^2}, \quad G_2 = \frac{I_2}{r}. \end{aligned} \tag{3.5}$$

In this study, we consider the dynamics of the dimensionless model (3.3) within the full six-dimensional parameter space (A, B, C, D, E, F) , with a particular emphasis on scenarios

involving treatment, i.e., when $G_1(\tau) \neq 0$ and $G_2(\tau) \neq 0$. Using Hopf bifurcation theory, we establish the existence of both single and multiple limit cycles, which give rise to various types of bistable behavior. The newly introduced parameters and their biological interpretations are summarized in Table 3.2.

Table 3.2: Parameters used in system (3.3) [15].

Parameter	Biological meaning	Value
A	Half-saturation constant of the tumor-killing rate	0.1
B	Maximum CD4 ⁺ T cells production rate	6
C	Half-saturation constant of the CD4 ⁺ T cells production rate	1
D	Death rate of the CD4 ⁺ T cells	3
E	Half-saturation constant of the cytokine production rate	0.1
F	Cytokine loss rate	5000

3.3 Solution Properties of Model (3.3)

To begin, we investigate the properties of solutions to the model (3.3), and establish the following result:

Theorem 3.3.1 *The solutions of the model (3.3) remain positive and bounded provided that the initial condition is positive.*

Proof We start by examining the well-posedness of the solutions to model (3.3). By the fundamental theory of ODEs the (3.3) admits a unique solution for any given set of initial conditions (3.4). Moreover, it is easy to verify that the solutions remain positive for all time, provided that the initial conditions are positive. Applying the method of variation of parameters, we obtain the explicit solutions to system (3.3) as follows:

$$\begin{aligned}
 X(\tau) &= X(0) e^{\int_0^\tau [1-X(s)-\frac{Z(s)}{A+X(s)}] ds}, \\
 Y(\tau) &= Y(0) e^{\int_0^\tau [\frac{BX(s)}{C+X(s)}-D] ds} + G_1 \int_0^\tau e^{\int_s^\tau [\frac{BX(u)}{C+X(u)}-D] du} ds, \\
 Z(\tau) &= e^{-F\tau} \left[Z(0) + \int_0^\tau \frac{X(s)Y(s)}{E+X(s)} e^{Fs} ds \right] + G_2 \int_0^\tau e^{\int_s^\tau [\frac{X(u)Y(u)}{E+X(u)}] e^{Fu}} du ds.
 \end{aligned}$$

It is obvious that $X(\tau)$ and $Y(\tau)$ are positive for $\tau > 0$, provided that $X(0)$ and $Y(0)$ are positive. Then, $Z(\tau) > 0$ for $\tau > 0$ due to $X(\tau) > 0$ and $Y(\tau) > 0$.

Proving the boundedness of solutions is less straightforward and requires a comparison argument. From the first equation in system (3.3), we observe that the variable $X(\tau)$ satisfies the differential inequality:

$$\frac{dX}{d\tau} \leq X(1 - X).$$

The solution to this auxiliary inequality is well known to be bounded and, in fact, converges to the equilibrium point $X = 1$. Therefore, $X(\tau)$ is bounded for all $\tau > 0$.

To show that $Y(\tau)$ and $Z(\tau)$ are also bounded, we proceed by contradiction. First, assume that $Z(\tau)$ is unbounded. Then, from the X -equation in model (3.3), it follows that $\lim_{\tau \rightarrow \infty} X(\tau) = 0$, due to the unbounded negative influence from the Z -dependent term. Substituting this into the Y -equation yields the limiting form,

$$\frac{dY}{d\tau} = -DY + G_1,$$

which implies that $\lim_{\tau \rightarrow \infty} Y(\tau) = \frac{G_1}{D}$. Now consider the Z -equation under the assumption that $X(\tau)$ approaches zero and $Y(\tau)$ remains bounded. In this case, the equation reduces asymptotically to

$$\frac{dZ}{d\tau} = -FZ + G_2,$$

indicating that $\lim_{\tau \rightarrow \infty} Z(\tau) = \frac{G_2}{F}$, a contradiction to the assumption that $Z(\tau)$ is unbounded. Therefore, $Z(\tau)$ must be bounded.

Similarly, assume that $Y(\tau)$ is unbounded. From the structure of the Z -equation, this would imply that $Z(\tau)$ becomes unbounded as well (since Z depends on the product XY), which in turn forces $X(\tau) \rightarrow 0$, as previously argued. Substituting $\lim_{\tau \rightarrow \infty} X(\tau) = 0$ into the Y -equation again gives

$$\frac{dY}{d\tau} = -DY + G_1,$$

implying that $Y(\tau)$ tends to the finite steady-state value $\frac{G_1}{D}$, which contradicts the assumption that $Y(\tau)$ is unbounded. Hence, both $Y(\tau)$ and $Z(\tau)$ are bounded for all $\tau > 0$.

From these arguments, it follows that all solutions of system (3.3) remain positive and bounded for all $\tau > 0$, and the system admits a positively invariant, bounded region.

In the subsequent sections, we investigate the impact of immunotherapy on tumor regression through a series of targeted analyses. We begin by exploring the role of cytokine therapy in modulating tumor dynamics. This is followed by an examination of limit cycle bifurcations and an assessment of their stability. We then analyze the effects of treatments involving CD4⁺ T cells and explore the emergence and stability of multiple limit cycles. Finally, we study the combined effects of cytokine therapy and CD4⁺ T cell treatment, with particular emphasis on the efficacy of polytherapy.

3.4 Treatment with Cytokine ($G_1 = 0$, $G_2 > 0$).

The dynamics of the tumor, CD4⁺ T and cytokines, including the impact of cytokine treatment, are described by the following system, based on model (3.3):

$$\begin{aligned}\frac{dX}{d\tau} &= X\left(1 - X - \frac{Z}{A + X}\right), \\ \frac{dY}{d\tau} &= Y\left(\frac{BX}{C + X} - D\right), \\ \frac{dZ}{d\tau} &= \frac{XY}{E + X} - FZ + G_2,\end{aligned}\tag{3.6}$$

where $G_2 > 0$ denotes that immunotherapy involves the constant administration of cytokine at rate G_2 per unit time to the tumor site. By setting $\frac{dX}{d\tau} = \frac{dY}{d\tau} = \frac{dZ}{d\tau} = 0$, the equilibrium

solutions are obtained as follows:

$$\begin{aligned}
 E_0 &= (0, 0, \frac{G_2}{F}), \\
 E_1 &= (X_1, 0, \frac{G_2}{F}), \quad \text{or} \quad E_{1\pm} = (X_{1\pm}, 0, \frac{G_2}{F}), \quad \text{with} \quad X_{1\pm} = \frac{1}{2}(1 - A \pm \sqrt{\Delta_1}), \\
 E_2 &= \left(\frac{CD}{B-D}, \frac{[E(B-D) + CD](G_{2t} - G_2)}{CD}, \frac{[B - D(1 + C)][A(B-D) + CD]}{(B-D)^2} \right),
 \end{aligned} \tag{3.7}$$

where E_0 and E_1 (or $E_{1\pm}$) represent boundary equilibria, while E_2 is the interior (positive) equilibrium. Note that E_1 may include two solutions, with $X_1 = X_{1\pm}$.

For convenience, define the following auxiliary quantities:

$$\begin{aligned}
 R_0 &= \frac{FA}{G_2}, \\
 C_t &= \frac{1}{2D}(B-D)(1 - A + \sqrt{\Delta_1}), \\
 G_{2t} &= \frac{F[B - D(C + 1)][A(B-D) + DC]}{(B-D)^2}, \\
 \Delta_1 &= (1 + A)^2 - \frac{4G_2}{F},
 \end{aligned} \tag{3.8}$$

where the quantity R_0 is called a basic reproduction number because it determines the growth of the tumor cell population X near the tumor-free equilibrium $E_0 = (0, 0, \frac{G_2}{F})$. If $R_0 > 1$, X grows, indicating that small tumor perturbations can expand; if $R_0 < 1$, X decays, so the tumor-free state remains stable. Thus, R_0 acts as a threshold parameter controlling the stability of E_0 .

3.4.1 Stability and bifurcation analysis

We now present two theorems: one regarding the existence of the equilibria, and the other addressing the stability of the boundary equilibria E_0 and E_1 . The stability of E_2 and the occurrence of Hopf bifurcation will also be discussed in the second theorem.

Theorem 3.4.1 *The existence conditions for the equilibrium solutions of system (3.6) are given below.*

1. *The boundary equilibrium E_0 exists for all positive parameter values.*

2. *For the boundary equilibrium E_1 , three cases arise:*

(a) *If $A > 0$ and $G_2 < AF$, there exists one equilibrium, $E_1 = (\frac{1}{2}(1-A + \sqrt{\Delta_1}), 0, \frac{G_2}{F})$.*

(b) *If $A < 1$ and $G_2 = AF$, there is one equilibrium $E_1 = (1-A, 0, \frac{G_2}{F})$.*

(c) *If $A < 1$ and $AF < G_2 < \frac{(A+1)^2 F}{4}$, then two equilibria $E_{1\pm}$ exist.*

3. *The interior (endemic) equilibrium E_2 exists if and only if $B > D(1+C)$ and $G_2 < G_{2t}$.*

Proof The existence of E_0 is immediate since it requires only positive parameter values.

To analyze the equilibrium E_1 , we set $Y_1 = 0$ and $Z_1 = \frac{G_2}{F}$, and solve the steady-state condition for X_1 :

$$F_1(X_1) = X_1^2 - (1-A)X_1 + \frac{G_2}{F} - A = 0. \quad (3.9)$$

This is a quadratic equation. A positive root $X_1 = X_{1+}$ always exists when $G_2 < AF$. When $G_2 = AF$, a single positive root $X_1 = 1 - A$ exists if $A < 1$. If $G_2 > AF$ and $\Delta_1 > 0$, two positive roots exist provided $A < 1$. These correspond to the boundary equilibria E_1 or $E_{1\pm}$.

For the interior equilibrium E_2 , setting $\frac{dX}{dt} = 0$ yields $Z_2 = (1 - X_2)(A + X_2) > 0$, which implies $X_2 < 1$. Next, setting $\frac{dY}{dt} = 0$ gives $X_2 = \frac{CD}{B-D}$, which requires $B > D(1 + C)$ for positivity.

Substituting $X_2 = \frac{CD}{B-D}$ into the steady-state equation for Z , we obtain

$$Y_2 = \frac{(E + X_2)(FZ_2 - G_2)}{X_2} = \frac{[E(B - D) + CD](G_{2t} - G_2)}{CD},$$

so $Y_2 > 0$ requires $G_2 < G_{2t}$ (i.e., $C < C_t$).

Finally, substituting X_2 into the expression for Z_2 yields

$$Z_2 = (1 - X_2)(A + X_2) = \frac{[B - D(1 + C)][A(B - D) + CD]}{(B - D)^2},$$

which is positive when $B > D(1 + C)$.

Theorem 3.4.2 *The stability conditions for the equilibrium solutions of system (3.6) are given as follows:*

1. *The boundary equilibrium E_0 is locally asymptotically stable (LAS) for $R_0 < 1$, and unstable for $R_0 > 1$.*
2. *The boundary equilibrium E_{1-} is unstable (a saddle). A transcritical bifurcation occurs at $R_0 = 1$ (i.e., at $G_2 = FA$) between E_0 and E_{1-} .*
3. *When $G_2 \leq FA$, (i.e., $R_0 \geq 1$), the boundary equilibrium E_{1+} is LAS for $C > C_t$, and unstable for $C < C_t$. Note that $A < 1$ if $G_2 = FA$.*
4. *Further details about E_{1+} are as follows:*
 - (a) *If $A < 1$ and $AF < G_2 < \frac{1}{4}F(1 + A)^2$, then E_{1+} is LAS for $C > C_t$, and unstable for $C < C_t$.*
 - (b) *A transcritical bifurcation occurs between E_{1+} and E_2 at the critical point $C = C_t$, which is equivalent to $G_2 = G_{2t}$.*
 - (c) *No Hopf bifurcation can occur from the equilibrium E_{1+} .*
5. *A Hopf bifurcation can occur from the interior equilibrium E_2 at the critical point $G_2 = G_{2H}$ when F is sufficiently large. (An explicit expression for G_{2H} is given in the proof).*
6. *System (3.6) does not exhibit a Bogdanov-Takens (B-T) bifurcation (A Bogdanov-Takens (B-T) bifurcation occurs when an equilibrium point of a dynamical system*

has a double zero eigenvalue and satisfies certain non-degeneracy conditions. It is a codimension-2 bifurcation, meaning that two parameters must be varied simultaneously to observe it. Near a B–T point, the system can exhibit saddle-node, Hopf, and homoclinic bifurcations, all emerging from the same critical equilibrium.)

Proof The stability of equilibrium solutions is determined from the Jacobian matrix of (3.6), given by

$$J(X, Y, Z) = \begin{bmatrix} \frac{(1-2X)A^2 - (4X^2 - 2X + Z)A - 2X^3 + X^2}{(A+X)^2} & 0 & -\frac{X}{A+X} \\ \frac{BCY}{(C+X)^2} & \frac{BX}{C+X} - D & 0 \\ \frac{EY}{(E+X)^2} & \frac{X}{E+X} & -F \end{bmatrix}. \quad (3.10)$$

Evaluating the Jacobian at E_0 and E_1 , we obtain

$$J(E_0) = \begin{bmatrix} 1 - \frac{G_2}{FA} & 0 & 0 \\ 0 & -D & 0 \\ 0 & 0 & -F \end{bmatrix},$$

and

$$J(E_1) = \begin{bmatrix} \frac{X_1(1-A-2X_1)}{A+X_1} & 0 & -\frac{X_1}{A+X_1} \\ 0 & \frac{(B-D)X_1 - CD}{C+X_1} & 0 \\ 0 & \frac{X_1}{E+X_1} & -F \end{bmatrix}.$$

Since these matrices are triangular, their eigenvalues lie on the diagonal. Therefore, E_0 is LAS if $1 - \frac{G_2}{FA}$ (i.e., $R_0 < 1$), and unstable otherwise.

To analyze E_1 , note that

$$X_{1-} = \frac{1}{2}(1 - A - \sqrt{\Delta_1}) \implies 1 - A - 2X_{1-} = \frac{1}{2}(1 - A + \sqrt{\Delta_1}) > 0 \quad \text{for } A < 1.$$

This implies that E_{1-} is unstable when it exists ($A < 1$, $AF < G_2 < \frac{1}{4}F(1 + A)^2$). At $G_2 = AF$, $X_{1-} = 0$ and one eigenvalue of J_{E_1} is zero, indicating a transcritical bifurcation at $G_2 = AF$. However, both E_0 and E_{1-} are unstable near this point, so the bifurcation occurs on a submanifold.

Next, consider E_{1+} . Three cases arise.

(a) $G_2 < AF$ and $A > 0$:

$$1 - A - 2X_{1+} = -\frac{1}{2}[\sqrt{\Delta_1} - (1 - A)] = -\frac{2(A - \frac{G_2}{F})}{\sqrt{\Delta_1} + 1 - A} < 0,$$

regardless whether $A \geq 1$ or $A < 1$. So the sign of the second eigenvalue, $(B - D)X_{1+} - CD$, determines the stability. Setting this equal zero defines a critical value $C = C_t$. Then,

- E_{1+} is LAS if $C > C_t$, unstable if $C < C_t$.
- At $C = C_t$ (i.e., $G_2 = G_{2t}$), a transcritical bifurcation occurs between E_{1+} and E_2 .

Indeed, at this critical point,

$$X_{1+} = \frac{1}{2}(1 - A + \sqrt{\Delta_1}) = \frac{\frac{1}{2D}(B - D)(1 - A + \sqrt{\Delta_1})D}{B - D} = \frac{C_t D}{B - D} = X_2.$$

(b) $G_2 = AF$ and $A < 1$: The characteristic polynomial is

$$P_{E_{1+}}(\lambda) = (\lambda + F)(\lambda + (1 - A)^2) \left(\lambda + \frac{CD - (1 - A)(B - D)}{C + 1 - A} \right),$$

which implies that E_{1+} is

- LAS if $C > (1 - A)\left(\frac{B}{D} - 1\right)$,
- unstable otherwise, with a transcritical bifurcation at $C = (1 - A)\left(\frac{B}{D} - 1\right)$.

(c) $AF < G_2 < \frac{1}{4}F(1 + A)^2$ and $A < 1$: Same conclusion as in (a):

- E_{1+} is LAS if $C > C_t$, unstable if $C < C_t$.
- A transcritical bifurcation occurs at $C = C_t$.

Thus, no Hopf bifurcation arises from E_1 . The bifurcation diagram is shown in Figure 3.3.

Now, consider the interior equilibrium E_2 . Evaluating the Jacobian at E_2 , we obtain

$$J(E_2) = \begin{bmatrix} -\frac{C[(-A + 2C + 1)D + B(A - 1)]D}{(B - D)[(C - A)D + AB]} & 0 & -\frac{CD}{(C - A)D + AB} \\ -\frac{[(C - E)D + EB](G_2 - G_{2t})(B - D)^2}{C^2BD} & 0 & 0 \\ -\frac{(G_2 - G_{2t})(B - D)^2E}{[(C - E)D + EB]CD} & \frac{CD}{(C - E)D + EB} & -F \end{bmatrix}, \quad (3.11)$$

which has the characteristic polynomial,

$$P_{E_2}(\lambda) = \lambda^3 + a_1\lambda^2 + a_2\lambda + a_3,$$

where

$$\begin{aligned} a_1 &= \frac{F(B - D)[A(B - D) + CD] + CD[2CD - (1 - A)(B - D)]}{(B - D)[A(B - D) + CD]}, \\ a_2 &= \frac{CDF(B - D)^3[E(B - D) + CD][2CD - (1 - A)(B - D)] + E(B - D)^3(G_{2t} - G_2)}{(B - D)[A(B - D) + CD][E(B - D) + CD]}, \\ a_3 &= \frac{D(B - D)^2(G_{2t} - G_2)}{B[A(B - D) + CD]}. \end{aligned} \quad (3.12)$$

For $A < 1$, system (3.6) exhibits *bistability*, where the tumor-free equilibrium E_0 and

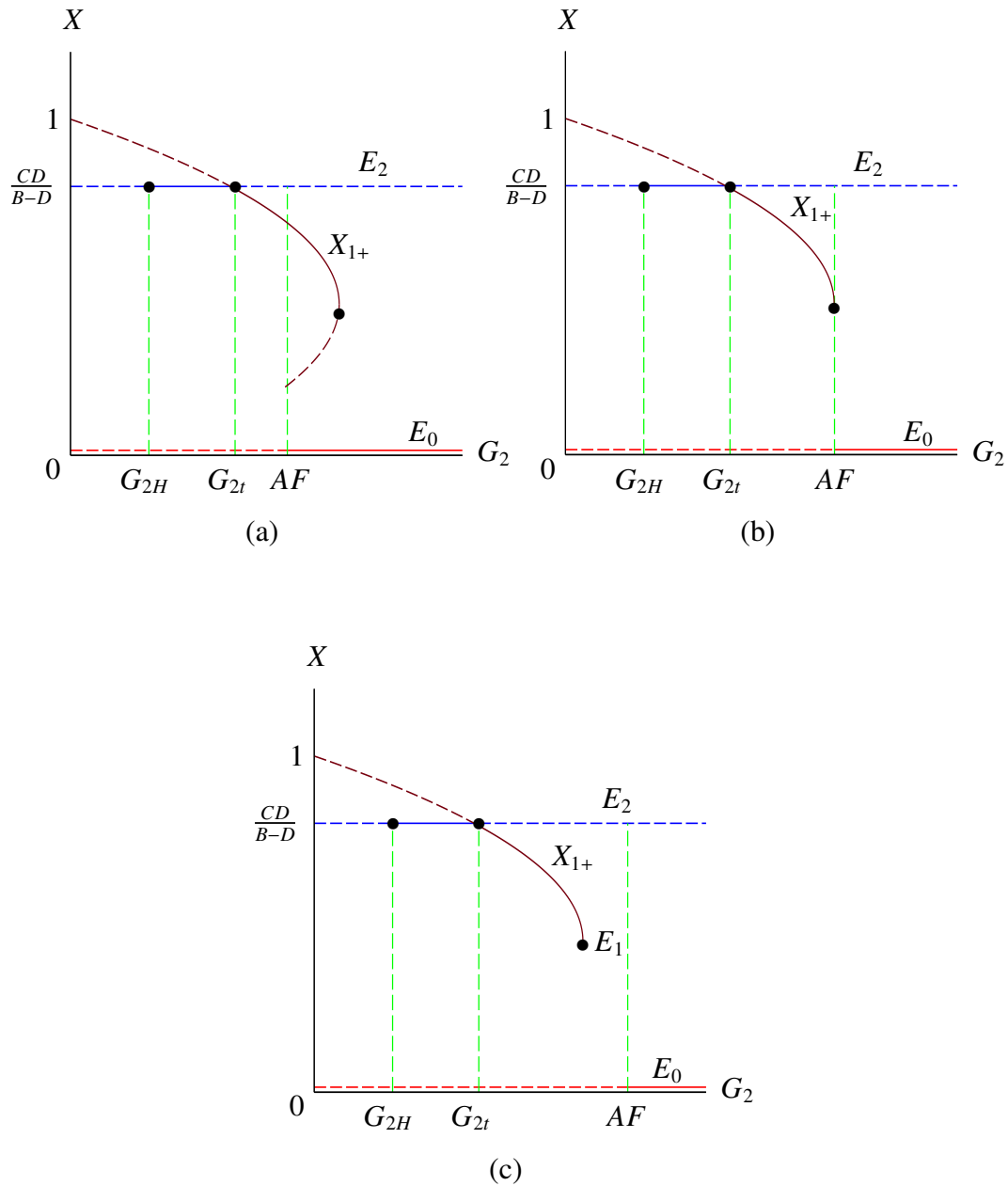


Figure 3.3: Bifurcation diagram of system (3.6) for (a) $A < 1$, (b) $A = 1$, and (c) $A \geq 1$, projected on the G_2 - X plane, showing the equilibria E_0 , E_1 and E_2 , marked by red, brown and blue colors, respectively. Solid and dotted lines/curves denote stable and unstable equilibria, respectively.

the tumor-present equilibrium E_2 are both stable, separated by an unstable saddle E_1 . The long-term outcome depends on the initial tumor load $X(0)$: if $X(0) < X_1$, the tumor is eradicated (E_0); if $X(0) > X_1$, the tumor persists (E_2). Biologically, cytokine treatment (G_2)

must exceed a critical threshold G_{2H} for tumor elimination, illustrating threshold-dependent therapeutic success.

Since the existence of E_2 requires $B > D(1 + C)$ and $G_2 < G_{2t}$ (i.e., $C < C_t$), we have $a_3 > 0$. At the critical point $G_2 = G_{2t}$ (equivalently, $C = C_t$), $a_3 = 0$. In this case, the condition $2C_tD - (1 - A)(B - D) = (B - D)\sqrt{\Delta_1} > 0$ guarantees that $a_1 > 0$ and $a_2 > 0$. The absence of a double zero eigenvalue at $E_2 = E_{1+}$ confirms that no Bogdanov–Takens bifurcation occurs in system (3.6).

Furthermore, it can be shown that at the critical point $G_2 = G_{2t}$ (or $C = C_t$),

$$X_2 = \frac{C_t D}{B - D} = \frac{1}{2}(1 - A + \sqrt{\Delta_1}) = X_{1+}, \quad Y_2 = \frac{[E(B - D) + CD](G_{2t} - G_2)}{CD} = 0,$$

$$Z_2 = \frac{(B - D - C_t D)[A(B - D) + C_t D]}{(B - D)^2} = A + \frac{1}{4}(1 - A - \sqrt{\Delta_1})(1 - A + \sqrt{\Delta_1}) = \frac{G_2}{F},$$

which confirms that a transcritical bifurcation occurs between E_{1+} and E_2 at $G_2 = G_{2t}$.

To determine whether Hopf bifurcation occurs at E_2 , which exists for $B > D(1 + C)$ and $G_2 < G_{2t}$ (i.e., $C < C_t$), we analyze the Routh-Hurwitz determinant $\Delta_2 = a_1 a_2 - a_3$. To simplify the analysis, let

$$G_2 = G_{2t} - h, \quad (0 < h < G_{2t}).$$

Then we have

$$a_1 = \frac{F(B - D)[A(B - D) + CD] + CD[2CD - (1 - A)(B - D)]}{(B - D)[A(B - D) + CD]},$$

$$a_2 = \frac{CDF[E(B - D) + CD][2CD - (1 - A)(B - D)] + E(B - D)^3 h}{(B - D)[A(B - D) + CD][E(B - D) + CD]},$$

$$a_3 = \frac{D(B - D)^2 h}{B[A(B - D) + CD]},$$

which clearly shows that $a_3 > 0$ for $h > 0$. Moreover, $a_1 > 0$ and $a_2 > 0$ for $h > 0$ and $\max\{0, \frac{(1-A)(B-D)}{2D}\} < C < C_t$.

Let

$$\Delta_2 = \frac{\Delta_{2a}}{2B(B-D)^2[A(B-D) + CD]^2[E(B-D) + CD]},$$

where

$$\Delta_{2a} = M_0 + M_1 h,$$

with

$$\begin{aligned} M_0 &= BCDF[E(B-D) + CD][(A-1)(B-D) + 2CD] \\ &\quad \times \{[(A-1)(B-D) + 2CD][F(B-D) + 2CD] + F(B-D)^2(1+A)\} \\ M_1 &= 2(B-D)^3\{E[(B-D)(A(B-D) + CD)(B(F-D) + D^2) \\ &\quad + BCD((A-1)(B-D) + 2CD)] - D^2C(B-D)[A(B-D) + CD]\}. \end{aligned}$$

Consider the condition $\Delta_2 = 0$ for $B > D(1 + C)$, which can be rewritten as $B > D$ and $C < \frac{B}{D} - 1$ to get the following conditions:

$$B > D, \quad \max\left\{0, \frac{(1-A)(B-D)}{2D}\right\} < C < \min\left\{C_t, \frac{B}{D} - 1\right\} = C_t, \quad (3.13)$$

where the condition $G_2 < G_{2t}$ has been replaced by $C < C_t$. To investigate the possibility of a Hopf bifurcation at E_2 , we require a positive solution for h from the equation $M_0 + M_1 h = 0$. Define the Hopf bifurcation point as

$$h_H = -\frac{M_0}{M_1}, \quad \text{with } 0 < h_H < G_{2t}.$$

Under condition (3.13), it is seen that $M_0 > 0$. Thus, a Hopf bifurcation requires $M_1 < 0$. The bracketed term in M_1 must be positive, which is linear expression in E with a positive coefficient if $F > D$, a condition typically satisfied in applications where F is large. Hence,

define the critical value,

$$E_c = \frac{D^2 C(B-D)[A(B-D) + CD]}{(B-D)[A(B-D) + CD][B(F-D) + D^2] + BCD[(A-1)(B-D) + 2CD]}. \quad (3.14)$$

Then, $M_1 < 0$ for $E < E_c$. Moreover, we must ensure $h_H < G_{2t}$, leading to

$$h_H - G_{2t} = E N_1 - 2CD^2 N_2,$$

where

$$\begin{aligned} N_1 &= (B-D)\{BCD[(A-1)(B-D) + 2CD] \\ &\quad \times [((A-1)(B-D) + 2CD)(F(B-D) + 2CD) \\ &\quad + F(B-D)^2(1+A) + 2(B-D(1+C))(A(B-D) + CD)] \\ &\quad + 2(B-D)[B-D(1+C)][A(B-D) + CD][A(B-D) + CD][B(F-D) + D^2]\}, \\ N_2 &= -FCB(B-D)[A(B-D) + CD][(A-1)(B-D) + 2CD] \\ &\quad + \frac{1}{8}(B-D)^5(1+A)^3 + [(A-1)(B-D) + 2CD] N_3, \\ N_3 &= -2BD^2 C^3 + \frac{1}{2}D(B-D)[2(1-A)B - (B-D)D] C^2 \\ &\quad + \frac{1}{4}D(B-D)^3(1-3A)C + \frac{1}{8}(B-D)^4[1 + A(4-A)]. \end{aligned}$$

It is evident that $N_1 < 0$. Therefore, $h_H - G_{2t} < 0$ yields the condition: $0 < E < E_* = \frac{2CD^2 N_2}{N_1}$,

which in turn requires $N_2 > 0$. This can be achieved by imposing the condition $F < F_c$,

where

$$F_c = \frac{\frac{1}{8}(B-D)^5(1+A)^3 + [(A-1)(B-D) + 2CD] N_3}{CB(B-D)[A(B-D) + CD][(A-1)(B-D) + 2CD]}, \quad (3.15)$$

provided $N_3 > 0$. To ensure $N_3 > 0$, assume

$$A < \min \left\{ \frac{1}{3}, 1 - \frac{D(B-D)}{2B} \right\},$$

along with $2B > BD + D^2$, which holds for $B > D$ if $D \leq 2$, or $D < B < \frac{D^2}{D-2}$ if $D > 2$. With these, all terms in N_3 except the first are positive. Since $N_3(C)$ is a cubic polynomial in C , it satisfies the following properties:

$$\begin{aligned} \lim_{C \rightarrow -\infty} N_3 &= +\infty, \\ N_3(0) &= \frac{1}{8}(B-D)^4[(1+A)(4-A)] > 0 \\ \left. \frac{dN_3}{dC} \right|_{C=0} &= \frac{1}{4}D(B-D)^3(1-3A) > 0, \\ N_3\left(\frac{(1-A)(B-D)}{2D}\right) &= \frac{1}{8}(B-D)^4(1+A)^2 > 0 \\ N_3\left(\frac{B}{D}-1\right) &= -\frac{1}{8D}(B-D)^3(1+A)[(A+1)D(B-D)+8B] < 0, \\ \lim_{C \rightarrow +\infty} N_3 &= -\infty. \end{aligned}$$

These properties imply that N_3 has one local minimum for $C < 0$ and one local maximum for $C > 0$, and thus a unique positive root $C = C_* \in (0, \frac{B}{D} - 1)$. Since C_t is the upper bound ensuring $Y_2 > 0$, it follows that $C_* < C_t$.

Summarizing the above discussions, we conclude that Hopf bifurcation at E_2 occurs when

$$\begin{aligned} B > D \text{ if } D \leq 2, \quad \text{or} \quad 2 < D < B < \frac{D^2}{D-2}, \\ A < \min \left\{ \frac{1}{3}, 1 - \frac{D(B-D)}{2B} \right\}, \\ \frac{(1-A)(B-D)}{2D} < C < C_* = \frac{2CD^2N_2}{N_1}, \\ F < F_c, \quad E < E_*. \end{aligned} \tag{3.16}$$

Finally, we prove that $E_* < E_c$ by computing

$$\begin{aligned} h_H - G_{2t}|_{E=E_c} &= E_c N_2 - 2CD^2 N_2 \\ &= \frac{C^2 D^2 B^2 [(A-1)(B-D)+2CD] \{ [(A-1)(B-D)+2CD][F(B-D)+2CD] + F(B-D)^2(1+A) \}^2}{[(A-1)(B-D)+2CD] \{ (B-D)(B(F-D)+D^2) + 2CBD \} + (A+1)(B-D)^2 [B(F-D)+D^2]} \\ &> 0, \end{aligned}$$

which confirms that $EN_2 - 2CD^2N_2 = 0$ has a unique positive solution $E = E_* \in (0, E_c)$.

Thus, $h_H < G_{2t}$ for all $E < E_*$. Returning to the original bifurcation parameter G_2 , define the Hopf critical point as

$$G_{2H} = G_{2t} - h_H.$$

Therefore, a Hopf bifurcation arises from E_2 at $G_2 = G_{2H}$ under the conditions specified in (3.16).

The proof of Theorem 3.4.2 is complete.

3.4.2 Limit cycle bifurcation and its stability

Once the Hopf bifurcation point is identified, where a set of limit cycles (isolated periodic motions) emerges, the next step is to determine the stability of these bifurcating limit cycles. While numerical simulations can provide insight into stability, they do not yield analytical expressions that describe how the stability depends on changes in parameters.

In planar dynamical systems, it is well established that the stability of limit cycles is determined by the sign of the first-order focus value, which can be computed using a relatively straightforward formula involving second- and third-order derivatives of the vector field at the Hopf critical point. However, for higher-dimensional systems, these analytical expressions become significantly more complex, often requiring the reduction of the system to its center manifold. As a result, symbolic computation tools such as Maple are commonly used to calculate the first-order focus value. Among the various available methods, the normal form method is particularly efficient for computing focus

values, especially in higher-dimensional systems and for obtaining higher-order values.

We employ normal form theory in conjunction with the Maple program developed in [44] to analyze the Hopf bifurcation in system (3.6). The normal form of the Hopf bifurcation, capturing dynamics on the two-dimensional center manifold near the critical point, is given in polar coordinates as

$$\begin{aligned}\frac{dr}{d\tau} &= r(v_0\mu + v_1r^2 + v_2r^4 + \dots), \\ \frac{d\theta}{d\tau} &= \omega_c + t_0\mu + t_1r^2 + t_2r^4 + \dots\end{aligned}$$

where $\mu = G_2 - G_{2H}$, and r and θ represent the amplitude and phase of motion, respectively. The coefficient v_k is the k th-order focus value, which governs the stability of the bifurcating limit cycles. If $v_1 < 0$, the Hopf bifurcation is supercritical and the resulting limit cycles are stable; if $v_1 > 0$, the Hopf bifurcation is subcritical and the limit cycles are unstable. We have established that system (3.6) always undergoes a Hopf bifurcation, leading to emergence of limit cycles. In this paper, we focus on the case of a single limit cycle and leave the analysis of multiple limit cycles to future work.

To identify the Hopf bifurcation point, $G_2 = G_{2H}$, we apply the formulas given in (3.25). We fix the parameter values as follows:

- $B = 6$ and $D = 3$;
- Based on the condition $A < 1 - \frac{(B-D)D}{2B} = \frac{1}{4}$, we set $A = \frac{1}{10}$;
- From $\frac{(1-A)(B-D)}{2D} = \frac{9}{20} < C < C_* = 0.622346\dots$, we choose $C = \frac{1}{2}$;
- Calculating $F_c = \frac{107}{12}$, we set $F = 6 < F_c$;
- Then, with $E < E_* = \frac{35}{806}$, we choose $E = \frac{1}{30}$.

Thus, the critical Hopf value is $G_{2H} = \frac{183}{1075}$, and the full parameter set is:

$$A = \frac{1}{10}, \quad B = 6, \quad C = \frac{1}{2}, \quad D = 3, \quad E = \frac{1}{30}, \quad F = 6. \quad (3.17)$$

The numerical coefficients in the transformation matrix come directly from evaluating the Jacobian matrix of system (3.6) at the Hopf equilibrium point E_2 , using the chosen parameter set in (3.17). In other words, these numbers are obtained by linearizing the system at the equilibrium, computing the eigenvectors, and normalizing them to construct the coordinate change that reduces the system to its canonical Hopf form. To apply normal form theory to compute the first-order focus value (also known as the first Lyapunov constant), we introduce the affine transformation,

$$\begin{pmatrix} X \\ Y \\ Z \end{pmatrix} = \begin{pmatrix} \frac{1}{2} \\ \frac{9344}{5375} \\ \frac{3}{10} \end{pmatrix} + \begin{bmatrix} -\frac{2150}{20951} & \omega_c & \frac{5}{36} \\ -\omega_c & \frac{64\sqrt{215}}{1435} & -\frac{128}{1075} \\ 1 & 0 & 1 \end{bmatrix} \begin{pmatrix} u \\ v \\ w \end{pmatrix}, \quad (3.18)$$

where $\omega_c = \frac{96\sqrt{215}}{5375}$, into system (3.6), yielding a system,

$$\begin{aligned} \frac{du}{d\tau} &= \frac{1}{125(5329\sqrt{215}+5400\omega_c)} \left\{ 219 \left(8 - \frac{32250u}{20951} + \frac{21600\sqrt{215}v}{20951} + \frac{25w}{12} \right) \left(1 - \frac{2150u}{20951} + \frac{1440\sqrt{215}v}{20951} + \frac{5w}{36} \right) \right. \\ &\quad \times \left[10 \left(-\frac{2150u}{20951} + \frac{1440\sqrt{215}v}{20951} + \frac{5w}{36} \right)^2 + \frac{207360u}{20951} + \frac{1440\sqrt{215}v}{20951} + \frac{365w}{36} \right] \dots \left. \right\}, \\ \frac{dv}{d\tau} &= \frac{1}{\omega_c} \left\{ \frac{-73}{86000(5329\sqrt{215}+5400\omega_c)} \left(8 - \frac{32250u}{20951} + \frac{21600\sqrt{215}v}{20951} + \frac{25w}{12} \right) \left(1 - \frac{2150u}{20951} + \frac{1440\sqrt{215}v}{20951} + \frac{5w}{36} \right) \right. \\ &\quad \times \left[10 \left(-\frac{2150u}{20951} + \frac{1440\sqrt{215}v}{20951} + \frac{5w}{36} \right)^2 + \frac{207360u}{20951} + \frac{1440\sqrt{215}v}{20951} + \frac{365w}{36} \right] \dots \left. \right\}, \\ \frac{dw}{d\tau} &= \frac{1}{\omega_c} \left\{ \frac{-219}{125(5329\sqrt{215}+5400\omega_c)} \left(8 - \frac{32250u}{20951} + \frac{21600\sqrt{215}v}{20951} + \frac{25w}{12} \right) \left(1 - \frac{2150u}{20951} + \frac{1440\sqrt{215}v}{20951} + \frac{5w}{36} \right) \right. \\ &\quad \times \left[10 \left(-\frac{2150u}{20951} + \frac{1440\sqrt{215}v}{20951} + \frac{5w}{36} \right)^2 + \frac{207360u}{20951} + \frac{1440\sqrt{215}v}{20951} + \frac{365w}{36} \right] \dots \left. \right\}. \end{aligned} \quad (3.19)$$

We then expand around (u, v, w) and apply the Maple program to compute the normal form up to third order:

$$\frac{dr}{d\tau} = r[v_0\mu + v_1r^2 + O(r^4)], \quad (3.20)$$

Here, $\mu = G_2 - G_{2H}$ is the bifurcation parameter, and v_0, v_1 are the zero-order and

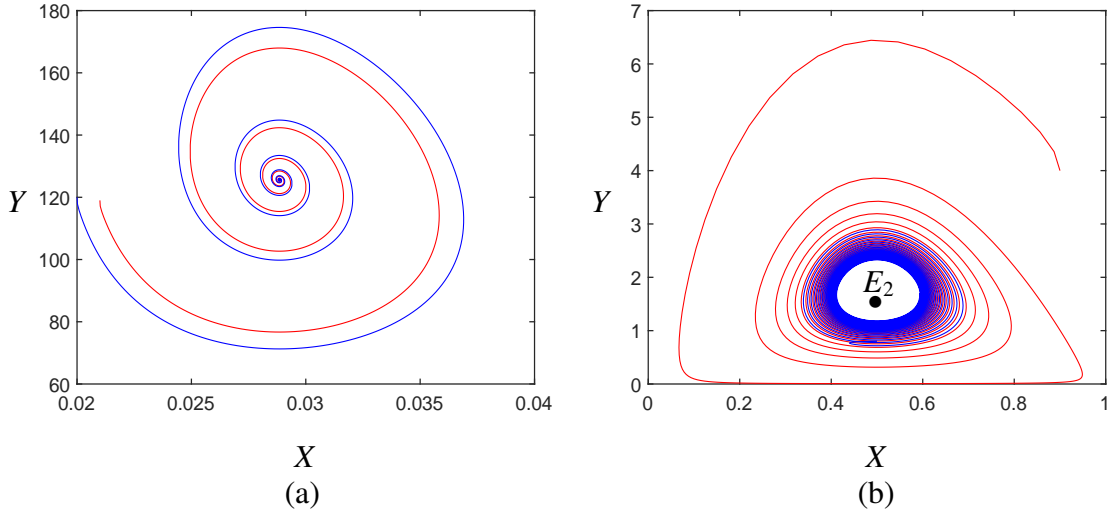


Figure 3.4: Simulated trajectories of system (3.6) for (a) $G_2 = \frac{9}{5}$, converging to the equilibrium E_2 ; and (b) $G_2 = \frac{183}{1075}$, converging to a stable limit cycle.

the first-order focus values. The sign of v_1 determines whether the Hopf bifurcation is supercritical or subcritical. While v_0 is obtained via linear perturbation, v_1 is calculated using the Maple program [44]. We find that

$$v_0 = -\frac{9245}{1166471} < 0, \quad (3.21)$$

and the output of the Maple program gives v_1 as

$$v_1 = -\frac{13060070986532235}{120109436621281436}, \quad (3.22)$$

indicating a supercritical Hopf bifurcation and hence a stable bifurcating limit cycle.

Figure 3.4 illustrates simulation results of system (3.6) for two values of the cytokine influx rate G_2 . When $G_2 = \frac{9}{5} > G_{2H}$, the solution converges to the equilibrium E_2 (Figure 3.4(a)). When $G_2 = \frac{183}{1075} < G_{2H}$, the solution converges to a stable limit cycle (Figure 3.4(b)). This transition reflects a supercritical Hopf bifurcation as G_2 crosses the threshold G_{2H} from above.

Remark: Since in applications, F is large. Although the above example uses a relative

small F value, large values of F are also possible when other parameters are adjusted. For instance, keeping $A = \frac{1}{10}$, $B = 6$, and $D = 3$, we set $C = \frac{181}{400}$, yielding $F_c = \frac{1604394089}{8000200} \approx 200.54$, allowing us to choose $F = 200$. To satisfy the Hopf bifurcation condition, we select $E = \frac{9}{1000000} < E_* \approx 0.00000921$, resulting in $G_{2H} = \frac{29941878877}{7979142685600} \approx 0.003753$.

With this new parameter set, we compute

$$v_1 = -\frac{1391102075195670479483673557445760794191386164214908353476363130412184}{24306898262926014305188937887225796653006867824061673857862519664991437} \approx -0.057231 < 0,$$

confirming once again that the Hopf bifurcation is supercritical and the bifurcating limit cycle is stable.

3.4.3 Stability at $G_2 = G_{2t}$ and center manifold reduction

In this section, we analyze the stability and bifurcation behavior of system (3.6) at the transcritical point $G_2 = G_{2t}$ using center manifold theory.

Theorem 3.4.3 *For system (3.6) at the critical point $G_2 = G_{2t}$, the equilibria E_{1+} and E_2 coincide, forming a degenerate stable node. There is no backward bifurcation for this critical point.*

Proof At $G_2 = G_{2t}$, the Jacobian matrix of system (3.6) evaluated at the equilibrium $E_2 = E_{1+}$ has a simple zero eigenvalue, Therefore, E_2 is a degenerate node. To analyze its stability, we reduce the system to its center manifold by applying an affine transformation:

$$\begin{pmatrix} X \\ Y \\ Z \end{pmatrix} = \begin{pmatrix} X_2 \\ Y_2 \\ Z_2 \end{pmatrix} + \begin{pmatrix} \frac{-(B-D)}{2CD+(A-1)(B-D)} & 1 & 1 \\ \frac{F[E(B-D)+CD]}{CD} & 0 & 0 \\ 1 & \frac{FA(B-D)}{CD} + F - \frac{2CD}{B-D} - (A-1) & 0 \end{pmatrix} \begin{pmatrix} u_1 \\ u_2 \\ u_3 \end{pmatrix}, \quad (3.23)$$

where

$$X_2 = \frac{CD}{B-D}, \quad Y_2 = 0, \quad Z_2 = \frac{[B-D(1+C)][A(B-D)+CD]}{(B-D)^2},$$

and $G_2 = G_{2t}$. Substituting this transformation into (3.6), we obtain

$$\begin{aligned} \frac{du_1}{d\tau} &= -\frac{(B-D)^3 u_1^2}{BC[(A-1)(B-D)+2CD]} + \frac{(B-D)^2 u_1 u_2}{BC} + \frac{(B-D)^2 u_1 u_3}{BC}, \\ \frac{du_2}{d\tau} &= -Fu_2 + \frac{u_2}{F} \\ &\quad + \frac{(B-D)^3 [BE(D-F)+D^2(C-E)]u_1(u_2+u_3)}{B[F(B-D)[A(B-D)+CD]-CD[A(B-D)+2CD]+CD(B-D)][E(B-D)+CD]}, \\ \frac{du_3}{d\tau} &= \frac{-1}{A(B-D)+CD} \left\{ \frac{CD[(A-1)(B-D)+2CD]u_3}{B-D} + \frac{[AF(B-D)^2+C^2D^2]u_2^2}{CD} \right. \\ &\quad \left. + \frac{[A(A-1)(B-D)^2+3ACD(B-D)+C^2D^2]u_3^2}{A(B-D)+CD} + \dots \right\}. \end{aligned} \quad (3.24)$$

The linearized system is in Jordan canonical form with eigenvalues 0, $-F$ and $-\frac{CD[2CD+(A-1)(B-D)]}{(B-D)[A(B-D)+CD]}$.

The third eigenvalue is clearly negative when $G_2 = G_{2t}$. To obtain the center manifold, we

assume $u_2 = c_2 u_1^2$, $u_3 = c_3 u_1^2$, and apply the chain rule:

$$\frac{du_2}{d\tau} = 2c_2 u_1 \frac{du_1}{d\tau}, \quad \frac{du_3}{d\tau} = 2c_3 u_1 \frac{du_1}{d\tau}.$$

Solving for c_2 and c_3 , we obtain

$$c_2 = \frac{(B-D)^4 [BE(D-F) + D^2(C-E)]}{c_{2d}}, \quad c_3 = \frac{-F(B-D)^3 c_{3n}}{C^2 D c_{2d}}.$$

where

$$\begin{aligned}
 c_{2d} &= BF[E(B - D) + CD][(A - 1)(B - D) + 2CD] \\
 &\quad \times \{F(B - D)[A(B - D) + CD] - CD[(A - 1)(B - D) + 2CD]\}, \\
 c_{3n} &= F(B - D)[A(B - D) + CD] \\
 &\quad \times \{E(B - D)[A(B - D)^3 + (1 - A)BC(B - D) + CD((B - D)^2 - BC)] \\
 &\quad \quad + CD[A(B - D)^3 + CD((B - D)^2 + BC)]\} \\
 &\quad - BC^3D^2[E(B - D) + CD][(A - 1)(B - D) + 2CD].
 \end{aligned}$$

Thus, the center manifold up to the second order is given by

$$W^c = \{(u_1, u_2, u_3) | u_2 = c_2u_1^2 + O(u_1^3), u_3 = c_3u_1^2 + O(u_1^3)\}.$$

and the reduced dynamics on the center manifold is

$$\frac{du_1}{d\tau} = - \frac{(B - D)^3}{BC[(A - 1)(B - D) + 2CD]} u_1^2 + O(|u_1^3|^3). \quad (3.25)$$

The negative coefficient of u_1^2 indicates that the equilibrium E_2 is a locally asymptotically stable degenerate node.

To ensure that the equilibrium remains in the interior after perturbation, we require the positivity of the Y -coordinate:

$$Y = 0 + \frac{F[E(B - D) + CD]}{CD} u_1 > 0,$$

which implies that $u_1 > 0$. Under this condition, we can further explore the bifurcations at E_2 near this critical case.

To illustrate the local structure of equilibria, let us consider the transformation:

$$X = X_2 + u, \quad Y = Y_2 + v, \quad Z = Z_2 + w,$$

and substitute it into (3.6), which yields two equilibrium solutions:

$$(u_0, v_0, w_0) = (0, 0, 0), \quad (u_1, v_1, w_1) = \left(-\frac{CD}{B-D}, 0, 0\right).$$

The first equilibrium corresponds to $(X_2, 0, Z_2)$, previously shown to be a degenerate stable node. The second corresponds to $(X_3, Y_3, Z_3) = (0, 0, Z_2)$, which matches equilibrium E_0 at $G_2 = G_{2t}$. A straightforward linear stability analysis confirms that this equilibrium is also a stable node.

3.5 Treatment with CD4⁺ T cells ($G_1 > 0$, $G_2 = 0$).

If CD4⁺ T cells are utilized for treatment, then the interaction is described by the following model:

$$\begin{aligned} \frac{dX}{d\tau} &= X\left(1 - X - \frac{Z}{A + X}\right), \\ \frac{dY}{d\tau} &= Y\left(\frac{BX}{C + X} - D\right) + G_1, \\ \frac{dZ}{d\tau} &= \frac{XY}{E + X} - FZ. \end{aligned} \tag{3.26}$$

with non-negative initial conditions, $G_1 > 0$ represents the immunotherapy, where G_1 denotes the constant volume of CD4⁺ T administered to the tumor site of the patient per unit time.

In the following, we focus on investigating the existence and stability conditions of the equilibria of system (3.26). For this purpose, the equilibrium solutions of this system can

be easily determined by setting $\frac{dX}{d\tau} = \frac{dY}{d\tau} = \frac{dZ}{d\tau} = 0$ as

$$\begin{aligned} E_1 &= \left(0, \frac{G_1}{D}, 0\right), \\ E_2 &= (X_2, Y_2, Z_2) = \left(X_2, \frac{F(E + X_2)Z_2}{X_2}, (1 - X_2)(A + X_2)\right), \quad 0 < X_2 < 1. \end{aligned} \quad (3.27)$$

A boundary equilibrium of the form $(X, 0, 0)$ does not exist because $G_1 > 0$. Similarly, $(0, Y, 0)$ represents a state with immune cells present but no tumor and no cytokines. Biologically, this scenario is unrealistic because immune cells require activation usually triggered by tumor antigens to produce or sustain cytokines. Without tumor presence or cytokine signaling, immune cells cannot remain at a positive level.

To determine the existence of an interior steady state E_2 , where X_2 is determined from the fourth degree polynomial,

$$F_{2a} = X_2(C + X_2)G_1 - FF_{2b}, \quad \text{where} \quad F_{2b} = [CD - (B - D)X_2](1 - X_2)(E + X_2)(A + X_2).$$

There exists only one boundary steady state E_1 and its stability depends on the eigenvalues of the Jacobian matrix evaluated at E_1 : $1, -D, -F$, which show that E_1 is always a saddle-focus point. Observe that if $X(0) = 0$, then $X(\tau) = 0$ for $\tau > 0$, $\lim_{\tau \rightarrow \infty} Z(\tau) = 0$ and $\lim_{\tau \rightarrow \infty} Y(\tau) = \frac{G_1}{D}$. This implies that the stable manifold of E_1 is situated on the non-negative YZ plane. This indicates that the tumor may not be eliminated completely even with immunotherapy by adopting $CD4^+$ T cells to enhance the immune response. However, the boundary steady state $(1, 0, 0)$, which represents the tumor at its carrying capacity, does not exist in this model. The model shows bistability at high doses of $CD4^+$ T cells. The tumor may either be maintained at a small size or grow near its maximum capacity. This implies that the tumor's long-term behavior, when treated with $CD4^+$ T cells, depends on its size at the point of detection.

3.5.1 Stability and bifurcation of system (3.26)

In this subsection, we consider the stability and bifurcations of system (3.26), mainly focused on the equilibrium solutions. We have the following two theorems for the existence of E_2 and the stability of the equilibrium solutions, with the proof and more details on the Hopf bifurcation will be given in the next theorem.

Theorem 3.5.1 *For system (3.26), there exists at least one positive real solution for X_2 from the equation $F_{2a} = 0$:*

1. $0 < X_2 < 1$ if $B \leq D(1 + C)$;
2. $0 < X_2 < \frac{CD}{B-D}$ if $B > D(1 + C)$.

Proof To ensure that $F_{2a} = 0$ have positive solutions, a necessary condition is that $F_{2b} > 0$, or $DC - (B - D)X_2 > 0$ with $0 < X_1 < 1$, which yields that

- (a) $B \leq D(1 + C)$, $0 < X_2 < 1$,
- (b) $B > D(1 + C)$, $0 < X_2 \leq X_{2c} = \frac{CD}{B - D}$.

To further assess the sign of F_{2b} , consider the derivative of F_{2b} with respect to X_2 :

$$\begin{aligned} F'_{2b}(X_2) = \frac{dF_{2b}}{dX_2} &= 4(B - D)X_2^3 + 3[(1 - A - C - E)D + B(A + E - 1)]X_2^2 \\ &\quad + 2\{[A(1 - C - E) + (1 - C)E + C]D + B[(E - 1)A - E]\}X_2 \\ &\quad + \{A[(1 - C)E + C] + CE\}D - ABE \end{aligned}$$

Evaluating the derivative at specific points:

- $F'_{2b}(0) = (A + E - AE)CD - AE(B - D)$,
- $F'_{2b}(1) = (A + 1)(E + 1)(B - (1 + C)D)$,

$$\bullet F'_{2b}(X_{2c}) = - \frac{(B - (1 + C)D)((B - D)E + CD)((B - D)A + CD)}{(B - D)^2}.$$

Now we analyze the two cases based (a) and (b) according to the value of B : For the cases (a), we have $F_{2b}(0) = CDEA > 0$, and $F_{2b}(X_{2c}) = 0$. Moreover,

- If $B = D$, then $F_{2b} = CD(1 - X_2)(X_2 + E)(X_2 + A) > 0$ for all $0 < X_2 < 1$.
- If $B < D$, then $F_{2b} \rightarrow -\infty$ as $X_2 \rightarrow \pm\infty$. The quartic nature of F_{2b} implies four real roots: one negative and three positive roots, including $X_2 = X_{2c}$ and $X_2 = 1$. Therefore, $F_{2b} > 0$ on two intervals: $(0, X_2^*)$ and $(X_{2c}, 1)$, for some $0 < X_2^* < X_{2c}$.
- If $D < B < D(1 + C)$, then $F_{2b} \rightarrow +\infty$ as $X_2 \rightarrow \pm\infty$, and $F'_{2b}(X_{2c}) < 0$, $F'_{2b}(1) > 0$. F_{2b} has four positive real roots: $X_2^* \in (0, X_{2c})$, X_{2c} , 1 and one greater than 1. Hence, $F_{2b} > 0$ on two intervals: $(0, X_2^*)$ and $(X_{2c}, 1)$.
- If $B = D(1 + C)$, then $F_{2b} = CD(1 - X_2)^2(E + X_2)(A + X_2)$ in which $F_{2b} > 0$ for $X_2 \in (0, X_{2c}) \cup (X_{2c}, 1)$.

Thus, for case (a), $F_{2a} = 0$ admits at least one positive real solution for $X_2 \in (0, 1)$.

Next, consider the case (b). For this case, $F_{2b} \rightarrow +\infty$, as $X_2 \rightarrow \pm\infty$, with $F_{2b}(0) > 0$ and $F_{2b}(X_{2c}) = F_{2b}(1) = 0$. Now examine $F'_{2b}(0)$. $F'_{2b}(0) > 0$ implies $F_{2b} > 0$ on $(0, X_{2c})$. This leads to constraints on B , depending on the sign of $(A + E - AE)CD - AE(B - D)$. Moreover, if the second derivative of F_{2b} at $X_2 = 0$ is negative, then a local maximum exists in $(0, X_{2c})$, further confirming $F_{2b} > 0$ over that interval. Therefore,

$$B > \max \left\{ D(1 + C), D \left(1 + \frac{C(-AE + A + E)}{AE} \right) \right\},$$

we conclude that $F_{2a} = 0$ admits at least one solution in $(0, X_{2c})$. Given that the equilibrium condition is defined by $F_{2a} = 0$, we can explicitly solve for D as a function of X_2 as

$$D = \frac{X_2[FB(1 - X_2)(E + X_2)(A + X_2) + (C + X_2)G_1]}{F(1 - X_2)(E + X_2)(C + X_2)(A + X_2)}.$$

Since this expression only requires $0 < X_2 < 1$, the cases (a) and (b) described earlier are not needed here. Therefore, for any $X_2 \in (0, 1)$, a corresponding D can be found to ensure $F_{2a} = 0$.

Next, we consider the stability of E_2 , and have the following result.

Theorem 3.5.2 *The interior equilibrium E_2 undergoes a Hopf bifurcation when the Routh-Hurwitz determinant Δ_2 (defined in the proof) vanishes. There is no transcritical bifurcation if*

$$F_3 = 2X_2^3 + (A + E - 1)X_2^2 + AE \geq 0, \quad (3.28)$$

and E_2 is unstable for $F_3 < 0$. Moreover, no Hopf bifurcation occurs for sufficiently large F ; and E_2 is locally asymptotically stable (LAS) when $F_3 > 0$. The Hopf critical point occurs at $B = B_H$, as shown in the proof below.

Proof We analyze the Jacobian matrix of system (3.26) evaluated at the equilibrium E_2 , which is given by

$$J(E_2) = \begin{bmatrix} \frac{X_2(1 - 2X_2 - A)}{(A + X_2)} & 0 & -\frac{X_2}{A + X_2} \\ -\frac{(X_2 - 1)(A + X_2)(E + X_2)FBC}{X_2(C + X)} & \frac{BX_2}{C + X_2} - D & 0 \\ -\frac{(X_2 - 1)(X_2 + A)EF}{X_2(E + X)} & \frac{X_2}{E + X_2} & -F \end{bmatrix}. \quad (3.29)$$

This yields the characteristic polynomial,

$$P_{E_2}(\lambda) = \lambda^3 + a_1\lambda^2 + a_2\lambda + a_3, \quad (3.30)$$

where

$$a_1 = \frac{1}{(A + X_2)} \left[(A + F - 1 + 2X_2)X_2 + FA + \frac{G_1 X_2}{F(1 - X_2)(E + X_2)} \right],$$

$$a_2 = \frac{1}{F(1 - X_2)(E + X_2)(A + X_2)^2} a_{2a},$$

$$a_3 = \frac{X_2}{(A + X_2)^2(C + X_2)^2(E + X_2)^2(1 - X_2)} a_{3a},$$

with

$$a_{2a} = G_1 X_2 ((A + F - 1 + 2X_2)X_2 + FA) + F^2(1 - X_2)(A + X_2)(2X_2^3 + (A + E - 1)X_2^2 + AE),$$

$$a_{3a} = (FBC(1 - X_2)^2(E + X_2)^2(A + X_2)^2 + G_1(C + X_2)^2((A + E - 1 + 2X_2)X_2^2 + AE)).$$

According to the Routh-Hurwitz criteria, the equilibrium E_2 is LAS if

$$a_1 > 0, a_3 > 0, \quad \text{and} \quad \Delta_2 = a_1 a_2 - a_3 > 0$$

We now analyze this in cases:

(a) If $A + E \geq 1$, then $F'_3(X_2) > 0$ for $X_2 > 0$, which implies $F_3 > 0$, $a_3 > 0$ and $a_2 > 0$ for large F .

(b) If $E < 1$ and $A < 1 - E$, then $F'_3(0) = F'_3(\frac{1-A-E}{3}) = 0$, and F_3 may change sign.

Minimizing F_3 with respect to X_2 , we obtain

$$F_{3 \min} = AE - \frac{(1 - A - E)^3}{27}.$$

Solving $F_{3 \min} = 0$ yields the critical value $A = A^* = (1 - E^{\frac{1}{3}})^3$.

- If $A \geq A^*$, then $F_3 \geq 0$, so $a_2 > 0$ and $a_3 > 0$.
- If $A < A^*$, then $F_3 < 0$ for some $X_2 \in (0, 1)$, causing $a_2 < 0$ and instability of E_2 .

For large F , a_1, a_2, a_3 are all positive, but Δ_2 may cross zero, implying that a Hopf bifurcation can occur when $a_1, a_2 > 0, a_3 > 0$, but $\Delta_2 = 0$. From this, $F_3 \geq 0$ holds if one of the following conditions is satisfied:

$$\begin{aligned}
 & \text{(i)} \quad A + E \geq 1, \\
 & \text{(ii)} \quad 0 < E < 1, (1 - E^{\frac{1}{3}})^3 \leq A < 1 - E, \\
 & \text{(iii)} \quad 0 < E < 1, (1 - E^{\frac{1}{3}})^3 > A > 0, X_2 \in (0, X_2^{(1)}] \cup [X_2^{(2)}, 1).
 \end{aligned} \tag{3.31}$$

These ensure $a_1 > 0, a_2 > 0, a_3 > 0$ for large F , precluding a transcritical bifurcation. Otherwise, if $F_3 < 0$, then $a_2 < 0$, and E_2 is unstable. Under the above three conditions, $F_3 > 0$ and $\Delta_2 > 0$, meaning no Hopf bifurcation occurs for large F , and E_2 remains LAS.

When $F_3 = 0$, we have $0 < A \leq (1 - E^{\frac{1}{3}})^3$, and $X_2 = X_2^{(1)}$ or $X_2 = X_2^{(2)}$. When $A = (1 - E^{\frac{1}{3}})^3$, the roots coincide: $X_2^{(1)}(A) = X_2^{(2)}(A)$.

We now identify conditions for Hopf bifurcation, which occurs when $a_1 > 0, a_3 > 0$, and $\Delta_2 = 0$. The explicit form of Δ_2 is

$$\Delta_2 = \frac{\Delta_{2a}}{F^2(1 - X_2)^2(E + X_2)^2(A + X_2)^3(C + X_2)^2}$$

where

$$\Delta_{2a} = -F^3(1 - X_2)^3(A + X_2)^3CX_2(E + X_2)^2B + \Delta_{2aa} \tag{3.32}$$

and

$$\begin{aligned}
 \Delta_{2aa} = & (C + X_2)^2[FA + X_2(F - 1 + A + 2X_2)] \\
 & \times \{X_2^2G_1^2 + FX_2(1 - X_2)(E + X_2)[FA + X_2(F - 1 + A + 2X_2)]G_1 \\
 & + F^3(1 - X_2)^2(E + X_2)(A + X_2)[2X_2^3 + (A + E - 1)X_2^2 + AE]\}.
 \end{aligned}$$

Define the critical value,

$$B_c = \frac{(1 + C)(C + X_2)X_2G_1}{CF(1 - X_2)^2(E + X_2)(A + X_2)},$$

so that when $B \leq B_c$, we have $\Delta_{2a} > \Delta_{2b}$, where

$$\begin{aligned} \Delta_{2b} = & F^3(1 - X_2)^2(E + X_2)(C + X_2)^2(A + X_2)F_{4a}F_{4b} \\ & + F^2G_1X_2(1 - X_2)(C + X_2)(E + X_2)(A + X_2)[F(C + X_2)(A + X_2) + X_2F_{4c}] \\ & + X_2^2(C + X_2)^2G_1[FX_2(1 - X_2)(E + X_2)(A - 1 + 2X_2)^2 + G_1F_{4a}], \end{aligned}$$

with the auxiliary terms:

$$F_{4a} = FA + X_2(A + 2X_2) + (F - 1)X_2,$$

$$F_{4b} = 2X_2^3 + (A + E - 1)X_2^2 + AE,$$

$$F_{4c} = 4X_2^2 + [2A + 3(C - 1)]X_2 + (A - 2)C - A,$$

where $F_{4b} = F_3$. Clearly, $F_{4a} > 0$ whenever $F \geq 1$. For $F_{4b} = F_3$, as discussed above, $F_{4b} > 0$ if one of the conditions given in (3.31) is satisfied. For F_{4c} , evaluating endpoints yields:

$$F_{4c}(0) = (A - 2)C - A, \quad F_{4c}(1) = (1 + A)(1 + C).$$

Root structure of $F_{4c} = 0$ depends on A and C :

1. If $A \leq 2, C > 0$: one positive root X_{2p} .
2. If $A > 2, C \geq \frac{A}{A-2}$: then $F_{4c} \geq 0$ for all X_2 , so $\Delta_{2a} > 0$ and E_2 is LAS.
3. If $A > 2, C < \frac{A}{A-2}$: again one positive root X_{2p} .

The general expression for this root is

$$X_{2p} = \frac{1}{8} [3(1 - C) - 2A + \sqrt{4A^2 - 4CA + 9C^2 + 4A + 14C + 9}].$$

- If $X_{2p} < 1$, then for $X_2 \in [X_{2p}, 1)$, $\Delta_{2b} > 0$ and E_2 is LAS.
- For $X_2 \in (0, X_{2p})$, stability depends on sign of F_{4c} and thus on F .

Define a threshold:

$$F_{4d} = -\frac{F_{4c}X_2}{(C + X_2)(A + X_2)}, \quad \text{so} \quad \left. \frac{dF_{4d}}{dX_2} \right|_{X_2=0} = \frac{A - AC + 2C}{AC} > 0.$$

This implies F_{4d} has a unique positive maximum in $(0, 1)$, which is estimated to be less than 1. Therefore, if $F > 1$, then $F(C + X_2)(A + X_2) + X_2F_{4c} > 0$, so remains LAS.

Finally, when $\Delta_2 = 0$, the critical value of B at which Hopf bifurcation occurs is

$$B_H = \frac{\Delta_{2aa}}{F^3(1 - X_2)^3(A + X_2)^3CX_2(E + X_2)^2}. \quad (3.33)$$

Since the numerator $\Delta_{2aa} > 0$ whenever $F_3 \geq 0$, and the denominator is always positive, we conclude $B_H > 0$. Thus, a Hopf bifurcation emerges at $B = B_H$ when $\Delta_2 = 0$.

This completes the proof.

3.5.2 Bifurcation of multiple limit cycles

We aim to determine the maximum number of limit cycles that can bifurcate from the Hopf critical point B_H in system (3.33) when the relevant conditions are satisfied. To this end, we apply the normal form of the Hopf and generalized bifurcations to compute the focus values, which in turn allow us to estimate the number of bifurcating limit cycles.

The following theorem (see the detailed proof in [45, 46]) provides a sufficient condition for a dynamical system to exhibit multiple limit cycles emerging from a Hopf critical point. Without loss of generality, assume the amplitude equation of the normal form for a general n -dimensional dynamical system $\dot{x} = f(x, \mu)$ with a Hopf bifurcation takes the form,

$$\frac{dr}{d\tau} = r[v_0\mu + v_1r^2 + v_2r^4 + \cdots + v_kr^{2k} + O(r^{2k+2})], \quad (3.34)$$

where v_k is the k th-order focus value, expressed in terms of the system parameters. If one

can identify k parameters, say, $\mu = (\mu_1, \mu_2, \dots, \mu_k)$, such that

$$v_0 = v_1 = \dots = v_{k-1} = 0, \quad \text{but } v_k \neq 0,$$

at the critical point defined by $\mu_c = (\mu_{1c}, \mu_{2c}, \dots, \mu_{kc})$, and

$$\text{rank} \left[\frac{\partial(v_0, v_1, \dots, v_{k-1})}{\partial(\mu_1, \mu_2, \dots, \mu_k)} \right]_{\mu=\mu_c} = k,$$

then k small-amplitude limit cycles can bifurcate from the equilibrium via suitable perturbations to μ .

For system (3.26), we have the following result.

Theorem 3.5.3 *System (3.26) admits at least two limit cycles bifurcating from the Hopf critical point, with outer limit cycle is stable and the inner one is unstable, and both enclose the stable equilibrium E_2 .*

Proof We begin by selecting the following typical parameter values:

$$A = \frac{1}{10}, \quad C = 1, \quad E = \frac{1}{10}, \quad F = 5000, \quad X_2 = \frac{139}{1000},$$

which yield

$$B_H = \frac{258364405203497(1932100000G_1^2 + 17089223906265651G_1 - 45289032746370525)}{144136018732388476605918750000},$$

$$D = \frac{139(49181181B_H + 227800G_1)}{56017365159}.$$

The numerical coefficients in the transformation matrix come directly from evaluating the Jacobian matrix of system (3.26) at the Hopf equilibrium point E_2 , using the chosen parameter set in (3.27). In other words, these numbers are obtained by linearizing the system at the equilibrium, computing the eigenvectors, and normalizing them to construct the coordinate change that reduces the system to its canonical Hopf form. Next, we apply the

affine transformation,

$$\begin{pmatrix} X \\ Y \\ Z \end{pmatrix} = \begin{pmatrix} \frac{139}{1000} \\ \frac{49181181}{27800} \\ \frac{205779}{1000000} \end{pmatrix} + \begin{bmatrix} T_{11} & \omega_c & T_{13} \\ T_{21} & T_{22} & T_{23} \\ 1 & 0 & 1 \end{bmatrix} \begin{pmatrix} u \\ v \\ w \end{pmatrix}, \quad (3.35)$$

where

$$\omega_c = \frac{1139 \sqrt{18988026562517390G_1 - 50321147495967250}}{1435000000000},$$

and

$$\begin{aligned} T_{11} &= \frac{206081872391500}{-7208009907872487+2768216372300000G_1}, \\ T_{13} &= \frac{28603281}{200(139G_1+1229529525)}, \\ T_{21} &= \frac{237986947115000(-36834441+13900000G_1)}{139(-7208009907872487+2768216372300000G_1)}, \\ T_{22} &= \frac{199152257(100000G_1-63997269)\sqrt{2}\sqrt{-25160573747983625+9494013281258695G_1}}{342965(-7208009907872487+2768216372300000G_1)}, \\ T_{23} &= -\frac{1932100000G_1^2+17089223906265651G_1-45289032746370525}{14301640500(139G_1+1229529525)}. \end{aligned} \quad (3.36)$$

Using the Maple program [44] to compute the normal forms up to 5th-order terms yields

$$\frac{dr}{d\tau} = r [v_0\mu + v_1r^2 + v_2r^4 + O(r^6)], \quad (3.37)$$

where $\mu = B - B_H$ is a bifurcation parameter, and v_0, v_1 and v_2 are the rare the focus values of respective orders. The transversal condition v_0 is obtained via linear analysis, while v_1 and v_2 are derived using the Maple implementation. Explicitly,

$$v_0 = \frac{7415041449683042081872338614062500000 \sqrt{5}}{v_{0d}},$$

where,

$$v_{0d} = 1297321 \sqrt{9494013281258695G_1 - 25160573747983625} \\ \times (193210000000000G_1^2 + 5126767171879695300000G_1 \\ + 15115236593113258444867492881).$$

The focus values v_1 and v_2 are obtained as rational functions of G_1 , with

$$v_1 = \frac{v_{1a}}{v_{1d}}, \quad v_2 = \frac{v_{2a}}{v_{2d}},$$

where

$$v_{1a} = 2045935700091608210829854100189377942433066332860083259000000000000000000000G_1^8 \\ - 5428834985470406256857944336083837579851485354711685925479385390987000000000000000000000G_1^7 \\ - 202753425242783398022059724449609898334272953997733558997218098536161308436776540000000000000000G_1^6 \\ - 1793418493201348141320270871524186185042437678611616576265878296652089851399807220899517307400000000000G_1^5 \\ - 542680622655228041465748791480437908485233406576787803671891171130212670081550753980199045979710997269000000G_1^4 \\ - 369157757122969816758541413301376845424437510969117234668879992063589128971999617708111227024532362867065558753203G_1^3 \\ + 1947948663746889874680512396097152932290309822949706541568386921253561210083246157824766315782717294054693635410650G_1^2 \\ - 50558077097980849691001099318777637574562241131673815785975042277888320993488277874803289276362135859946756203076875G_1 \\ + 127179621555089854334238366643965401721315519156874085704916938433667580912530705300557057990086231974505283203125000, \\ v_{1d} = 219634736175833190992500(13900000G_1 + 122944056879609)(27682163723G_1 - 73361928325) \\ \times (2768216372300000G_1 - 7208009907872487)(1390000000000G_1^2 + 73766434127765400000G_1 + 108742611556859241249712179) \\ \times (193210000000000G_1^2 + 5126767171879695300000G_1 + 15115236593113258444867492881), \\ v_{2a} = \dots, \\ v_{2d} = \dots,$$

Exact coefficients are kept because rounding them alters the computed focus values and affects reproducibility. Including the full integers guarantees verifiable, machine-accurate results. The detailed expressions for v_{2a} and v_{2d} are omitted for brevity.

Because the focus values depend on a single parameter G_1 , it is possible to choose G_1 such that $v_1 = 0$, but $v_2 \neq 0$, leading to the emergence of two limit cycles. Solving $v_{1a} = 0$ numerically for G_1 yields two positive real solutions, one of which is $G_{1c} = 2.65021346 \dots$, for which $v_2 = -6.52662498 \dots$. Perturbing G_1 slightly as $G_1 = G_{1c} + \varepsilon_1$ with $\varepsilon_1 =$

-0.0000005 , and letting $B = B_H + \varepsilon_2$ with $\varepsilon_2 = -0.0018$ gives

$$v_0\mu + v_1r^2 + v_2r^4 = -0.16607551 * 10^{-7} + 0.00241040 \cdots r^2 - 6.52662498 \cdots = 0.$$

Solving this equation yields approximate amplitudes of two limit cycles:

$$r_1 \approx 0.002650, \quad r_2 = 0.019034.$$

Since $\varepsilon_2 < 0$, the parameter B decreases as it crosses the Hopf critical point B_H . Given $v_2 < 0$, the outer limit cycle is stable and the inner one is unstable. The equilibrium E_2 at this critical point is a stable focus.

For this example, at the critical point, we have

$$B_H = 0.00192194 \cdots, \quad \text{and} \quad D = 0.00173260 \cdots,$$

both of which are small due to the large value of F . The corresponding simulated phase portraits are shown in Figure 3.5.

The proof is complete.

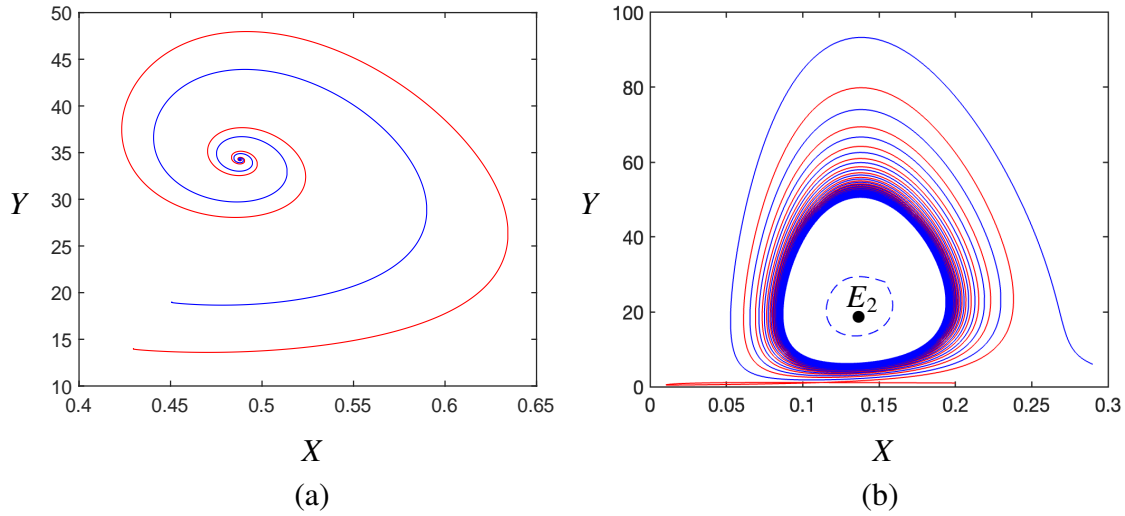


Figure 3.5: Simulated trajectories of system (3.26): (a) with parameters $A = \frac{9}{10}$, $B = 9$, $C = 1$, $D = 3$, $E = 1/10$, $F = 40$, $G_1 = \frac{165021347}{100000000}$, converging to equilibrium E_2 ; and (b) with parameters $A = \frac{2}{5}$, $B = 55$, $C = 1$, $D = \frac{1343113}{200000}$, $E = \frac{9}{10}$, $F = 6$, $G_1 = \frac{278715}{105167}$, converging to a stable limit cycle.

3.6 Treatment with both $CD4^+$ T cells and Cytokine ($G_1 > 0$, $G_2 > 0$).

When the treatment strategy involves both $CD4^+$ T cells and cytokine, the interaction dynamics can be described by the following model:

$$\begin{aligned}
 \frac{dX}{d\tau} &= X\left(1 - X - \frac{Z}{A + X}\right), \\
 \frac{dY}{d\tau} &= Y\left(\frac{BX}{C + X} - D\right) + G_1, \\
 \frac{dZ}{d\tau} &= \frac{XY}{E + X} - FZ + G_2,
 \end{aligned} \tag{3.38}$$

where $G_1 > 0$ and $G_2 > 0$ represent constant administrations of $CD4^+$ T cells and cytokine, respectively, to the tumor site per unit time. To determine the equilibria of the system, we solve the algebraic equations corresponding to the right-hand sides of the differential

equations. This yields two biologically relevant equilibria:

$$\begin{aligned} E_1 &= \left(0, \frac{G_1}{D}, \frac{G_2}{F}\right), \\ E_2 &= \left(X_2, \frac{G_1(C + X_2)}{CD - (B - D)X_2}, (1 - X_2)(A + X_2)\right), \end{aligned} \quad (3.39)$$

The equilibrium E_1 is a tumor-free state ($X = 0$) where immune cells and cytokines remain positive due to the constant therapeutic inflows G_1 and G_2 . This state is biologically meaningful only when both $G_1 > 0$ and $G_2 > 0$. In this case, E_1 represents a successful treatment outcome in which the tumor is eliminated and the immune response is sustained by continuous therapy.

where the second equilibrium E_2 is valid only under certain conditions. Specifically, consider the expression,

$$S_1 = -\frac{S_{1a}}{(E + X_2)[(B - D)X_2 - CD]},$$

where

$$S_{1a} = G_1 X_2 (C + X_2) - (E + X_2)(D(C + X_2) - B X_2)(F(A + X_2)(1 - X_2) - G_2).$$

When $G_2 \geq F(A + X_2)(1 - X_2)$, the numerator S_{1a} becomes positive, but no real solution for X_2 to exist. Therefore, for the interior equilibrium E_2 to exist, the following inequality must hold:

$$G_2 < F(A + X_2)(1 - X_2).$$

Under this condition, the corresponding value of G_1 required to ensure equilibrium is given by

$$G_1 = \frac{(E + X_2)[D(C + X_2) - X_2 B][F(1 - X_2)(A + X_2) - G_2]}{X_2(C + X_2)}.$$

Alternatively, solving for G_2 in terms of G_1 yields

$$G_2 = \frac{F(1 - X_2)(A + X_2)(E + X_2)[D(C + X_2) - X_2B] - X_2(C + X_2)G_1}{[D(C + X_2) - X_2B](E + X_2)}.$$

To ensure G_2 remains positive, G_1 must satisfy

$$G_1 < \frac{F(1 - X_2)(A + X_2)(E + X_2)[D(C + X_2) - BX_2]}{X_2(C + X_2)}.$$

Thus, a biologically meaningful interior equilibrium E_2 exists if both $0 < G_2 < F(A + X_2)(1 - X_2)$ and the corresponding G_1 lies within the above bounds. Additionally, the value of G_1 can also be directly related to G_2 via

$$G_1 = \frac{(E + X_2)((B - D)X_2 - CD)G_2}{X_2(C + X_2)},$$

which must be positive. Thus, the conditions for existence of the interior equilibrium are summarized as follow:

1. $G_2 < F(A + X_2)(1 - X_2) = G_{2e}$, with $X_2 < 1$, and $B < D(1 + \frac{C}{X_2})$, or
2. $B \leq D$, then $0 < X_2 < 1$; and if $B > D$, then $X_2 < \min\{1, \frac{CD}{(B-D)}\}$.

These criteria ensure the system admits a biologically relevant non-trivial equilibrium when both CD4⁺ T cell and cytokine therapies are applied appropriately.

Theorem 3.6.1 *For system (3.38), the equilibrium E_1 is a stable node when $G_2 > FA$, and becomes a saddle when $G_2 < FA$, under which condition the interior equilibrium E_2 exists. There is no bifurcation of limit cycles occurring for $F > D$.*

Proof To determine the stability of the equilibria, we evaluate the Jacobian matrix of system (3.38) at E_1 and E_2 . At the boundary equilibrium $E_1 = (0, \frac{G_1}{D}, \frac{G_2}{F})$, the Jacobian matrix yields the eigenvalues: $-D$, $-F$ and $1 - \frac{G_2}{FA}$. From this, we see that E_1 is a stable node

when $G_2 > FA$, and a saddle point when $G_2 < FA$, indicating a change in stability and the possibility of a new interior equilibrium E_2 .

To examine the stability of E_2 , we compute the Jacobian at E_2 and determine the characteristic polynomial, which takes the form:

$$J(E_2) = \begin{bmatrix} \frac{X_2(1 - 2X_2 - A)}{(A + X_2)} & 0 & -\frac{X_2}{A + X_2} \\ \frac{B(FX_2^2 + F(A - 1)X_2 - AF + G_2)C(E + X_2)}{(C + X_2)^2X_2} & \frac{BX_2}{C + X_2} - D & 0 \\ -\frac{(FX_2^2 + F(A - 1)X_2 - AF + G_2)E}{(E + X_2)X_2} & \frac{X_2}{E + X_2} & -F \end{bmatrix}. \quad (3.40)$$

The characteristic polynomial is

$$\lambda^3 + a_1\lambda^2 + a_2\lambda + a_3 = 0,$$

where

$$\begin{aligned}
 a_1 &= D - \frac{BX_2}{C + X_2} + X_2 + \frac{FA + (F - 1 + X_2)X_2}{A + X_2}, \\
 a_2 &= \frac{1}{(A + X_2)(C + X_2)(E + X_2)} a_{2a}, \\
 a_{2a} &= \{(-2B + 2D + 2F)X_2^4 \\
 &\quad + [(-2B + 2D + F)E + (A - B + 2C + D - 1)F + (A + 2C - 1)D - B(A - 1)]X_2^3 \\
 &\quad + [((-B + C + D)F + (A + 2C - 1)D - B(A - 1))E + ((A + C)D + (-B + C)A - C)F \\
 &\quad + CD(A - 1)]X_2^2 + [(((A + C)D - A(B - 1))F + CD(A - 1) - G_2)E + ACDF]X_2 \\
 &\quad + C(A(D + 1)F - G_2)E\}, \\
 a_3 &= -\frac{F}{(A + X_2)(C + X_2)^2(E + X_2)} a_{3a}, \\
 a_{3a} &= -2F(B - D)X_2^5 - F((3B - 4D)C + (B - D)(A + E - 1))X_2^4 \\
 &\quad - 2FC(-CD + (B - D)(A + E - 1))X_2^3 \\
 &\quad + ((D(A + E - 1)C^2 - B((A - 1)E - A)C - AE(B - D))F - G_2(BC - E(B - D)))X_2^2 \\
 &\quad + 2CDE(AF - G_2)X_2 \\
 &\quad + C^2DE(AF - G_2).
 \end{aligned}$$

where the coefficients a_1 , a_2 , and a_3 are explicitly derived in terms of the system parameters and X_2 . For the interior equilibrium E_2 to exist and be locally asymptotically stable, the Routh-Hurwitz conditions must be satisfied: $a_1 > 0$, $a_3 > 0$, and $\Delta_2 = a_1 a_2 - a_3 > 0$.

We consider the existence condition for E_2 , which requires $G_2 < F(A + X_2)(1 - X_2) = G_{2e}$. Let $G_2 = F(A + X_2)(1 - X_2) - h$, where $h > 0$ is a small perturbation. Substituting this into the characteristic polynomial, we analyze the discriminant Δ_2 , denoted as

$$\Delta_{2b} = \Delta_{2b0} + \Delta_{2b1}h$$

where Δ_{2b0} and Δ_{2b1} are parameter dependent expressions:

$$\begin{aligned}\Delta_{2b0} = & (E + X_2)(F(C + X_2) + D(C + X_2) - BX_2) \\ & \times (F(A + X_2) + (A + 2X_2 - 1)X_2)((A + X_2) \\ & \times (D(C + X_2) - BX_2) + X_2(C + X_2)(A + 2X_2 - 1))\end{aligned}$$

and

$$\begin{aligned}\Delta_{2b1} = & C(A + X_2)(E + X_2)(D(C + X_2) - BX_2) \\ & + E(C + X_2)^2 X_2(A + 2X_2 - 1) \\ & + E(C + X_2)^2 (A + X_2) \left(F - \frac{CD(E + X_2)}{E(C + X_2)} \right).\end{aligned}$$

It can be shown that $\Delta_{2b0} > 0$ under the condition $A + 2X_2 - 1 > 0$, and that $a_1 > 0$, $a_3 > 0$ also hold under this condition. For $\Delta_2 = 0$, we require $\Delta_{2b1} > 0$, which is satisfied

$$F - \frac{CD(E + X_2)}{E(C + X_2)} > 0.$$

Noting that

$$\frac{CD(E + X_2)}{E(C + X_2)} < \frac{CD}{C} = D,$$

we conclude that the inequality holds when $F > D$. Therefore, for typical parameter values where $F > D$, the conditions $a_1 > 0$, $a_3 > 0$, and $\Delta_2 > 0$ are all satisfied, and the equilibrium E_2 is stable.

When $F > D$, the system does not undergo a Hopf bifurcation because none of the eigenvalues cross the imaginary axis. Additionally, a Bogdanov–Takens bifurcation is not possible, as this would require a degenerate case with two zero eigenvalues, which does not occur at either equilibrium.

To explore the possibility of Hopf bifurcation when $F < D$, we require

$$F - \frac{CD(E + X_2)}{E(C + X_2)} < 0,$$

which would make $\Delta_{2b1} < 0$. In this case, a more detailed bifurcation analysis would be needed. However, under the typical regime $F > D$, we conclude that no limit cycle bifurcation occurs.

Remark

Although the characteristic polynomial of the system may suggest the possibility of a Hopf bifurcation under certain parameter regimes, our analysis shows that this does not occur within biologically meaningful conditions. Specifically, for typical parameter values satisfying $F > D$, the system does not admit purely imaginary eigenvalues, and thus no limit cycle arises. We expect $F > D$ because cytokines decay much faster than immune cells. Therefore, the cytokine clearance rate F is higher than the immune-cell decay rate D , making $F > D$ biologically realistic. Mathematically, a Hopf bifurcation may occur when $F < D$, but this condition is not aligned with observed or realistic biological parameters. Therefore, while a Hopf bifurcation is theoretically possible, it is biologically irrelevant in this context.

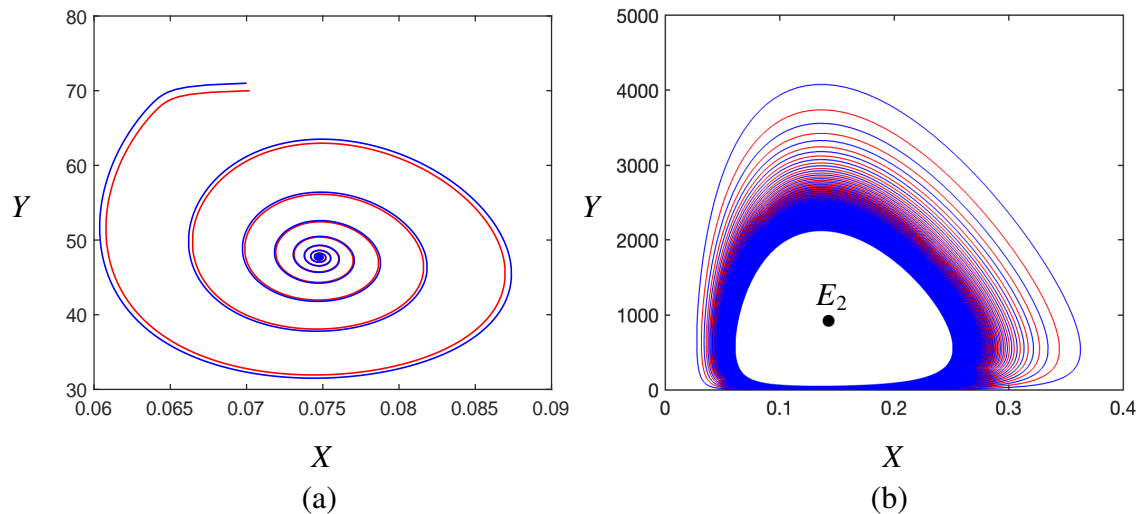


Figure 3.6: Simulated trajectories of system (3.38): (a) when $A = \frac{1}{10}$, $B = 57$, $C = 1$, $D = 4$, $E = \frac{3}{10}$, $F = 70$, $G_1 = \frac{165021347}{100000000}$, $G_2 = \frac{9}{5}$, converging to the equilibrium E_2 ; and (b) when $A = \frac{1}{10}$, $B = 50$, $C = 1$, $D = 6$, $E = 40$, $F = 10$, $G_1 = \frac{278715}{105167}$, $G_2 = \frac{183}{1075}$, converging to a stable limit cycle.

Biologically, this implies that while the immune system may transiently respond to tumor fluctuations, it does not enter a state of sustained rhythmic behavior. Despite the combined action of CD4⁺ T cells (stimulated by G_1) and cytokines (administered via G_2), the tumor–immune dynamics do not exhibit periodic cycles. Instead, the immune system drives the tumor toward a steady-state level, without the oscillatory patterns often associated with immune surveillance and escape. Thus, while a Hopf bifurcation may appear mathematically feasible in theory, it is not realized within biologically meaningful parameter ranges. This highlights the importance of aligning mathematical predictions with biologically realistic constraints.

3.7 Conclusion

In this work, we presented a detailed analysis of a mathematical model describing tumor–immune–cytokine interactions under three immunotherapy strategies: (i) cytokine administration only, (ii) CD4⁺ T-cell infusion only, and (iii) combined administration of CD4⁺ T cells and cytokine. For each case, we identified equilibria, derived the existence conditions, and analyzed stability and bifurcations.

For cytokine therapy, the model predicts three possible outcomes: tumor eradication, partial reduction, or coexistence with immune cells, depending on the cytokine dose relative to threshold values. High doses eliminate small tumors, intermediate doses reduce but do not remove them, and low doses allow stable coexistence. Transcritical and Hopf bifurcations at these thresholds can shift the system between states, highlighting the need for precise dosing.

For CD4⁺ T-cell therapy, effectiveness depends on both dose and initial tumor size. Although complete eradication is unlikely, high G_1 values can maintain small tumor at low levels. However, bistability means that large initial tumors may still progress. Under certain conditions, a Hopf bifurcation can induce sustained oscillations in tumor-size.

For combination therapy, the model yields a stable boundary equilibrium when $G_2 > FA$, and an interior equilibrium when $G_2 < FA$. If the cytokine decay rate exceeds the T-cell loss rate ($F > D$), oscillations are suppressed, and the system approaches a steady state. This combined approach enhances tumor control by coupling cytokine, driven immune activation with sustained T-cell cytotoxicity.

Biologically, treatment success depends not only on dose but also on clearance rates, immune activation thresholds, and initial tumor size. Cytokine therapy requires careful titration to avoid destabilizing dynamics; T-cell therapy is most effective when initiated early; and combination therapy broadens the stability range for long-term control.

References

- [1] R. A. Weinberg, *The Biology of Cancer*, 2nd ed., Garland Science, London, UK, 2013.
- [2] Cancer Research UK, Stages of cancer, 2017. <https://www.cancerresearchuk.org/about-cancer/what-is-cancer/stages-of-cancer>
- [3] Cancer.Net, Stages of cancer, 2018. <https://www.cancer.net/navigating-cancer-care/diagnosing-cancer/stages-cancer>
- [4] R. Rockne, E. C. Alvord Jr., J. K. Rockhill, K. R. Swanson, A mathematical model for brain tumor response to radiation therapy, *J. Math. Biol.* 58 (2009) 561–578.
- [5] J. Malinzi, Mathematical analysis of a mathematical model of chemovirotherapy: Effect of drug infusion method, *Comput. Math. Methods Med.*, Article ID 7576591 (2019) 16 pages.
- [6] Y. Tao, Q. Guo, K. Aihara, A partial differential equation model and its reduction to an ordinary differential equation model for prostate tumor growth under intermittent hormone therapy, *J. Math. Biol.* 69(4) (2014) 817–838.

- [7] L. Pang, L. Shen, Z. Zhao, Mathematical modelling and analysis of the tumor treatment regimens with pulsed immunotherapy and chemotherapy, *Comput. Math. Methods Med.*, Article ID 6260474 (2016) 12 pages.
- [8] E. Bastiaannet, J. C. Beukema, H. J. Hoekstra, Radiation therapy following lymph node dissection in melanoma patients: Treatment, outcome, and complications, *Cancer Treat. Rev.* 31(1) (2005) 18–26.
- [9] T. P. Kingham, O. I. Alatise, V. Vanderpuye *et al.*, Treatment of cancer in Sub-Saharan Africa, *Lancet Oncol.* 10(4) (2013) 158–167.
- [10] A. Arabameri, D. Asemani, J. Hajati, Mathematical modeling of in-vivo tumor-immune interactions for cancer immunotherapy using matured dendritic cells, *J. Biol. Syst.* 26(1) (2018) 1–22.
- [11] A. Cesano, S. Warren, Bringing the next generation of immuno-oncology biomarkers to the clinic, *Biomedicines* 6(14) (2018) 14–24.
- [12] R. Eftimie, J. L. Bramson, D. J. D. Earn, Interaction between the immune system and cancer: A brief review of non-spatial mathematical models, *Bull. Math. Biol.* 73 (2011) 2–32.
- [13] G. E. Plautz *et al.*, T-cell adoptive immunotherapy of metastatic renal cell carcinoma, *Adult Urology* 54 (1999) 617–623.
- [14] S. A. Rosenberg *et al.*, Use of tumor-infiltrating lymphocytes and interleukin-2 in the immunotherapy of patients with metastatic melanoma, *N. Engl. J. Med.* 319 (1988) 1676–1680.
- [15] L. Anderson, S. Jang, J. L. Yu, Qualitative behaviour of system of tumor-CD4+-cytokine interactions with treatments, *Math. Meth. Appl. Sci.* 38 (2015) 4330–4344.

- [16] M. F. Sanmamed, L. Chen, A paradigm shift in cancer immunotherapy: From enhancement to normalization, *Cell* 175(2) (2018) 313–326.
- [17] Petersen, Brenden K and Yang, Jiachen and Grathwohl, Will S and Cockrell, Chase and Santiago, Claudio and An, Gary and Faissol, Daniel M Deep reinforcement learning and simulation as a path toward precision medicine *Journal of Computational Biology* 26 (2019) 597-604
- [18] Chaplin, D. D. Overview of the immune response. *The Journal of Allergy and Clinical Immunology*, 125(2 Suppl 2), (2010) S3–S23.
- [19] Kantari, C., Pederzoli-Ribeil, M., & Witko-Sarsat, V. The role of neutrophils and monocytes in innate immunity. *Contributions to Microbiology*, 15, (2008) 118–146.
- [20] Cano, R. L. E., & Lopera, H. D. E. (2013). Introduction to T and B lymphocytes. In: Anaya, J. M., Shoenfeld, Y., Rojas-Villarraga, A., et al. (Eds.), *Autoimmunity: From Bench to Bedside*. Bogota (Colombia): El Rosario University Press. Chapter 5. Accessed on July 10, 2023.
- [21] Wilkinson, T. M., Li, C. K. F., Chui, C. S. C., Huang, A. K. Y., Perkins, M., Liebner, J. C., Lambkin-Williams, R., Gilbert, A. S., Oxford, J., Nicholas, B., et al. (2012). Preexisting influenza-specific CD4+ T cells correlate with disease protection against influenza challenge in humans. *Nature Medicine*, 18, 274–280.
- [22] Janeway, C. A., Travers, P., Walport, M., & Shlomchik, M. J. (2001). *Immunobiology: The Immune System in Health and Disease* (5th ed.). Garland Science.
- [23] Alberts, B., Johnson, A., Lewis, J., Raff, M., Roberts, K., & Walter, P. (2002). *Molecular Biology of the Cell* (4th ed.). Garland Science.
- [24] Murphy, K., Travers, P., Walport, M., & Janeway, C. (2012). *Janeway's Immunobiology* (8th ed.). Garland Science.

- [25] Harty, J. T., Tvinnereim, A. R., & White, D. W. (2000). CD8+ T cell effector mechanisms in resistance to infection. *Annual Review of Immunology*, **18**, 275–308.
- [26] Niazi, Sarfaraz K mRNA Vaccines: A Prospective Analysis of Long-term, Multi-target, and Autoimmune Disorders *Distributed under a Creative Commons CC BY license* (2023)
- [27] J. Saravia, N. M. Chapman, H. Chi, “Helper T cell differentiation, *Cellular & Molecular Immunology*, 2019. Available at: <https://www.nature.com/articles/s41423-019-0230-7>
- [28] P. Berraondo, M. F. Sanmamed, M. C. Ochoa *et al.*, Cytokines in clinical cancer immunotherapy, *Br. J. Cancer* 120(1) (2019) 6–15.
- [29] M. Mamat, Subiyanto, A. Kartono, Mathematical model of cancer treatments using immunotherapy, chemotherapy, and biochemotherapy, *Appl. Math. Sci.* 7(5) (2013) 247–261.
- [30] S. Sharma, G. P. Samanta, Dynamical behaviour of a tumor-immune system with chemotherapy and optimal control, *J. Nonlinear Dyn.*, Article ID 608598 (2013) 13 pages.
- [31] L. G. de Pillis, K. R. Fister, W. Gu *et al.*, Optimal control of mixed immunotherapy and chemotherapy of tumors, *J. Biol. Syst.* 16(1) (2008) 51–80.
- [32] A. D’Onofrio, Tumor-immune system interaction: Modeling the tumor-stimulated proliferation of effectors and immunotherapy, *Math. Models Methods Appl. Sci.* 58 (2006) 1375–1401.
- [33] V. Kuznetsov *et al.*, Nonlinear dynamics of immunogenic tumors: Parameter estimation and global bifurcation analysis, *Bull. Math. Biol.* 2 (1994) 295–321.

- [34] S. Michelson *et al.*, Tumor micro-ecology and competitive interactions, *J. Theor. Biol.* 128 (1987) 233–246.
- [35] H. de Vladar, J. González, Dynamic response of cancer under the influence of immunological activity and therapy, *J. Theor. Biol.* 227 (2004) 335–348.
- [36] V. A. Kuznetsov, G. D. Knott, Modeling tumor regrowth and immunotherapy, *Math. Comput. Model.* 33 (2001) 1275–1287.
- [37] B. Goldstein, J. Faeder, W. Hlavacek, Mathematical and computational models of immune-receptor signaling, *Nat. Rev. Immunol.* 4 (2004) 445–456.
- [38] L. De Pillis, A. E. Radunskaya, C. L. Wiseman, A validated mathematical model of cell-mediated immune response to tumor growth, *Cancer Res.* 65 (2005) 7950–7958.
- [39] N. Kronik *et al.*, Improving alloreactive CTL immunotherapy for malignant gliomas using a simulation model of their interactive dynamics, *Cancer Immunol. Immunother.* 57 (2008) 425–439.
- [40] N. Kronik *et al.*, Improving T-cell immunotherapy for melanoma through a mathematically motivated strategy: Efficacy in numbers?, *J. Immunol.* 35 (2012) 116–124.
- [41] C. R. Parish, Cancer immunotherapy: The past, the present, and the future, *Immunol. Cell Biol.* 81 (2003) 106–113.
- [42] D. Kirschner, J. C. Panetta, Modeling immunotherapy of the tumor–immune interaction, *J. Math. Biol.* 37 (1998) 235–252.
- [43] R. Amin, P. Yu, “Bifurcation analysis on immunotherapy of a tumor model without treatment,” *Discrete and Continuous Dynamical Systems - Series S*, 2025.
- [44] P. Yu, Computation of normal forms via a perturbation technique, *J. Sound Vib.* 211 (1998) 19–38.

- [45] P. Yu, M. Han, Four limit cycles from perturbing quadratic integrable systems by quadratic polynomials, *Int. J. Bifurcation Chaos* 22 (2012) 1250254.

- [46] M. Han, P. Yu, Normal forms, Melnikov functions, and bifurcation of limit cycles, Springer-Verlag, London, (2012).

Chapter 4

4 Bifurcation Analysis and Complex Dynamics of a Virotherapy Model

4.1 Introduction

Oncolytic virotherapy is an innovative and developing cancer treatment that uses modified viruses to specifically target and replicate within cancer cells, causing their destruction while sparing healthy tissue. The idea originated in the early 20th century when spontaneous tumor shrinkage was observed in cancer patients after natural viral infections. However, it wasn't until the mid-20th century that the potential of viruses as a therapeutic tool was seriously explored [1]. In the 1950s and 1960s, early clinical observations revealed that some cancer patients showed tumor reduction during or after viral infections like measles or influenza [2].

Although early virotherapy trials showed assurance, progress was limited due to a lack of tools for viral modification and concerns about safety. The field remained underdeveloped until the rise of recombinant DNA technology in the 1990s, which enabled scientists to genetically modify viruses. This advancement allowed for enhanced tumor targeting, reduced toxicity, and increased replicative potential of the viruses [3]. Many oncolytic viruses are designed as vectors for gene delivery. A particularly promising approach involves engineering these viruses to produce pro-inflammatory cytokines and co-stimulatory molecules, which help stimulate a targeted immune response against the tumor [4, 5]. These foundational advancements established the foundation for understanding how oncolytic viruses can selectively target tumor cells and modulate the immune system, connecting historical development with modern therapeutic strategies.

Oncolytic viruses (OVs) are designed or selected to utilize deficiencies in tumor cells.

These viruses work through two main mechanisms: Direct Oncolysis and Immune System Activation. In Direct Oncolysis, OV's particularly infect and reproduce in cancer cells which leads to cell bursting (lysis) and death. After the cell dies, new viral particles are released, which can infect neighboring tumor cells and continue the cycle of infection and destruction [6]. In Immune System Activation, tumor lysis releases tumor-associated antigens and signals the danger which stimulate the host immune system, often converting a "cold" (non-immunogenic) tumor microenvironment into a "hot" (immunogenic). This can lead to an adaptive immune response against the tumor, enhancing the overall therapeutic effect [7]. The dual mechanism of action highlights the potential of OV's to both directly destroy tumor cells and prime the immune system for a sustained antitumor response, linking molecular action to immune activation.

Selectivity for cancer cells is achieved in multiple ways. For example, many OV's are altered to target defects in cellular antiviral responses that are frequently found in tumor cells but remain functional in healthy cells. Others are modified to replicate only in rapidly dividing cells or under the control of tumor-specific promoters [8]. Several viruses have been investigated for their oncolytic potential, including: Adenoviruses, Herpes simplex virus (HSV), Vaccinia virus, Reovirus, Measles virus. These strategies underscore the precision with which OV's can distinguish between healthy and cancerous cells, enhancing safety and efficacy while preparing for clinical applications.

Oncolytic viruses (OV's) are replication-competent viruses with low pathogenicity, engineered to selectively infect and replicate within tumor cells, causing their destruction through direct lysis, while leaving normal cells unharmed. Growing evidence in oncolytic virotherapy shows that OV infection can also stimulate specific antitumor immune responses. Proteins released from OV-lysed tumor cells activate the innate immune system by triggering dendritic cells, which then promote adaptive immunity (Figure 4.1) [9]. The immune stimulating effects of OV's complement their direct oncolytic activity, providing a bifurcated approach to tumor elimination that bridges cell-level and systemic responses.

With continuous progress in treatment methods, research has shown that the virus holds

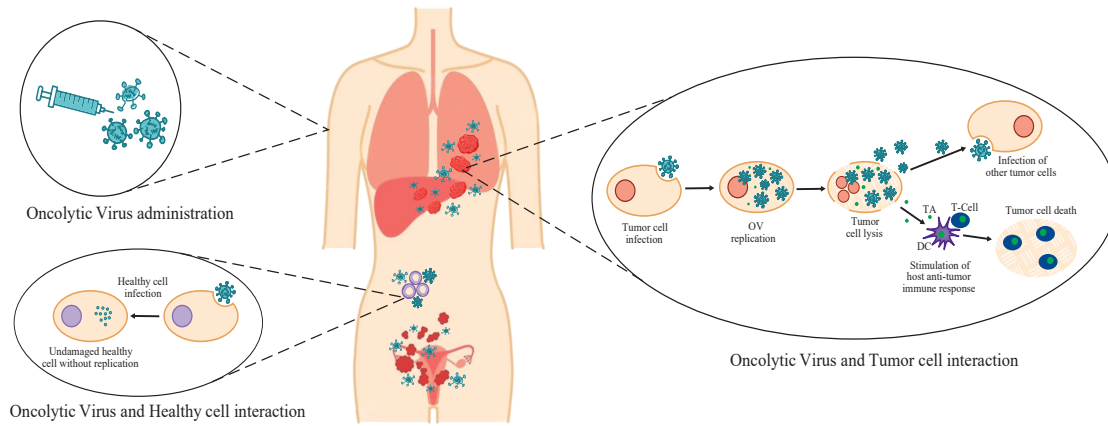


Figure 4.1: Function of oncolytic virotherapy (TA: Tumor Antigen, DC: Dendritic Cell) [9].

significant promise for cancer therapy [10]. Many important advances have been achieved, some of which are highlighted below. The first oncolytic virus drug to be approved was T-Vec (*Talimogene la-herparepvec*), which was created by modifying herpes simplex virus type 1 (HSV-1) and adding GM-CSF. It was approved in the USA in October 2015, in Europe in January 2016, and in Australia in May 2016. T-Vec works by halting tumor growth, helping to extend patient survival [11]. This approval, considered one of the major milestones in the field, marked a significant validation of the approach, as T-VEC became the first oncolytic virus therapy to be permitted in the United States [12]. This landmark approval paved the way for research on other viruses with oncolytic potential, linking regulatory success to ongoing experimental exploration.

Beyond T-VEC, research on the Zika virus (ZIKV) to treat glioblastoma in mice shows promising results, with ZIKV killing glioblastoma stem cells and potentially extending survival. Genetically modified strains may benefit adult patients [13, 14]. Oncolytic viruses are also showing potential against various cancers, including liver, pancreatic, and breast cancers, as well as mesotheliomas and myelomas [15]. In preclinical models of hepato-

cellular carcinoma (HCC), oncolytic viruses have demonstrated strong anti-tumor efficacy [16]. These successes in both clinical and preclinical settings highlight the therapeutic promise of oncolytic viruses and motivate further exploration into their mechanisms of action, maintaining continuity with prior approval milestones.

The interaction between viruses and their host cells plays a fundamental role in understanding the progression and control of infectious diseases, particularly in virotherapy, immunology, and tumor-virus dynamics. Mathematical models serve as indispensable tools in capturing the complex interplay between susceptible (uninfected) cells, infected cells, and free virus particles, providing insights into disease dynamics and guiding therapeutic strategies. Mathematical modeling thus provides a framework for quantifying and predicting the behavior of oncolytic virus therapies in complex biological systems, connecting experimental evidence to theoretical understanding.

To better understand the complex interactions involved in this process, mathematical modeling has played an increasingly important role, helping researchers predict outcomes, design optimal treatment procedures, and identify critical thresholds for therapy success or failure. We analyzed a nonlinear dynamical system that models the interaction between tumor cells, oncolytic viruses, and the immune response. Our objective is to explore the qualitative behavior of the system under various therapeutic conditions.

We considered the mathematical model [17] and applying suitable simplifications to reduce its complexity while conserving key dynamical features. We then thoroughly investigate fundamental properties of the model, including the existence, uniqueness, and boundedness of its solutions. Next, we identify and classify equilibrium points of the system, analyzing their local stability to understand the potential long-term outcomes of the therapy. In particular, we examine how variations in critical parameters can cause significant changes in the system's behavior, including the formation of oscillatory dynamics or persistent tumor-virus coexistence. To discover these phenomena, we perform a bifurcation analysis using tools from nonlinear dynamical systems theory. Specifically, we apply

center manifold theory and normal form analysis to examine the local dynamics near bifurcation points and determine the conditions under which stable limit cycles can arise. Finally, we support our analytical results with numerical simulations that illustrate the system's rich dynamical behavior and provide biological interpretation of the findings. The insights gained from this study enhance our theoretical understanding of oncolytic virus therapy and may contribute to the design of more effective treatment procedures.

4.2 Modeling and Reduction

The interactions between tumors, oncolytic viruses, and the host immune system are complex, involving multiple biological processes that occur on different timescales, affecting the population over time. Mathematical modeling provides a powerful framework for capturing these interactions, offering insights into the mechanisms underlying virotherapy and guiding potential therapeutic strategies.

In this study, we consider a three-component model that describes the essential dynamics of virotherapy by tracking three interacting populations: uninfected cancer cells $x(t)$, infected cancer cells $y(t)$, and free virus particles $v(t)$. The following set of differential equations describes how these populations evolve over time (arbitrary units), capturing the dynamics of their development [18]:

$$\begin{aligned}\frac{dx}{dt} &= rx\left(1 - \frac{x+y}{\omega}\right) - dx - \beta xv, \\ \frac{dy}{dt} &= \beta xv - (d+a)y, \\ \frac{dv}{dt} &= ky - \mu v,\end{aligned}\tag{4.1}$$

All the parameters r , k , β , ω , a , d and μ are positive constants. The meanings of these parameters are explained in Table 4.1 [19].

The first equation models the net growth of uninfected cancer cells. In the absence

Table 4.1: Model parameters for system (4.1) and their biological interpretation.

Parameter	Biological meaning	Value
r	Intrinsic growth rate of uninfected tumor cells	1/2
ω	Tumor carrying capacity (cell density scale)	10
d	Natural death rate of uninfected tumor cells	1/10
β	Infection rate constant (virus–cell contact efficacy)	3/2
a	Virus–induced death rate of infected cells	1/5
k	Virion production rate per infected cell	1/10
μ	Clearance rate of free virions	1/10

of infection, these cells proliferate at a rate rx , following logistic growth with carrying capacity ω , reflecting limitations due to space, nutrients, and other resources. They also die naturally at rate dx , so their average lifespan is $1/d$. Infection occurs when free virus particles encounter uninfected cells at rate βxv , where β , accounts for both the probability of successful viral entry and the rate at which encounters occur.

The second equation describes the population of infected cancer cells. These cells arise from successful infection events and are lost through two processes: natural death at rate dy and virus-induced death at rate ay . Thus, the mean lifespan of an infected cell is $1/(d + a)$.

The third equation governs the dynamics of free virus particles. Each infected cell produces virus at rate k , giving a total “burst size” of $k/(a + d)$ particles per infected cell over its lifetime. Free viruses are cleared from the system at rate μv , yielding an average viral lifespan of $1/\mu$.

To facilitate analysis, we introduce the following non dimensional variables and time rescaling:

$$x = \omega X, \quad y = \omega Y, \quad v = \frac{k\omega}{r} Z, \quad t = \frac{1}{r} \tau$$

Substituting these into (4.1) yields the dimensionless system

$$\begin{aligned}\frac{dX}{d\tau} &= X(1 - X - Y - D - BZ), \\ \frac{dY}{d\tau} &= BXZ - AY, \\ \frac{dZ}{d\tau} &= Y - CZ,\end{aligned}\tag{4.2}$$

where $X(\tau)$, $Y(\tau)$, $Z(\tau)$ represent the scaled populations of uninfected cells, infected cells, and free virus particles, respectively. The parameters

$$A = \frac{d+a}{r}, \quad B = \frac{\beta k \omega}{r^2}, \quad C = \frac{\mu}{r}, \quad D = \frac{d}{r}.$$

All values are positive and represent biologically relevant rates in a non-dimensional form: A is the death rate of infected cells, B measures the effective infection strength, C is the clearance rate of free virus particles, and D reflects the death rate of uninfected cells.

The system (4.2) is studied subject to the non-negative initial conditions

$$X(0) = X_0 \geq 0, \quad Y(0) = Y_0 \geq 0, \quad Z(0) = Z_0 \geq 0.\tag{4.3}$$

Our analysis focuses on the generic dynamics of (4.2) in the four-dimensional parameter space (A, B, C, D) . In particular, we investigate the onset and nature of oscillatory dynamics through Hopf bifurcation theory. By examining the interplay of these parameters, we identify conditions under which multiple limit cycles may arise, leading to distinct bistable regimes. This exploration of Hopf and generalized Hopf bifurcations provides deeper insight into how changes in biological rates can qualitatively alter the virotherapy outcome.

4.3 Positivity and Boundedness of Solutions

In biological models, variables such as cell densities and virus concentrations must remain nonnegative and typically stay bounded for all time. We now establish that the system under consideration satisfies these properties.

Theorem 4.3.1 *Let the initial conditions (X_0, Y_0, Z_0) be nonnegative. Then the corresponding solution $(X(\tau), Y(\tau), Z(\tau))$ exists, is unique, remains nonnegative for all $\tau \geq 0$, and is uniformly bounded.*

Proof Existence and uniqueness follow from the standard theory of ordinary differential equations, since the right-hand side of (4.2) is locally Lipschitz on \mathbb{R}^3 . It remains to show positivity and boundedness. We begin with the tumor equation in the absence of viral infection. By the variation-of-constants formula applied to the uninfected cells equation in (4.2), we obtain

$$X(\tau) = X(0) e^{\int_0^\tau [1 - X(s) - Y(s) - D - BZ(s)] ds},$$

Since exponential factor is strictly positive, it follows that $X(\tau) \geq 0$, for all $\tau \geq 0$ whenever $X(0) \geq 0$. Similarly, from the infected tumor cell equation in (4.2) we have

$$Y(\tau) = e^{-A\tau} \left[Y(0) + \int_0^\tau BX(s)Z(s)e^{As} ds \right],$$

and from the virus particle equation in (4.2),

$$Z(\tau) = e^{-C\tau} \left[Z(0) + \int_0^\tau Y(s)e^{Cs} ds \right].$$

These expressions show that $Y(\tau)$ and $Z(\tau)$ are mutually nonnegative: if $Y(\tau) \geq 0$ for $\tau \geq 0$, then $Z(\tau) \geq 0$, and conversely.

We now claim that both $Y(\tau) \geq 0$ and $Z(\tau) \geq 0$ for all $\tau \geq 0$. Suppose, for contradiction, that one of them first crosses zero. Without loss of generality, assume $Y(\tau)$ crosses zero at

$\tau = \tau_1$ and $Z(\tau)$ at $\tau = \tau_2$. Then $Y(\tau_1) = 0$ with $Y(\tau) > 0$ for $\tau < \tau_1$, and $Z(\tau_2) = 0$ with $Z(\tau) > 0$ for $\tau < \tau_2$.

If $\tau_1 \leq \tau_2$, then $Z(\tau) > 0$ for $\tau < \tau_2$, and hence

$$Y(\tau_1) = e^{-A\tau_1} \left[Y(0) + \int_0^{\tau_1} BX(s)Z(s)e^{As} ds \right] > 0,$$

which contradicts $Y(\tau_1) = 0$. Thus, $Y(\tau) \geq 0$ for all $\tau \geq 0$. On the other hand, if $Y(\tau) > 0$ for $\tau < \tau_1$, and

$$Z(\tau_2) = e^{-C\tau_2} \left[Z(0) + \int_0^{\tau_2} Y(s)e^{Cs} ds \right] > 0.$$

contradicting $Z(\tau_2) = 0$. Hence, $Z(\tau) \geq 0$ for all $\tau \geq 0$. Therefore, all three components remain nonnegative for all time.

Next, we prove boundedness of solutions to (4.2). Consider the Lyapunov function

$$V(X, Y, Z) = X + Y + AZ,$$

which is positive definite for positive solutions, radially unbounded, and whose level sets $V = h$ are planes in the first octant. Differentiating V with respect to time τ along the trajectories of system (4.2) we obtain

$$\frac{dV}{d\tau} = \frac{dX}{d\tau} + \frac{dY}{d\tau} + A \frac{dZ}{d\tau} = X(1 - X - Y - D) - ACZ.$$

Thus, the condition $\frac{dV}{d\tau} = 0$ define the surface,

$$S_V : X(1 - X - Y - D) - ACZ = 0,$$

in the first octant, with $\frac{dV}{d\tau} < 0$ outside S_V . Moreover, the plane,

$$\Pi : X + Y + AZ = 1 - D, \quad (D < 1),$$

encloses S_V , implying that $\frac{dV}{d\tau} < 0$ outside the plane Π . Hence, the region

$$\Omega = \{(X, Y, Z) \mid X \geq 0, Y \geq 0, Z \geq 0, X + Y + AZ \leq 1 - D\}.$$

is positively invariant and absorbing. Therefore, every trajectory of (4.2) starting in the first octant eventually enters and remains in Ω .

This finishes the proof for Theorem 4.3.1.

4.4 Equilibrium Solutions and Their Stability

The equilibrium states of system (4.2) are obtained by setting $\frac{dX}{d\tau} = \frac{dY}{d\tau} = \frac{dZ}{d\tau} = 0$. Solving these algebraic equations yields three biologically relevant equilibria:

$$\begin{aligned} \text{Trivial equilibrium:} & \quad E_0 = (0, 0, 0), \\ \text{Boundary equilibrium:} & \quad E_1 = (1 - D, 0, 0), \\ \text{Positive equilibrium:} & \quad E_2 = \left(\frac{AC}{B}, CZ_2, \frac{B(1 - D) - AC}{B(B + C)} \right). \end{aligned} \tag{4.4}$$

At the equilibrium E_0 , uninfected cells, infected cells, and free virus particles are all absent. The equilibrium E_1 corresponds to a virus-free state in which only uninfected cells persist. The uninfected cell density at equilibrium is $1 - D$, where D accounts for natural loss or immune clearance. No infection is present, and the virus population is zero. The coexistence equilibrium E_2 describes the situation in which uninfected cells, infected cells, and free virus particles all persist at constant positive levels. This state is feasible only when $B(1 - D) > AC$, ensuring that viral infection and production are sufficient to balance

losses from cell death and viral clearance. Two important thresholds emerge from these expressions. The basic reproduction number is given by

$$R_0 = \frac{B(1 - D)}{AC}. \quad (4.5)$$

which measures the average number of newly infected cells produced by one infected cell in an uninfected population. It accounts for both the virus infection rate and the fraction of susceptible cells, relative to losses from cell death and viral clearance. The condition $R_0 > 1$ ensures that the virus can invade and establish itself, making the coexistence equilibrium biologically feasible. when $R_0 < 1$, the virus dies out and the system remains virus-free.

A transcritical bifurcation occurs between E_1 and E_2 at

$$D_t = 1 - \frac{AC}{B}. \quad (4.6)$$

where the stability of the virus-free equilibrium changes, and the coexistence equilibrium emerges. In particular, a Hopf bifurcation may arise at the coexistence equilibrium when the parameter D reaches the critical value

$$D_H = 1 - \frac{AC}{B} - (B + C)Z_2, \quad (4.7)$$

leading to sustained oscillations in all three populations.

Theorem 4.4.1 *For system (4.2), the boundary equilibria E_0 and E_1 exist for all parameter values, whereas the interior equilibrium E_2 exists only when $D < D_t$. The equilibrium E_0 is always a saddle point. The equilibrium E_1 is locally asymptotically stable (LAS) when $D > D_t$ but becomes unstable for $D < D_t$. Conversely, the interior equilibrium E_2 is LAS when $D < D_H$ and loses stability when $D > D_H$, where D_H is the Hopf bifurcation threshold. A transcritical bifurcation occurs at $D = D_t$, marking an exchange of stability between E_1 and E_2 , and a Hopf bifurcation emerges from E_2 at $D = D_H$.*

Proof The two boundary equilibria E_0 and E_1 exist for all parameter values, while E_2 exists only when $B(1 - D) > AC$, i.e., $D < D_t$. The stability of the three equilibrium solutions can be easily determined by the Jacobian matrix of (4.2), evaluated at the steady states. The Jacobian matrix of (4.2) is given by

$$J(X, Y, Z) = \begin{bmatrix} 1 - 2X - Y - D - BZ & -X & -XB \\ & BZ & -A & XB \\ & 0 & 1 & -C \end{bmatrix}. \quad (4.8)$$

Evaluating J at the boundary equilibria E_0 and E_1 , we have

$$J(E_0) = \begin{bmatrix} 1 - D & 0 & 0 \\ 0 & -A & 0 \\ 0 & 1 & -C \end{bmatrix} \quad \text{and} \quad J(E_1) = \begin{bmatrix} D - 1 & D - 1 & (D - 1)B \\ 0 & -A & (1 - D)B \\ 0 & 1 & -C \end{bmatrix}.$$

It is easy to see from $J(E_0)$ that the population-free equilibrium E_0 is a saddle-node with a stable manifold lying on the non-negative Y - Z plane. In this case, E_0 is locally stable for $D > 1$, unstable for $D < 1$ and bifurcation between E_0 and E_1 for $D = 1$. If the condition $B(1 - D) < AC$ holds, all eigenvalues have negative real parts and E_1 is locally stable. Biologically, this implies that the infection fails to establish itself within the host population, and the virus is ultimately cleared. Conversely, if $B(1 - D) > AC$, the equilibrium E_1 becomes unstable. In this case, the virus successfully invades and persists in the population, potentially resulting in a stable endemic state. A transcritical bifurcation occurs between E_1 and E_2 at the critical point $D_t = 1 - \frac{AC}{B}$, but E_2 only exists for $D \geq D_t$. When the condition $D > D_t$ is met, the infection persists within the host, leading to a chronic state. This endemic equilibrium may be locally stable, meaning small perturbations in the system will not eliminate the infection but instead return to this chronic state.

Next, consider the stability of E_2 . Evaluating the Jacobian matrix of system (4.2) at the interior equilibrium E_2 , we obtain

$$J(E_2) = \begin{bmatrix} -\frac{AC}{B} & -\frac{AC}{B} & -AC \\ BZ_2 & -A & AC \\ 0 & 1 & -C \end{bmatrix}. \quad (4.9)$$

A direct computation yields the characteristic polynomial for E_2 :

$$P_{E_2}(\lambda) = \lambda^3 + a_1\lambda^2 + a_2\lambda + a_3, \quad (4.10)$$

where

$$\begin{aligned} a_1 &= \frac{AB + AC + BC}{B}, \\ a_2 &= \frac{AC(BZ_2 + A + C)}{B}, \\ a_3 &= AC(B + C)Z_2. \end{aligned} \quad (4.11)$$

It is easy to see that $a_3 > 0$ due to the existence condition $B > AC$ and $Z_2 < \frac{B-AC}{B(B+C)}$ for E_2 . At the critical point $D = 1$, $a_1 > 0$, $a_2 > 0$ and $a_3 = 0$, at which $E_1 = E_2$, implying that a transcritical bifurcation occurs between E_1 and E_2 .

According to the Routh–Hurwitz criteria, the equilibrium point E_2 is locally asymptotically stable (LAS) provided that $a_1 > 0$, $a_3 > 0$ and $\Delta_2 = a_1a_2 - a_3 > 0$. Consequently, Δ_2 is the first quantity to cross zero as the parameter varies, while a_1 and a_2 remain positive. This suggests that the only possible bifurcation emerging from E_2 is a Hopf bifurcation. A Bogdanov–Takens (B–T) bifurcation is ruled out, as it requires both $a_2 = 0$ and $a_3 = 0$, which is not the case here. To further examine the possibility of a Hopf bifurcation at E_2 , we now derive the explicit expression for Δ_2 .

$$\Delta_2 = \frac{AC\Delta_{2a}}{B^2},$$

where

$$\Delta_{2a} = B(AB + AC - B^2)Z_2 + (A + C)(AB + AC + BC).$$

A positive Z_2 solving $\Delta_{2a} = 0$ requires that $AB + AC - B^2 < 0$ implying that $A < \frac{B^2}{(B+C)}$. This yields the Hopf condition

$$Z_2 = \frac{(A + C)(AB + AC + BC)}{B[B^2 - A(B + C)]} > 0,$$

Substituting this into the equilibrium relations gives the explicit Hopf threshold

$$D_H = - \frac{B(B + C)A^2 + [C^3 + B(B + C)(3C + 1)]A - B(B^2 - BC^2 - C^3)}{B[B^2 - A(B + C)]}$$

The positivity condition $D_H > 0$ implies

$$B(B + C)A^2 + [C^3 + B(B + C)(3C + 1)]A - B(B^2 - C^2B - C^3) < 0$$

which leads to the parameter restrictions:

$$B > \frac{C(C + \sqrt{(C^2 + 4C)})}{2} \quad \text{and} \quad A < \min \left\{ \frac{B}{C}, \frac{B^2}{(B + C)}, A_c \right\},$$

where

$$A_c = \frac{A_{c1} - C^3 - B(B + C)(3C + 1)}{2B(B + C)},$$

in which

$$A_{c1} = \sqrt{(C^3 + B(B + C)(3C + 1))^2 + 4B^2(B + C)(B^2 - C^2B - C^3)}$$

Here A_c is the critical parameter marking the onset of oscillatory dynamics. When $D = D_H$, E_2 loses stability via a Hopf bifurcation, giving rise to sustained oscillations.

This completes the proof.

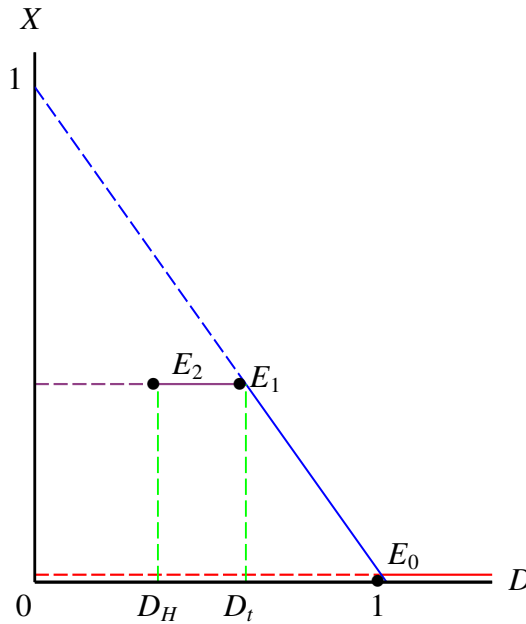


Figure 4.2: Bifurcation diagram for system (4.2) illustrating the equilibrium points E_0 , E_1 and E_2 . Stable equilibria are indicated by solid lines, while unstable equilibria are shown using dotted lines.

A bifurcation diagram of system (4.2), projected onto the D - X plane, is presented in Figure 4.2. This diagram illustrates the three equilibrium E_0 , E_1 and E_2 along with their corresponding stability properties. The diagram also highlights the critical points where bifurcations occurs: the transcritical bifurcation at $D = D_t$ and the Hopf bifurcation at $D = D_H$. The bifurcation point acts as a critical threshold for infection persistence.

4.5 Codimension of Hopf bifurcation

Having established the conditions necessary for the Hopf bifurcation at the endemic equilibrium E_2 , we now turn to an investigation of its codimension. The qualitative dynamics and bifurcations of system (4.2) can be summarized as follows. The disease-free equilibrium E_0 is always a saddle. The boundary equilibrium E_1 is locally asymptotically stable when $R_0 < 1$ but becomes unstable when $R_0 > 1$. The endemic equilibrium E_2 exists only for $R_0 > 1$. A transcritical bifurcation occurs at $R_0 = 1$, where stability is exchanged be-

tween E_1 and E_2 . We focus here on the regime $R_0 > 1$, under which a Hopf bifurcation can arise at E_2 , and in particular, we determine the codimension of this bifurcation.

When $R_0 = 1$, or equivalently $D = 1 - \frac{AC}{B}$, the system reaches a critical threshold. At this point, the equilibria E_1 and E_2 coincide at $D = D_t$, leading to rich and potentially complex dynamics unfolding on the center manifold. Meanwhile, the equilibrium point E_0 remains a saddle node.

To retain the explicit presence of B in the analysis of this critical case, we treat D as the bifurcation parameter and write $B = \frac{AC}{(1-D)}$ equivalently as $D = 1 - \frac{AC}{B}$. At $D = D_t = 1 - \frac{AC}{B}$, the basic reproduction number satisfies $R_0 = 1$, and the equilibrium states align accordingly.

$$E_0 = (0, 0, 0), \quad E_1 = E_2 = \left(\frac{AC}{B}, 0, 0\right). \quad (4.12)$$

In this degenerate situation, the transcritical bifurcation point lies precisely on the boundary between the virus-free and endemic states, and determining the stability properties requires a center manifold reduction at the critical point.

4.5.1 Center manifold reduction

We first use the center manifold theory to find the differential equation describing dynamics on the center manifold, and then discuss the stability of E_1 . The translation component of the transformation moves the equilibrium E_1 to the origin, while the linear part (diagonal and off-diagonal terms) is constructed from the corresponding eigenvectors of the Jacobian matrix evaluated at E_1 . To achieve this, we first introduce an affine transformation, given by

$$\begin{pmatrix} X \\ Y \\ Z \end{pmatrix} = \begin{pmatrix} \frac{AC}{B} \\ 0 \\ 0 \end{pmatrix} + \begin{bmatrix} -(B+C) & 1 & \frac{AC(B-A)}{(A+C)B-AC} \\ C & 0 & -A \\ 1 & 0 & 1 \end{bmatrix} \begin{pmatrix} u \\ v \\ w \end{pmatrix}, \quad (4.13)$$

into (4.2) with $D_t = 1 - \frac{AC}{B}$ to obtain the system,

$$\begin{aligned}
 \frac{du}{d\tau} &= -\frac{(B+C)B}{A+C}u^2 - \frac{BAC(A-B)}{(AB-AC+BC)(A+C)}w^2 + \frac{B}{A+C}uv \\
 &\quad - \frac{B[C(A-C)(A-B) + (A+C)B^2]}{(AB-AC+BC)(A+C)}uw + \frac{B}{A+C}vw, \\
 \frac{dv}{d\tau} &= -\frac{AC}{B}v + \frac{(B+C)(AC-B^2-BC)B}{(AB-AC+BC)}u^2 - v^2 \\
 &\quad - \frac{ABC(A-B)(A^2-AB+B^2)}{(AB-AC+BC)^2}w^2 + \frac{A(B^2-BC-C^2)+B(B+C)^2}{(AB-AC+BC)}uv \\
 &\quad - \left\{ \frac{B[A^3(B^2-2C^2) - A^2B(B^2-2BC-4C^2)]}{(AB-AC+BC)^2} \right. \\
 &\quad \quad \left. + \frac{B[AB^2(B^2-2BC-3C^2) + B^3C(B+C)]}{(AB-AC+BC)^2} \right\} uw \\
 &\quad + \frac{[A^2(B+C) + B(B^2-AB-AC)]}{AB-AC+BC}vw, \\
 \frac{dw}{d\tau} &= -(A+C)w + \frac{(B+C)B}{A+C}u^2 + \frac{BAC(A-B)}{(AB-AC+BC)(A+C)}w^2 \\
 &\quad - \frac{B}{A+C}uv + \frac{B[A^2C + AB^2 - C(A-B)(B+C)]}{(AB-AC+BC)(A+C)}uw - \frac{B}{A+C}vw.
 \end{aligned} \tag{4.14}$$

The linear part of system (4.12) is already in Jordan canonical form, with eigenvalues 0, $-\frac{AC}{B}$, $-(A+C)$. Proceeding with the application of center manifold theory and introducing

$$v = au^2, \quad w = bu^2,$$

and equating the corresponding coefficients in the equations:

$$\frac{dv}{d\tau} = 2au\dot{u}, \quad \text{and} \quad \frac{dw}{d\tau} = 2bu\dot{u}$$

combined with (4.12) gives

$$a = \frac{B^2(B+C)(AC-B^2-BC)}{AC(AB-AC+BC)}, \quad b = \frac{B(B+C)}{(A+C)^2}.$$

Thus, the center manifold, up to second order is given by

$$W^c = \{(u, v, w) | v = \frac{B^2(B+C)(AC-B^2-BC)}{AC(AB-AC+BC)}u^2 + O(u^3), w = \frac{B(B+C)}{(A+C)^2}u^2 + O(u^3)\},$$

and the differential equation governing the dynamics on the center manifold is

$$\frac{du}{d\tau} = -\frac{B(B+C)}{(A+C)}u^2 + O(u^3), \tag{4.15}$$

This clearly shows that the equilibrium E_2 is a saddle, as the coefficient of u^2 is negative. With $D = 1 - \frac{AC}{B}$, the system continues to have four parameters, A , B , C and D . Below, we briefly describe the dynamics and bifurcation structure of system (4.2). From (4.13), it is evident that $u = 0$ is a saddle point on the center manifold.

4.5.2 Bifurcation of limit cycles and their stability

To analyze the local dynamics near a non-hyperbolic equilibrium point in a nonlinear n -dimensional system, we employ center manifold theory and normal form reduction. These tools simplify the system while preserving the essential dynamics that determine bifurcations, particularly Hopf bifurcations and the emergence of limit cycles.

Consider a general autonomous system of ordinary differential equations:

$$\dot{u} = F(u, \mu), \quad u \in R^n, \quad \mu \in R, \tag{4.16}$$

where F is a smooth vector field, and μ is a bifurcation parameter. Let u_0 be an equilibrium of the system at $\mu = \mu_0$. Suppose the Jacobian matrix $J = D_u F(u_0, \mu_0)$ has a pair of purely imaginary eigenvalues $\pm i\omega_0$ and the remaining eigenvalues have negative real parts. Then u_0 is a non-hyperbolic equilibrium, and the dynamics near it are governed by the two-dimensional center manifold associated with the imaginary eigenvalues.

$$\frac{dz}{dt} = i\omega_0 z + \sum_{k=2}^{\infty} a_k(\mu) z |z|^{2k-2}, \quad z \in \mathbb{C},$$

or equivalently, in polar coordinates $z = re^{i\theta}$:

$$\frac{dr}{dt} = \sum_{k=1}^{\infty} v_k(\mu)r^{2k+1}, \quad \frac{d\theta}{dt} = \omega_0 + \sum_{k=1}^{\infty} \omega_k(\mu)r^{2k}.$$

The coefficients $v_k(\mu)$ are known as focus values, and they determine the nature and stability of limit cycles near the Hopf bifurcation point. The first nonzero focus value $v_k \neq 0$ provides the critical information about the type and multiplicity of limit cycles that bifurcate from the equilibrium. The normal form approach computes these focus values by performing a near-identity transformation that simplifies the nonlinear terms while preserving the qualitative behavior. This is essential for classifying the bifurcation type, determining the existence and stability of periodic solutions, and predicting complex dynamical behavior such as oscillations and multistability. Additional insights into the bifurcation behavior of limit cycles, including scenarios involving the emergence of multiple cycles and changes in stability, are extensively discussed in references [20, 21].

To compute the first-order focus value via normal form theory, we first perform an affine transformation of the system, which allows the system to be expressed in a form suitable for the analysis:

$$\begin{pmatrix} X \\ Y \\ Z \end{pmatrix} = \begin{pmatrix} \frac{AC}{B} \\ \frac{BC(1-D) - AC^2}{B(B+C)} \\ \frac{B(1-D) - AC}{B(B+C)} \end{pmatrix} + \begin{bmatrix} \frac{-AC(B+C)}{(A+B)C+AB} & \frac{B^2\omega_c - (B+C)A}{A(B+C)+BC} & \frac{AC(B^2 - AB - AC)}{B^2(A+C)} \\ C & \omega_c & -\frac{(B+C)A}{B} \\ 1 & 0 & 1 \end{bmatrix} \begin{pmatrix} u \\ v \\ w \end{pmatrix},$$

where

$$\omega_c = \sqrt{\frac{AC(B+C)(A+C)}{B^2 - A(B+C)}}, \quad (B^2 - AB - AC > 0),$$

is substituted into (4.2) to yield a system whose linear part is expressed in Jordan canonical form:

$$\begin{aligned} \frac{du}{d\tau} &= \omega_c v + \frac{AC(A+C)B^3(B+C)(B^2+BC+C^2)}{M_2M_3} u^2 \\ &\quad - \frac{ACB^3(A+C)^2(B+C)^2}{M_2M_3} v^2 - \frac{ACM_1^2M_4}{B^2(A+C)M_3} w^2 \\ &\quad + \frac{(A+C)B^3M_{11}\omega_c}{M_2M_3} uv + \frac{ACM_1M_5}{M_2M_3} uw + \frac{M_1M_6\omega_c}{M_2M_3} vw, \\ \frac{dv}{d\tau} &= -\omega_c u - \frac{ABC(B+C)M_7}{M_2M_3\omega_c} u^2 + \frac{B^2(A+C)(B+C)\omega_cM_1}{M_3} v^2 \\ &\quad - \frac{ACM_1M_8}{B^3(A+C)M_3\omega_c} w^2 - \frac{BM_9}{M_2M_3} uv + \frac{A^2C^2M_{10}}{B(A+C)M_2M_3\omega_c} uw \\ &\quad - \frac{M_1[M_8 - ABC(B+C)M_2^2]}{BM_2M_3} vw, \\ \frac{dw}{d\tau} &= -\frac{(A+C)B+AC}{B} w - \frac{AB^3C(A+C)(B+C)(B^2+BC+C^2)}{M_2M_3} u^2 \\ &\quad + \frac{AB^3C(A+C)^2(B+C)^2}{M_2M_3} v^2 + \frac{ACM_1^2M_4}{B^2(A+C)M_3} w^2 \\ &\quad - \frac{B^3(A+C)\omega_cM_{11}}{M_2M_3} uv - \frac{ACM_1M_5}{M_2M_3} uw - \frac{M_1M_6\omega_c}{M_2M_3} vw, \end{aligned} \tag{4.17}$$

where

$$\begin{aligned}
 M_1 &= B^2 - A(B + C), \\
 M_2 &= BC + A(B + C), \\
 M_3 &= A^3(B + C)^3 - A^2B(B + C)(B^2 - 2C^2) - 2AB^3C(B + C) - B^4C^2, \\
 M_4 &= A^2(B + C)^2 + AB(B^2 + 2BC + 2C^2) + B^2C(B + C), \\
 M_5 &= A^2(B + C)^3 + ABC(B + C)^2 + B^3C^2, \\
 M_6 &= A^3(B + C)^3 + A^2BC^2(B + C) - AB^3(B^2 + BC + C^2) - B^4C(B + C), \\
 M_7 &= A^3(B + C)^3 + A^2BC(B + 3C)(B + C) + ABC^2(B^2 + 3BC + C^2) \\
 &\quad + B^2C^3(B + C), \\
 M_8 &= A^4(B + C)^4 - A^3B(B^2 - BC - 3C^2)(B + C)^2 \\
 &\quad - A^2B^2C(B + C)(B^2 + BC - 3C^2) - AB^3C^2(B^2 + BC - C^2) - B^5C^3, \\
 M_9 &= A^4(B + C)^4 - A^3B(B^2 - BC - 4C^2)(B + C)^2 \\
 &\quad - A^2BC(B + C)(B^3 - 6BC^2 - 2C^3) \\
 &\quad - AB^2C^2(B + 2C)(B^2 - BC - C^2) - B^4C^3(B + C), \\
 M_{10} &= A^3(B^2 + BC + C^2)(B + C)^3 + A^2BC(B^2 + BC + 2C^2)(B + C)^2 \\
 &\quad + AB^2C^2(B^3 + C^3) + B^5C^3, \\
 M_{11} &= A(B + C)(B^2 + 2BC + 2C^2) - B^2(B^2 + BC + C^2).
 \end{aligned}$$

The system is first expanded about the equilibrium point (u, v, w) , after which we use a Maple implementation of normal form theory in [22] for Hopf bifurcation to derive the normal form up to terms of third order, as shown below:

$$\frac{dr}{d\tau} = r(v_0\mu + v_1r^2 + O(r^4)), \tag{4.18}$$

Here, $\mu = D - D_H$, serves as the perturbation parameter, and v_0, v_1 , denote the zeroth and first-order focus values, respectively. The transversality condition is derived through linear stability analysis, as follows:

$$v_0 = -\frac{BCA[B^2 - A(B + C)]^2}{2(B + C)\omega_c v_{0d}},$$

$$v_{0d} = [B^2 - A(B + C)][(B^2 + AC)(A + C)^2 + 3ABC(A + C) + A^2C^2] + A^2C(A + C)(AB + AC + 2BC + C^2), \quad (4.19)$$

which implies $v_{0d} > 0$ due to $B^2 - A(B + C) > 0$, and hence the transversal condition $v_{0d} < 0$.

The equation (4.18) serves as a foundation for bifurcation analysis. The sign of the first-order focus value, v_1 , determines the nature of the Hopf bifurcation: a positive value indicates a subcritical bifurcation, while a negative value indicates a supercritical one. Furthermore, the signs of higher-order focus values play a crucial role in assessing the stability and existence of multiple limit cycles emerging from the bifurcation. The general necessary and sufficient conditions for the occurrence of multiple limit cycles are shown in [23]. Applying this framework to our specific system given in (4.17) and utilizing the Maple program described in [22], we compute the first-order focus value v_1 as follows:

$$v_1 = -\frac{CAB^2[B^2 - A(B + C)] v_{1a}}{8(A + C)[A(B + C) + BC]^2 v_{1b}}$$

where

$$\begin{aligned}
 v_{1a} = & [B^2 - A(B + C)]^2 \{ (4A^2 - AC + 4C^2)(A + C)^2 B^4 \\
 & + (A + C)(2A^4 + 16A^3C + 31A^2C^2 + 15AC^3 + 6C^4) B^3 \\
 & + (2A^6 + 17A^5C + 68A^4C^2 + 129A^3C^3 + 105A^2C^4 + 33AC^5 + 3C^6) B^2 \\
 & + (2A^7 + 21A^6C + 97A^5C^2 + 217A^4C^3 + 243A^3C^4 + 125A^2C^5 + 23AC^6 + C^7) B \\
 & + A(2A^7 + 25A^6C + 135A^5C^2 + 361A^4C^3 + 488A^3C^4 + 330A^2C^5 + 98AC^6 \\
 & + 8C^7) \} + [B^2 - A(B + C)] A(A + C)^2 [B(2A^6 + 25A^5C + 127A^4C^2 \\
 & + 276A^3C^3 + 220A^2C^4 + 45AC^5 + 2C^6) + AC(4A^5 + 42A^4C + 165A^3C^2 \\
 & + 259A^2C^3 + 128AC^4 + 13C^5)] + CA^2(A + C)^2 [B(2A^6 + 23A^5C \\
 & + 93A^4C^2 + 158A^3C^3 + 105A^2C^4 + 21AC^5 + C^6) + AC(2A^5 + 21A^4C \\
 & + 74A^3C^2 + 101A^2C^3 + 46AC^4 + 5C^5)], \\
 v_{1b} = & \{ [B^2 - A(B + C)] [(A + C)^2 B^2 + 3AC(A + C)B + AC(A^2 + 3AC + C^2)] \\
 & + A^2C(A + C)[(A + C)(B + C) + BC] \} \\
 & \times \{ [B^2 - A(B + C)] [(A + C)^2 B^2 + 6AC(A + C)B + AC(4A^2 + 9AC + 4C^2)] \\
 & + 4A^2C(A + C)(A + C)(B + C) + BC \}.
 \end{aligned}$$

This clearly shows that $v_{1a} > 0$ and $v_{1b} > 0$ since $B^2 - A(B + C) > 0$ (i.e., $\omega_c > 0$). Hence, $v_1 < 0$, implying that the bifurcating limit cycle is stable.

The existence of a Hopf bifurcation in system (4.2) indicates the potential for cyclical tumor-virus dynamics, i.e., tumor growth and shrinkage occurring periodically over time.

4.6 Simulation

We now perform numerical simulations of model (4.2) in MATLAB to verify that the analytical predictions are consistent with the time domain dynamics. We also explore how variations in the parameters A , B , C and D influence system behavior. These parameters respectively represent the death rate of tumor cells, the strength of immune activity on tumor growth, the decay rate of the immune response, and the extent to which stress or damage reduces healthy cell growth. After non dimensionalization, we consider the parameter set

$$A = \frac{3}{5}, \quad B = 6, \quad C = \frac{1}{5}, \quad D = \frac{1}{5}.$$

When tumor cell growth is absent, the numerical simulation (Figure 4.3) shows that both the infected cells and the virus initially fluctuate over time but eventually decline to zero. The uninfected tumor cells, in turn, gradually decrease over time, eventually stabilizing at either zero or a constant positive level. With initial conditions $X(0) = 0.4$, $Y(0) = 0$, $Z(0) = 0.1$, the uninfected cells decrease to zero, and the solution trajectories approach the disease-free equilibrium $E_0 = (0, 0, 0)$, as depicted in Figure 4.3(a). However, when using the same initial conditions, but a different value of D , the uninfected tumor cells stabilize at a positive equilibrium level, and the solution curves converge to the equilibrium $E_1 = (0.1, 0, 0)$, as shown in Figure 4.3(b).

Numerical experiments show the following behavior depending on the value of D .

- For $D = 1.1 > 1$, the system converges to the trivial equilibrium E_0 .
- For $D = 0.9 \in (D_t, 1)$, where $D_t = \frac{8}{9}$, the system convergent to E_1 .

We also simulate using a new set of parameters:

$$A = \frac{19}{20}, \quad B = 9, \quad C = 1, \quad D = \frac{1569191919}{5000000000}.$$

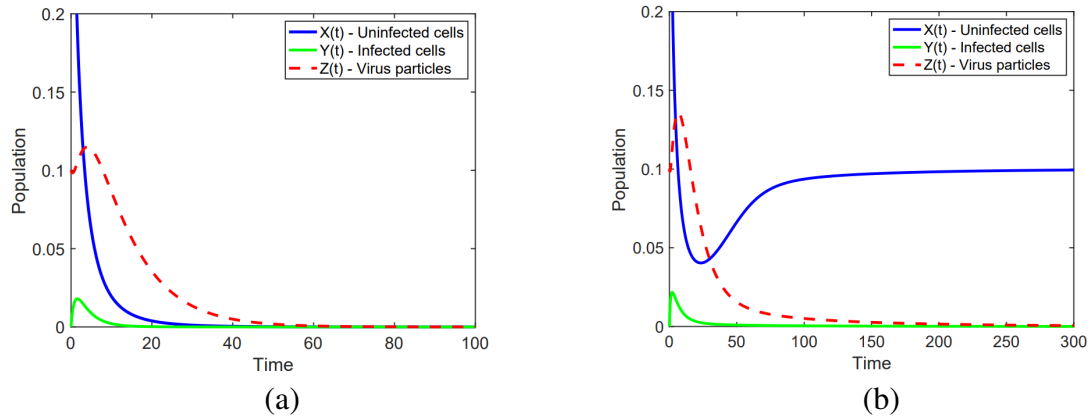


Figure 4.3: Simulations of model (4.2) for $A = 1$, $B = \frac{9}{10}$, $C = \frac{1}{10}$, $D_t = \frac{8}{9}$, with the initial condition: $X(0) = 0.4$, $Y(0) = 0$, $Z(0) = 0.1$ (a) $D = \frac{11}{10}$ and (b) $D = \frac{9}{10} \in (D_t, 1)$.

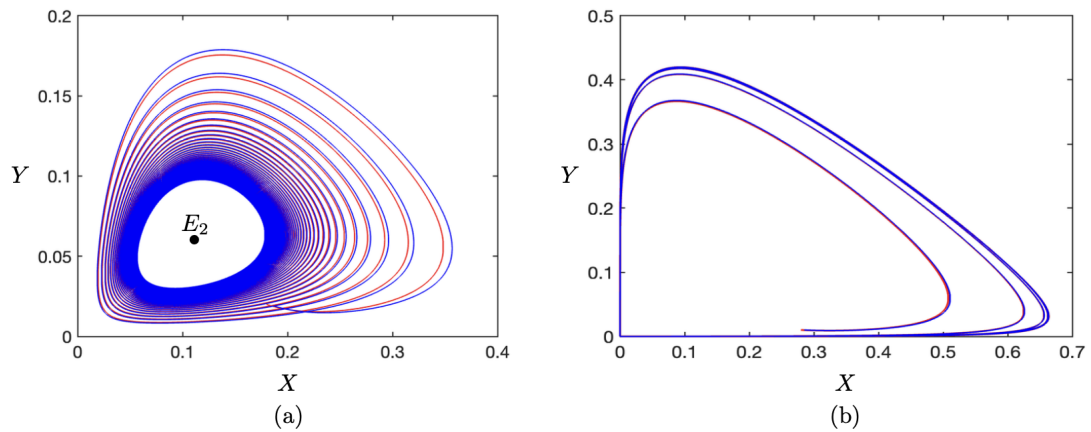


Figure 4.4: Simulations of model (4.2) showing stable limit cycles: (a) $A = \frac{19}{20}$, $B = 9$, $C = 1$, $D = \frac{3107}{9900} < D_H = \frac{661}{1980}$, regular oscillation and (b) $A = \frac{3}{5}$, $B = 6$, $C = \frac{1}{5}$, $D = \frac{1}{5} < D_H = \frac{34459}{40350}$, slow faster motion.

Figure 4.4 (b) signifies the emergence of a stable limit cycle due to a supercritical Hopf bifurcation, representing bounded, biologically meaningful oscillations in the tumor–virus dynamics. This results in the Hopf bifurcation threshold $D_H = \frac{661}{1980}$, where $\nu_0 > 0$. Using these parameters in the system, we compute the value:

$$\nu_1 = - \frac{11260705348431}{5861501682208} < 0.$$

From these results, we conclude that the stable limit cycles correspond to supercritical Hopf

bifurcations, where the system exhibits controlled, bounded oscillations a scenario that may be therapeutically acceptable. To estimate the amplitude of the limit cycle, we observe that the difference $\mu = D_H - D = \frac{1}{50}$, indicating that D is decreasing and approaching the Hopf bifurcation value D_H . This leads us to the following normal form equation governing the amplitudes of the bifurcating limit cycles:

$$\frac{dr}{d\tau} = r[v_0\mu + v_1r^2 + O(r^4)].$$

Using this equation, we can approximate the solution representing the amplitude of the single limit cycle. Figure 4.4 illustrates the simulated limit cycles. The inner trajectory (blue) starts close to the equilibrium and seems to settle toward it, indicating the stability of E_2 . The outer trajectory (red) spirals inward toward the limit cycle, confirming the presence of a stable outer attractor. As D crosses the critical threshold, one fixed point becomes unstable, and a limit cycle emerges. Inside the limit cycle, the system exhibits stability, while outside the cycle, the trajectories spiral toward it, confirming the dynamical transition at the Hopf bifurcation.

4.7 Conclusion

In this study, we proposed and analyzed a mathematical model to investigate the dynamics of oncolytic virus therapy, a promising approach in cancer treatment. The model captures key biological interactions between tumor cells, oncolytic viruses, and the immune system. By connecting these theoretical insights, our findings bridge the gap between mathematical modeling and potential clinical applications. By performing a detailed qualitative analysis, we established the boundedness of solutions and identified the equilibrium states of the system along with their stability properties. Using bifurcation theory, particularly center manifold and normal form analysis, we uncovered the conditions under which the system undergoes qualitative transitions, such as the onset of oscillatory behavior or the emer-

gence of stable limit cycles. These results highlight how variations in critical parameters could guide treatment design and predict therapeutic outcomes. These findings offer important insights into the potential for recurrent tumor growth or remission under different therapeutic scenarios. The study developed a mathematical model to analyze oncolytic virotherapy, capturing interactions among tumor cells, viruses, and the immune system. Using bifurcation and normal form analysis, it identified equilibrium states, stability conditions, and transitions leading to oscillatory behavior or stable limit cycles. These findings provide valuable insights into how variations in treatment parameters can influence tumor remission or recurrence, supporting optimized therapy design. Although the model simplifies biological processes and lacks clinical calibration, it offers a foundation for future improvements—such as incorporating memory effects, exploring combination therapies, and developing optimal control strategies for dosing and scheduling. Numerical simulations were conducted to validate and illustrate these analytical results, demonstrating the model’s ability to reproduce complex dynamical patterns relevant to cancer progression and control.

While the model offers valuable insights into the dynamics of oncolytic virotherapy, it has several limitations. Biological processes were not explicitly included. The immune response is simplified, neglecting adaptive immunity and memory effects. The model also overlooks the potential for viral resistance and tumor evolution. Being deterministic, it ignores stochastic fluctuations that can be significant in small populations. Additionally, treatment parameters are assumed constant, whereas real therapies often involve time-dependent or adaptive dosing. Lastly, the model does not have tuning with experimental or clinical data, which is essential for making patient-specific predictions. Acknowledging these limitations provides direction for refining the model and aligning it more closely with biological reality.

Virotherapy has many directions to be addressed for future investigation. First, the model has been extended using fractional order derivatives to account for memory effects

and hereditary properties in biological systems, allowing for a more accurate and realistic description of tumor-virus interactions over time. Additionally, we plan to explore combination therapies, such as virotherapy coupled with chemotherapy or immunotherapy, to study potential harmonious effects and identify optimal treatment strategies. Finally, we aim to develop optimal control strategies to determine the best therapeutic dosing and scheduling procedures, subject to clinical constraints such as toxicity and patient variability. Together, these future directions emphasize the integrative potential of mathematical modeling to guide experimental and clinical advances in oncolytic virotherapy.

References

- [1] E. Kelly, S. J. Russell, History of oncolytic viruses: genesis to genetic engineering, *Molecular Therapy*, **15**(4), 651-659, 2007.
- [2] C. M. Southam, A. E. Moore, Clinical studies of viruses as antineoplastic agents, with particular reference to Egypt 101 virus, *Cancer*, vol. 5, no. 5, pp. 1025-1034, 1952.
- [3] E. A. Chiocca, Oncolytic viruses, *Nature Reviews Cancer*, **2**(12), 938–950, 2002. Nature Publishing Group, London.
- [4] N. B. Elsedawy, S. J. Russell, Oncolytic vaccines, *Expert Review of Vaccines*, **12**(10), 1155–1172, 2013.
- [5] A. Melcher, K. Parato, C. M. Rooney, J. C. Bell, Thunder and lightning: immunotherapy and oncolytic viruses collide, *Molecular Therapy*, **19**(6) (2011) 1008–1016.
- [6] S. J. Russell, K.-W. Peng, J. C. Bell, Oncolytic virotherapy, *Nature Biotechnology*, **30**(7), 658–670, 2012.

- [7] S. Gujar, J. G. Pol, Y. Kim, P. W. Lee, G. Kroemer, Antitumor benefits of antiviral immunity: an underappreciated aspect of oncolytic virotherapies, *Trends in Immunology*, vol. 39, no. 3, pp. 209–221, 2018.
- [8] A. Samson, K. J. Scott, D. Taggart, E. J. West, E. Wilson, G. J. Nuovo, S. Thomson, R. Corns, R. K. Mathew, M. J. Fuller, *et al.* Intravenous delivery of oncolytic reovirus to brain tumor patients immunologically primes for subsequent checkpoint blockade, *Science Translational Medicine*, **10**(422), eaam7577, 2018.
- [9] S. Onnockx *et al.*, Oncolytic viruses: an inventory of shedding data from clinical trials and elements for the environmental risk assessment, *Frontiers in Bioengineering and Biotechnology*, vol. 11, pp. 1–20, 2023.
- [10] Y. Bai, P. Hui, X. Du, X. Su, Updates to the antitumor mechanism of oncolytic virus, *Thoracic Cancer*, 10(5), pp. 1031–1035, 2019.
- [11] H. Fukuhara, Y. Ino, T. Todo, Oncolytic virus therapy: A new era of cancer treatment at dawn, *Cancer Science*, **107**(10), 1373–1379, 2016.
- [12] R. H. I. Andtbacka, H. L. Kaufman, F. Collichio, T. Amatruda, N. Senzer, J. Chesney, K. A. Delman, L. E. Spitler, I. Puzanov, S. S. Agarwala, *et al.*, Talimogene laherparepvec improves durable response rate in patients with advanced melanoma, *Journal of Clinical Oncology*, **33**(25), 2780–2788, 2015.
- [13] C. Kaid, E. Goulart, L. C. Caires-Júnior, B. H. S. Araujo, A. Soares-Schanoski, H. M. S. Bueno, K. A. Telles-Silva, R. M. Astray, A. F. Assoni, A. F. R. Júnior, *et al.* Zika virus selectively kills aggressive human embryonal CNS tumor cells in vitro and in vivo, *Cancer Research*, **78**(12), 3363–3374, 2018.
- [14] Z. Zhu, M. J. Gorman, L. D. McKenzie, J. N. Chai, C. G. Hubert, B. C. Prager, E. Fernandez, J. M. Richner, R. Zhang, C. Shan, *et al.*, Zika virus has oncolytic

- activity against glioblastoma stem cells, *Journal of Experimental Medicine*, **214**(10), 2843–2857, 2017.
- [15] M. Zheng, J. Huang, A. Tong, H. Yang, Oncolytic viruses for cancer therapy: barriers and recent advances, *Molecular Therapy-Oncolytics*, **15** (2019), 234–247. doi:10.1016/j.omto.2019.10.007
- [16] Y. Luo, C. Lin, W. Ren, F. Ju, Z. Xu, H. Liu, Z. Yu, J. Chen, J. Zhang, P. Liu, et al., Intravenous injections of a rationally selected oncolytic herpes virus as a potent virotherapy for hepatocellular carcinoma, *Molecular Therapy-Oncolytics*, vol. 15, pp. 153–165, 2019. Oxford: Elsevier. doi:10.1016/j.omto.2019.09.001
- [17] D. Wodarz, Viruses as antitumor weapons: defining conditions for tumor remission, *Cancer Research*, **61**(8), 3501–3507, 2001.
- [18] D. Wodarz, et al., Computational approaches to study oncolytic virus therapy: insights and challenges, *Gene Therapy and Molecular Biology*, **8**, 137–146, 2004.
- [19] D. Wodarz, Computational modeling approaches to studying the dynamics of oncolytic viruses, *Mathematical Biosciences & Engineering*, **10**(3), 939–957, 2013.
- [20] M. Han, P. Yu, Normal forms, Melnikov functions and bifurcations of limit cycles, Springer, Vol. 181, 2012.
- [21] J. Jiang, P. Yu, Multistable phenomena involving equilibria and periodic motions in predator–prey systems, *International Journal of Bifurcation and Chaos*, **27**(3), 1750043, 2017. doi:10.1142/S0218127417500438
- [22] P. Yu, Computation of normal forms via a perturbation technique, *Journal of Sound and Vibration*, **211**(1), 19–38, 1998. doi:10.1006/jsvi.1997.1374
- [23] P. Yu, M. Han, Four limit cycles from perturbing quadratic integrable systems

by quadratic polynomials, *International Journal of Bifurcation and Chaos*, **22**(10), 1250254, 2012.

Chapter 5

5 Conclusion and Future Work

This thesis used mathematical models to study how tumors interact with immune cells, cytokines, and treatment methods such as immunotherapy and virotherapy. The results highlight the complex but important role of the immune system and treatment strategies in controlling tumor growth.

In the first study, we examined the role of $CD4^+$ T cells and their cytokine-mediated influence on tumor growth. While $CD4^+$ T cells do not directly destroy tumor cells, they can delay growth and push the tumor into a state of latency through cytokine release. Our analysis, using stability and bifurcation theory, showed that tumors always persist in the absence of treatment, regardless of their initial size. However, if the cytokine production rate or the tumor destruction rate is high, the tumor can be controlled to some extent, although not eliminated completely. These results suggest that while $CD4^+$ T cells play an important supportive role, additional intervention is required for complete tumor clearance.

In the second study, we extended the model to explore three immunotherapy strategies: cytokine therapy, $CD4^+$ T cell therapy, and their combination. The findings revealed that treatment success depends strongly on both the dose and the initial tumor size. Cytokine therapy can eliminate small tumors at high doses, partially reduce tumors at intermediate doses, or allow coexistence of tumor and immune cells at low doses. $CD4^+$ T cell therapy proved effective at keeping small tumors under control when started early, but it was unlikely to eliminate tumors completely, especially if the initial tumor size was large. Importantly, the combination of cytokine therapy and T cell infusion gave the best results, as it expanded the range of conditions under which tumors could be controlled and reduced oscillatory behavior. These findings underline that combined immunotherapy, with careful attention to dosing and timing, may offer better long-term control compared to cytokine therapy or $CD4^+$ T cell therapy alone.

The third study focused on oncolytic virotherapy, where viruses selectively infect and destroy tumor cells. The model incorporated tumor–virus–immune system interactions and revealed a variety of possible outcomes. Under some conditions, virotherapy could lead to complete tumor remission, while in other cases tumors recurred or oscillated in size due to immune–virus–tumor interactions. Bifurcation analysis showed how changes in viral replication and immune clearance rates could shift the system from stable tumor control to tumor returning or sustaining oscillations. Numerical simulations supported these findings, demonstrating the potential of virotherapy but also highlighting the need for precise dosing and consideration of the immune response.

Taken together, the findings from these studies show that the outcome of cancer treatment depends not only on the treatment type but also on biological parameters such as immune activity, tumor size, and treatment thresholds. While $CD4^+$ T cells alone cannot clear tumors, their cytokine-mediated effects are valuable in delaying growth. Immunotherapy strategies, particularly combination approaches, can significantly improve tumor control, and virotherapy provides an additional promising tool with complex but clinically relevant outcomes. Overall, this thesis establishes that mathematical modeling is not only capable of describing tumor–immune–therapy dynamics but can also serve as a foundation for future research aimed at improving cancer treatment outcomes.

5.1 Future Work

Although this thesis provides useful results, there are many ways the work can be extended in the future. The first model was simple and treated $CD4^+$ T cells as one type with limited interactions. A natural next step would be to include more realistic immune mechanisms, such as direct killing of tumor cells, memory effects, and the role of other immune cell types. Adding patient variability and spatial features of tumors would also make the model closer to real biology.

For the immunotherapy study, G_1 and G_2 are considered constant to represent continuous infusion. However, both can be extended as time dependent because therapy is often given in varying doses, cycles, or adaptive schedules. A future direction would be to include time-dependent treatment functions and test how different dosing patterns affect outcomes. It would also be valuable to compare the results directly with clinical or experimental data to check how well the model predictions match real treatment responses.

In the virotherapy study, we showed that viruses can produce complex tumor behaviors such as disappearance, recurrence, or oscillations. However, the model did not include viral resistance, tumor evolution, or random changes in small populations. These could be added to make predictions more reliable. Another direction is to explore fractional-order models, which can capture memory and long-term effects in biological systems.

Across all three studies, combination therapies remain an exciting area. Future research can look at how virotherapy works together with chemotherapy, radiation, or immunotherapy, and under what conditions these combinations are most effective. Finally, using mathematical methods to design the best treatment strategies that adjust dose and timing for each patient. This could lead to more personalized and effective cancer therapies, balancing treatment success with minimal side effects.

Education

- Ph.D. Applied Mathematics** 2020–Present
Western University, London, Ontario
Thesis: Nonlinear Dynamics and Bifurcations in Tumor–Immune Models with Therapies
Supervisor: Prof. Pei Yu
- M.Sc. Applied Mathematics** 2014–2016
The Maharaja Sayajirao University, Vadodara, India
Thesis: Mathematical Models of Cancer Under Various Therapies and Controllability
Supervisor: Prof. Purnima Pandit
- B.Sc. Mathematics** 2011–2014
The Maharaja Sayajirao University, Vadodara, India

Research Interests

Dynamical Systems

Stability analysis, Bifurcation theory, Nonlinear dynamics, Multi-stability

Mathematical Biology

Cancer modeling, Immunotherapy dynamics, Oncolytic virotherapy, Biological system interactions

Computational Modeling

Numerical simulations, Parameter estimation, Matlab/Maple implementations

Peer-Reviewed Publications

Ruchita Amin and Pei Yu, *Bifurcation Analysis on Immunotherapy of a Tumor Model Without Treatment*. *Discrete and Continuous Dynamical Systems - Series S*, 2025. <https://www.aims sciences.org//article/doi/10.3934/dcdss.2025076>

Ruchita Amin and Pei Yu, *Dynamical Analysis of a Tumor Model with Immunotherapy Treatment*. *Chaos, Solitons & Fractals*, 2025. <https://www.sciencedirect.com/science/article/pii/S0960077925016200>

Submitted Papers

Ruchita Amin and Pei Yu, *Bifurcation Analysis and Complex Dynamics of a Virotherapy Model*. International Journal of Bifurcation and Chaos, 2025.

Experience

Graduate Teaching Assistant Fall 2020-Fall 2024
Western University, London, Ontario

Mentor-Directed Reading Program Winter 2025
Western University, London, Ontario

Assistant Professor Fall 2016-Fall 2019
ITM Vocational University, Vadodara, Gujarat, India
Sardar Vallabhbhai Patel Institute of Technology, Vasad, Gujarat, India

Honors & Awards

AARMS Award Summer 2025
Poster Session at CMS Summer Meeting, Laval University, Québec, ON.

Robert and Ruth Lumsden Graduate Award Winter 2025

Henning Rasmussen Graduate Bursary Winter 2025

Kenneth Cooper Graduate Bursary Winter 2025
Western University, London, Ontario

Conferences & Presentations

Conference Research Paper Presentation Summer 2025
Bifurcation Analysis and Complex Dynamics of a Virotherapy Model.
Poster Presentation at CMS Summer Meeting, Laval University, Québec, ON.

Dynamical Analysis of a Tumor Model with Immunotherapy Treatment.
Student Research Sessions at CMS Summer Meeting, Laval University, Québec, ON.

Bifurcation Analysis on Immunotherapy of a Tumor Model Without Treatment.
Ottawa Mathematics and Statistics Conference (OMSC), Ottawa, ON.

Skills

Software & Programming
Maple, Matlab, LaTeX and Microsoft Office Suite